DISSERTATION

# MULTIPLE DOMAINS IN THE NDC80 COMPLEX ARE REQUIRED FOR GENERATING AND REGULATING KINETOCHORE-MICROTUBULE ATTACHMENTS IN MITOSIS

Submitted by

Lynsie Jill Radovich Sundin

Department of Biochemistry and Molecular Biology

In partial fulfillment of the requirements

For the Degree of Doctor of Philosophy

Colorado State University

Fort Collins, Colorado

Spring 2012

Doctoral Committee:

Advisor: Jennifer G. DeLuca

James Bamburg
Norman Curthoys
Susan Bailey

ABSTRACT

MULTIPLE DOMAINS IN THE NDC80 COMPLEX ARE REQUIRED FOR GENERATING AND REGULATING KINETOCHORE-MICROTUBULE ATTACHMENTS IN MITOSIS

The goal of mitosis is to accurately segregate chromosomes into two new daughter cells. It is critical that this process occurs appropriately because the consequences of chromosome nondisjunction or missegregation are severe, most notably birth defects and cancer. Kinetochores are built at the centromeric region of mitotic chromosomes and serve several functions during mitosis. First, the kinetochore is the physical scaffold at which microtubule binding sites are built. Second, kinetochores regulate the strength of the attachments to microtubules to ensure proper chromosome movements. Finally, the kinetochore is the origin of a soluble 'wait anaphase' signal that prevents premature entry into anaphase. Together these functions culminate with chromosome alignment at the spindle equator of a cell, ultimately resulting in accurate chromosome segregation in anaphase.

While the kinetochore can be considered the director of kinetochore-microtubule attachment, microtubules drive the process of cell division by providing the force behind chromosome movements. The mechanism of kinetochore-microtubule attachment remains elusive as kinetochores must generate and maintain connections to microtubules that are constantly

polymerizing and depolymerzing. Extensive studies into this process have revealed that the KMN (KNL1 complex, MIS12 complex, and NDC80 complex) network, a supercomplex of proteins at the outer kinetochore, comprises the core microtubule binding site in cells. As part of this network the NDC80 complex has been an attractive candidate as an essential part of the microtubule binding machinery. Here we have used a combination of in vivo, in vitro, and in silico methods to characterize three discrete domains of the NDC80 complex that each contribute to the process of kinetochore-microtubule attachment in distinct ways. Our data have elucidated some of the molecular details of how kinetochore-microtubule attachments are both generated and regulated. We show that the Hec1 CH domain is absolutely required for kinetochore-microtubule attachment. Our data suggest that the Hec1 CH domain makes direct contacts with microtubules, while the CH domain of Nuf2 does not, indicating functionally distinct roles for these protein domains in mitosis. We characterize the Hec1 loop domain, demonstrating that it is required for stable kinetochore-microtubule attachments and mitotic progression. Our data suggest that the Hec1 loop domain is required to recruit accessory proteins to the kinetochore during mitosis. Furthermore, we show that kinetochore-microtubule attachment strength is highly sensitive to small changes in Hec1 tail phosphorylation. Finally we also demonstrate that incremental phosphorylation of the Hec1 tail domain is a primary mechanism of regulating kinetochore-microtubule attachment strength.

Together our data highlight the diverse functions of a single kinetochore component and implicate the NDC80 complex as the principle site for direct binding to microtubules and as a site of regulation for these attachments.

ACKNOWLEDGEMENTS

I consider myself incredibly fortunate to have had the help and support of many people, without which the completion of this dissertation would not have been possible. I am grateful for the kindness and generosity I have been shown while being a part of the Department of Biochemistry and Molecular Biology.

As my advisor, Dr. Jennifer DeLuca has encouraged my development as a scientist and has given me the skills and confidence to transition from a young graduate student to an independent thinker. She has served not only as my mentor but also as a role model for developing a career in science.

I would like to thank my committee members, Dr. James Bamburg, Dr. Norman Curthoys, and Dr. Susan Bailey, for their support and encouragement. Their thoughtful advice and input have always pushed me to broaden my horizons and consider the big picture.

A million thanks are not enough for my labmates. I am so lucky to go to work each day and see my friends. I have always enjoyed the jokes and laughter, as well as our lively discussions about science and otherwise. Together you have taught me that you can find family even when you're far from home.

Adam, you have been at my side during this adventure and your support has been unwavering. You have the innate ability to know when I need to be pushed forward or when I need a strong person to lean on. Through all of the

ups and downs of graduate school, you have continued to bring out the best in me.

My parents and brother have always been an incredible support system for me. They have always encouraged me to chase my dreams and have been there to help pick up the pieces when the wheels fall off. My strength and confidence, my ‘sisu’, comes from each of you.

TABLE OF CONTENTS

# CHAPTER I

## Introduction

### 1.1 Overview of mitosis

Accurate progression through mitosis is critical for appropriate segregation of duplicated chromosomes into two daughter cells. Mitotic events are tightly regulated to prevent chromosome segregation errors, thus avoiding aneuploidy and the development of cancer and birth defects. The process of mitosis was first characterized nearly 150 years ago, but the exact mechanism by which chromosomes attach to dynamic microtubule plus-ends has yet to be determined and remains a widely studied topic.

Mitosis is initiated in prophase, when chromosomes are condensed and are held within the nucleus by the nuclear envelope (Figure 1.1). When the nuclear envelope breaks down the cell enters prometaphase and chromosomes begin to move toward the spindle equator and align in metaphase. During the entirety of mitosis, a surveillance system called the spindle assembly checkpoint (SAC) prevents premature entry into anaphase, avoiding chromosome nondisjunction and missegregation, thus preventing aneuploidy. When the SAC is satisfied, the cell enters anaphase and segregates chromosomes to two new daughter cells.

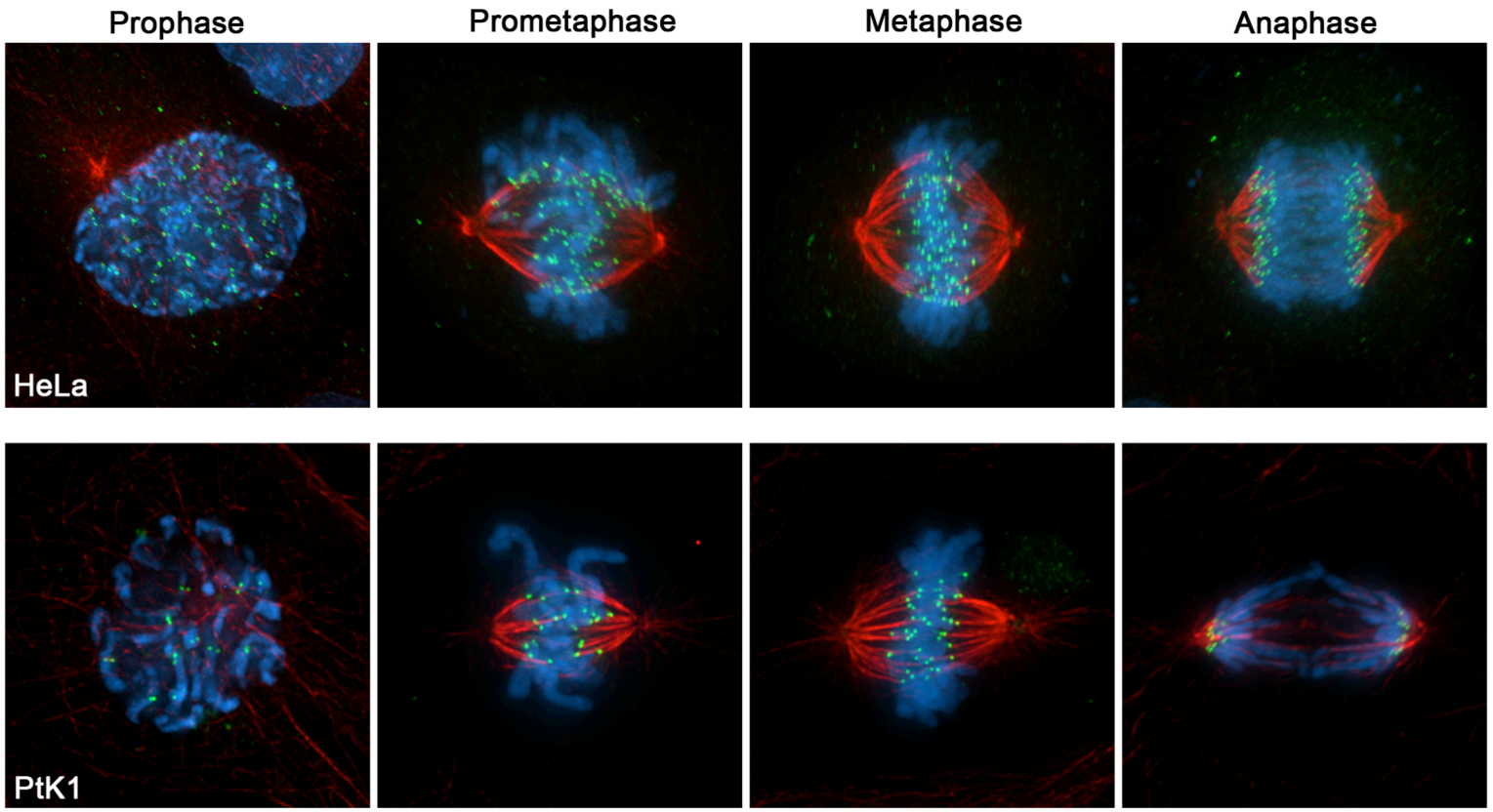


**Figure 1.1. The phases of mitosis shown by immunofluorescence in fixed mammalian cells.** In prophase, chromosomes are condensed and held within the nuclear envelope. As the nuclear envelope breaks down, chromosomes spill into the cytoplasm and begin making initial contacts with microtubules. When each kinetochore has made attachments to microtubules from opposing spindle poles, the chromosomes align at the spindle equator and the cell is in metaphase. Once the SAC has been satisfied, the cell can enter anaphase and segregate chromosomes to two new daughter cells. Top panel: HeLa cells; Bottom panel: PtK1 cells. Blue = DAPI, red = anti-tubulin, green = Hec1-GFP.

Central to chromosome movement during mitosis is the attachment of chromosomes to the microtubules of the mitotic spindle. The attachment site is built at a specialized area on mitotic chromosomes called the kinetochore. Not only is the process of kinetochore-microtubule attachment complex, but the kinetochore itself is also a large intricate structure made of at least 100 proteins. Many proteins and protein complexes have been identified that are required for correct attachment between kinetochores and microtubules, which has shed some light on the mechanism of kinetochore-microtubule attachment.

### 1.2 Kinetochore organization: structural overview of the microtubule attachment site

Microtubule dynamics drive cell division, and the kinetochore can be considered the director of chromosome movements in mitosis. The kinetochore is a large molecular machine that serves as a scaffold to physically link chromosomes to the mitotic spindle. Additionally, it serves as the site of control of progression through mitosis. The centromere, originally defined as the primary constriction site of a chromosome, provides the foundation for the kinetochore, which assembles during mitosis (Bloom, 2007). Budding yeast have the simplest and most well defined kinetochores. Built on 125 base pairs of DNA, these kinetochores bind a single microtubule and are made of approximately 60 proteins, most of which are further organized into protein complexes (Tanaka et al., 2005; Joglekar et al., 2006; Cheeseman et al., 2002; De Wulf et al., 2003). With only a few exceptions, these protein complexes are conserved from yeast to

humans (Santaguida and Musacchio 2009). The vertebrate kinetochore is comprised of over 100 proteins, assembles on a regional centromere that spans megabases of DNA, and binds multiple microtubules (~16 microtubules in humans) (Wendell et al., 1993; McEwen et al., 2001) (Figure 1.2). The high incidence of protein conservation from yeast to humans has led to the hypothesis that kinetochores in yeast represent the smallest microtubule binding unit and that human kinetochores, for example, are simply arrays of these smaller structures, though there is no structural evidence to support this idea directly (Zinkowski et al., 1991; Cimini et al., 2001; Joglekar et al., 2006; Dong et al., 2007). Not surprisingly, an ultrastructural visualization of the kinetochore has been a goal for decades and a clear picture of the kinetochore would certainly aid in determining how its many components come together to form the microtubule binding site.

### 1.2.1 Trilaminar structure

Early electron microscopy (EM) studies of mammalian kinetochores revealed a structure consisting of electron dense inner and outer kinetochore regions, and an interzone that largely lacks electron density (Brinkley and Stubblefield, 1966; Jokelainen, 1967; Rieder, 1981; Roos, 1973; McEwen et al., 1993). These observations led to the idea that the kinetochore has three discrete zones and what is classically thought of as a trilaminar structure. In total, the mammalian kinetochore spans about ~150nm from the inner to the outer region (McEwen et al., 1993). The inner kinetochore is the thinnest region with a

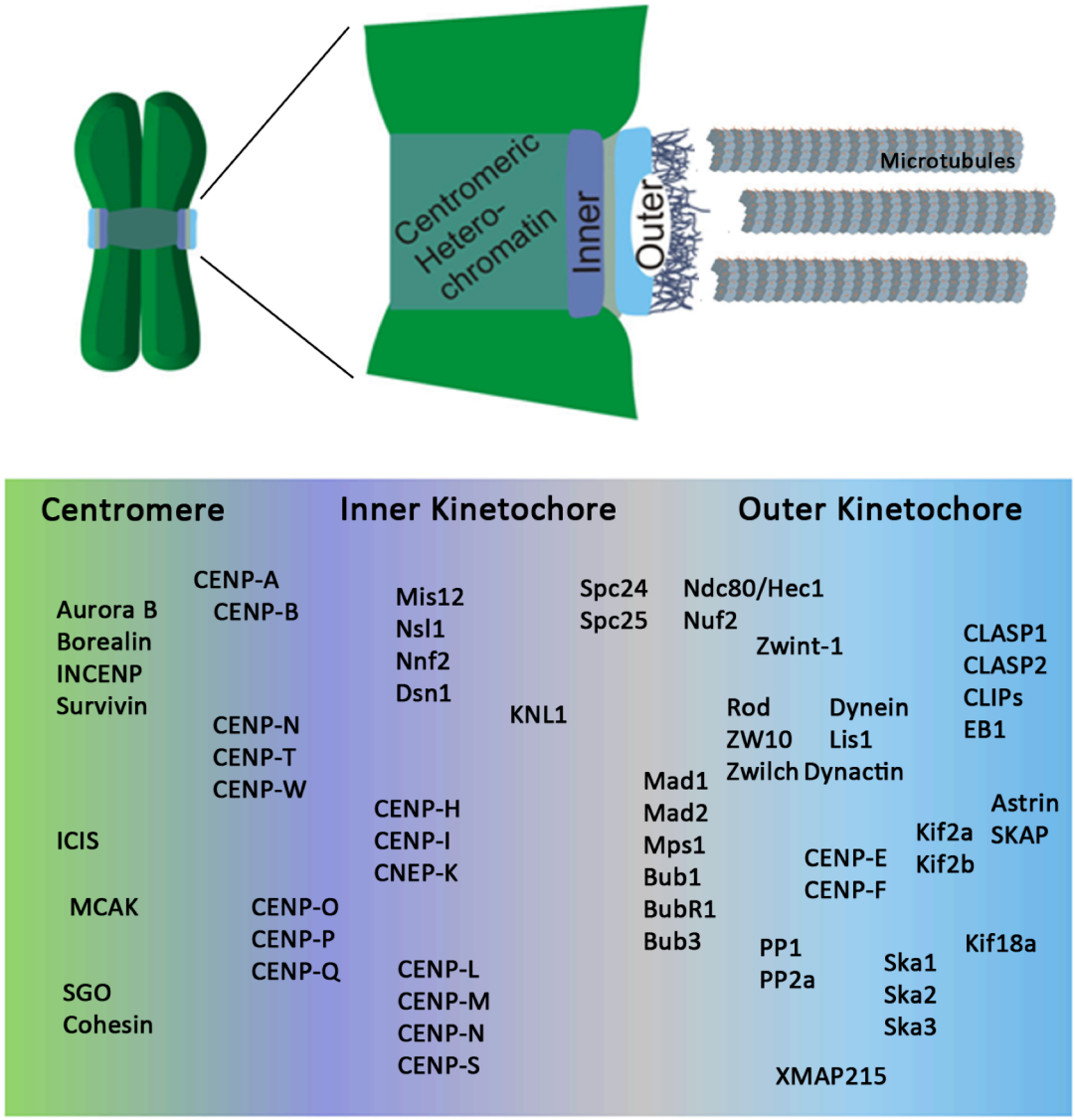


**Figure 1.2. Schematic of kinetochore structure.** The vertebrate kinetochore is made of at least 100 proteins that assemble on the centromeric heterochromatin of mitotic chromosomes. Shown here are some of the components of the kinetochore. Although this does not represent a complete list, it does highlight the complexity of the kinetochore as a molecular machine.

thickness up to 30nm. This region is proximal to the chromatin, and proteins here form a platform on which the outer kinetochore assembles. Measuring 50-60nm, the outer kinetochore is the thickest region, and is the area in which the microtubule binding site is assembled. Separating the inner and outer kinetochore regions is the 35nm interzone (Jokelainen 1967; Cheeseman and Desai 2008) (Figure 1.3, A and B). Although the interzone is less apparent in cells preserved using high-pressure freezing and freeze substitution instead of conventional fixation procedures, the tripartite structure of the kinetochore remains as a guide for explaining the relative positions of kinetochore proteins (McEwen et al.,1998). Electron tomography studies have revealed that the interzone may be comprised of fibrous links, which have been speculated to directly link the inner and outer kinetochore (McEwen et al., 1993; Dong et al., 2007).

Extending away from the outer kinetochore is an area of thin, fibril-like structures reaching up to ~150nm that are apparent only at kinetochores that are not attached to microtubules (Rieder and Salmon 1998). Termed the fibrous corona, this region has been shown to contain the microtubule motor proteins centromere associated protein-E (CENP-E) and dynein, both of which play roles in the process of kinetochore-microtubule attachment and also function in the SAC (Wojcik et al., 2001; Mao et al., 2005; Cooke et al., 1997; Maiato et al., 2004; Howell et al., 2001). Additionally, Spindly and CENP-F have been shown to localize to the fibrous corona and are important for chromosome alignment and anaphase entry (Bomont et al., 2005; Griffis et al., 2007; Barisic et al., 2010;

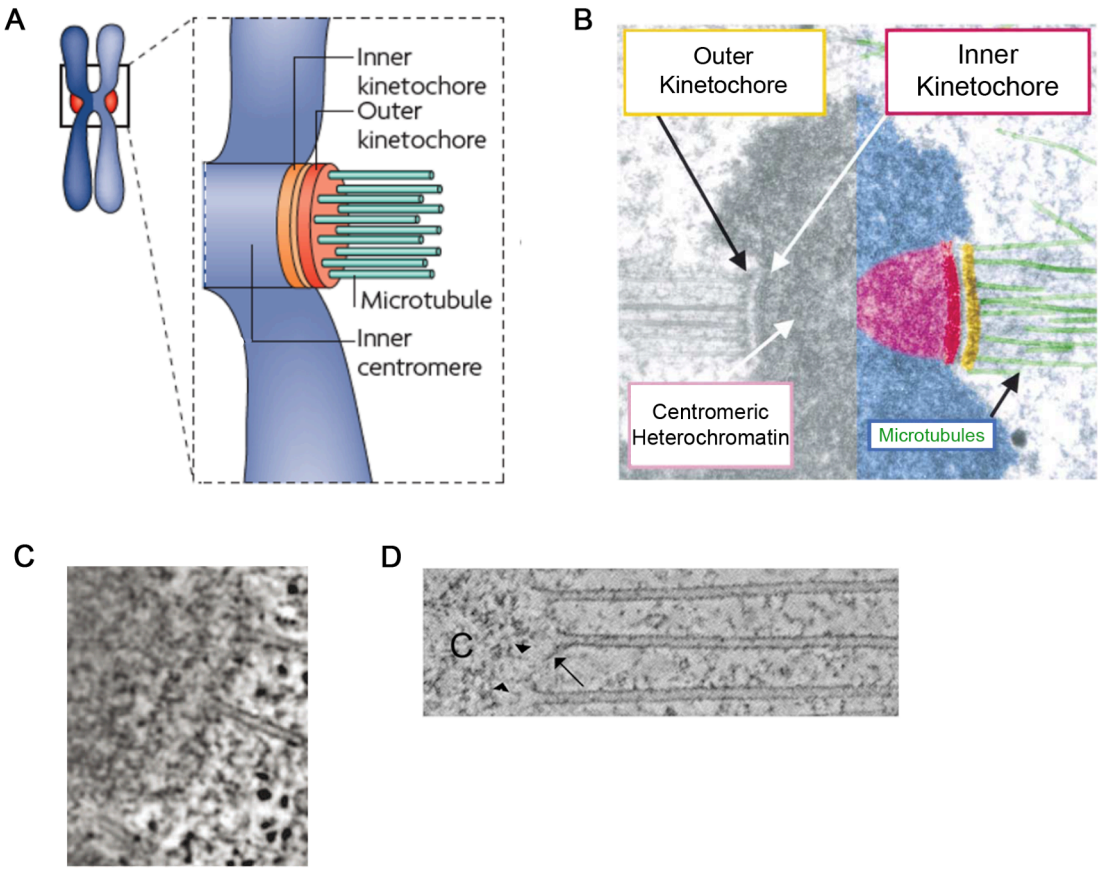


**Figure 1.3. Ultrastructure of the vertebrate kinetochore. A)** Schematic view of the kinetochore indicating the positions of the inner and outer kinetochore regions (Adapated from Cheeseman and Desai, 2008). **B)** Electron micrograph of kinetochores in vertebrate cells. The right panel has been pseudo-colored to highlight the often observed trilaminar structure and the presence of multiple microtubules terminating at the outer kinetochore (Adapted from Cleveland et al., 2003). **C)** An electron tomogram of a kinetochore from a rat kangaroo cell showing a mesh-like network at the outer region of the kinetochore (Adapted from Dong et al., 2007). **D)** Electron tomogram of a kinetochore from a rat kangaroo cell indicating the presence of thin fibrils (arrowheads) connecting the outer kinetochore to the flared plus-ends of microtubules (arrow). In this panel, "C" indicates chromatin (Adapted from McIntosh et al., 2008).

Gassmann et al., 2010). Considering their respective functions, it is not surprising that these proteins reside at the outermost “edge” of the kinetochore to monitor and respond to kinetochore-microtubule attachment status.

### 1.2.2 Fibrous network

Electron tomography studies using rapid freezing techniques on rat kangaroo (PtK1) cells have highlighted that the outer domain of the kinetochore appears to be a fibrous network of proteins rather than a dense plate (Figure 1.3C). From these preparations, the outer kinetochore appears to be comprised of fibers that are 80-90nm long and ~10nm in diameter. These fibers are only visible at kinetochores that are not bound to microtubules (McEwen et al., 1993; McEwen et al., 1998; Dong et al., 2007). Images of microtubule-bound kinetochores suggest that the outer fibers become less organized upon microtubule binding. It was also observed that microtubules terminated at the outer kinetochore at a variety of angles and that the outer kinetochore interacts with both the plus-ends and outer walls of microtubules. These data suggest that the outer kinetochore may be more like a flexible network of binding proteins rather than a rigid series of discrete binding sites (Dong et al., 2007). In addition to kinetochore ultrastructure, this study highlights that a flexible meshwork at the outer kinetochore would perhaps facilitate more efficient microtubule capture than predefined binding sites (Dong et al., 2007). Additionally, the “repeat subunit” model, or predefined binding site model, of kinetochore structure poses that vertebrate kinetochores that bind multiple microtubules are assemblages of

a minimal microtubule-binding unit, namely the kinetochore from budding yeast (Zinkowski et al., 1991; Joglekar et al., 2006). However, the flexible nature of the fibrous network of proteins observed at the outer kinetochore does not support the idea of discrete microtubule binding sites, but instead a less organized network of microtubule binding proteins (Dong et al., 2007).

### 1.2.3 Kinetochore fibrils

As tubulin subunits hydrolyze GTP to GDP they undergo a conformational change that does not support microtubule polymerization likely due to steric strain within a protofilament (Howard and Timasheff, 1986; Mandelkow and Mandelkow, 1992). The bending of protofilaments during microtubule depolymerization alleviates this strain, and this idea is supported by observations of curved or flared microtubule plus-ends in vitro (Mandelkow et al., 1991). Electron tomography studies have revealed that microtubule plus ends also take on a flared conformation in vivo. Interestingly, the curvature of flared microtubules bound to kinetochores is less than that of their in vitro counterparts, suggesting that a force is being applied to change the shape of the microtubule plus-end (McIntosh et al., 2008). In support of this, the same study showed the presence of fibrils extending from the kinetochore into the lumen of the microtubule (Figure 1.3D). Using mathematical modeling it was shown that these kinetochore fibrils could couple a depolymerizing microtubule to a chromosome to harness sufficient force to facilitate chromosome movements in mitosis. A fibril-mediated linkage between kinetochores and microtubules could explain how

microtubule depolymerization is coupled to chromosome movements. This type of coupler could resist the force of a bending microtubule protofiliment and translate the energy into a 'forced walk' between binding sites within the microtubule lattice (McIntosh et al., 2008; Joglekar et al., 2010). However, the underlying problem with this idea is that candidate microtubule binding proteins at the kinetochore that are known to be required for kinetochore-microtubule attachment have been shown to bind the outer lattice of the microtubule and not the luminal surface (Wilson-Kubalek et al., 2008; Alushin et al., 2010). However, the possibility exists that the fibrils represent a kinetochore protein that has yet to be identified and characterized (Ohta et al., 2010).

### 1.2.4 High-resolution microscopy studies delineate the relative position of major players and protein copy number at the kinetochore

Genetic screens and protein-protein interaction studies have been widely used to predict which kinetochore proteins interact, leading to an idea of how these proteins may be organized at the kinetochore (Maiato et al., 2004; Cheeseman and Desai 2008). Electron microscopy studies have been monumental in determining the structure of the kinetochore, but have been thus far unable to define the relative location of kinetochore proteins to one another. Using two-color, high-resolution fluorescence microscopy and SHREC (single-molecule high-resolution colocalization) analysis, a high-resolution map of the kinetochore was generated with proteins from each of the major kinetochore domains in both yeast and human cells (Churchman et al., 2005; DeLuca et al.,

2006; Joglekar et al., 2009; Wan et al., 2009). A summary of the relative positions of kinetochore components is shown in Figure 1.4. This nanometer-scale map shows the relative positions of 9 different kinetochore proteins in vivo and has been essential for supporting and interpreting previous studies that have shown interactions and recruitment requirements among kinetochore proteins.

In addition to the relative locations of various kinetochore proteins, the copy number of several components of the kinetochore has been determined by high-resolution fluorescence microscopy in cells. From initial studies using quantitative fluorescence microscopy in *Saccharomyces cerevisiae* the protein copy number of GFP (green fluorescent protein)- tagged kinetochore proteins was determined relative to the two CENP-A (Cse4 in budding yeast) molecules at the centromere (Joglekar et al., 2006). Using a fluorescence ratio method in chicken cell lines stably expressing different GFP-fused kinetochore components from endogenous loci, the number of protein components per microtubule was calculated (Johnston et al, 2010; Lawrimore et al., 2011). Interestingly, the protein copy number per kinetochore correlated with the number of microtubules bound, suggesting conservation of the structure of kinetochores from yeast to vertebrates (Johnston et al., 2010; Lawrimore et al, 2011; Joglekar et al., 2008) (Table 1.1). Undoubtedly, the continued coupling of high-resolution microscopy, biochemical and structural studies, and in vivo assays will lead to a detailed blueprint of the kinetochore.

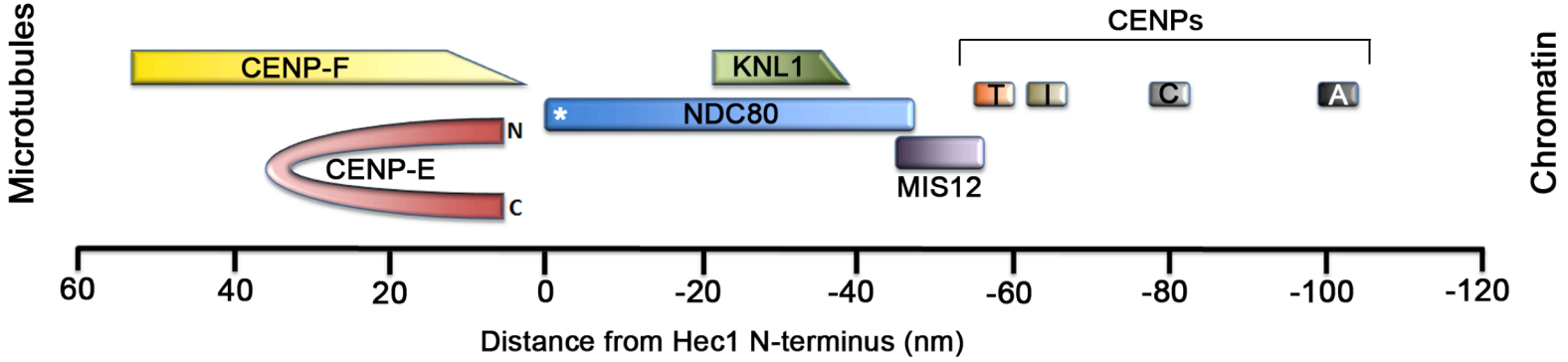


**Figure 1.4. Relative positions of major kinetochore components.** High-resolution microscopy studies coupled with SHREC analysis have resulted in a nanometer scale map of the vertebrate kinetochore. Shown here are the positions of major kinetochore components relative to the N-terminus of the NDC80 complex protein Hec1 (denoted by the white asterisk). On CENP-E, "N" and "C" indicate to the positions to which the N- and C-termini were mapped using two different antibodies. Additionally, CENP-F and KNL1 are both large, rod-shaped proteins of which the N-terminal and middle portions were mapped using multiple antibodies; the angled shape of each of these proteins indicates the lack of a mapped position for the C-termini (Adapted from Wan et al., 2009).

**Table 1.1. Kinetochore protein copy number calculated for human cells.** Quantitative fluorescence microscopy studies in *Saccharomyces cerevisiae* were used to determine the number of proteins per kinetochore-microtubule (kMT) for the proteins listed below. When the protein copy number was measured in DT40 (chicken) cells, the increase in protein copy number was commensurate with the number of microtubules bound per kinetochore. In human metaphase cells, the average number of kMTs is 16 (Wendell et al., 1993; McEwen et al., 2001). To calculate the average number of proteins per kinetochore in humans, the average protein copy number per kMT measured in yeast was multiplied by 16 (Modified from Wan et al., 2009).

| Protein Name | Average Number per Kinetochore | Average Number per kMT |
|---|---|---|
| CENP-C | 400 +/- 128 | 25 +/- 8 |
| CENP-T | 288 +/- 80 | 18 +/- 5 |
| CENP-I | 256 +/- 64 | 16 +/- 4 |
| MIS12 | 400 +/- 128 | 25 +/- 8 |
| KNL1 | 320 +/- 80 | 20 +/- 5 |
| Nuf2 | 384 +/- 112 | 24 +/- 7 |
| Hec1 | 336 +/- 96 | 21 +/- 6 |

### 1.3 Kinetochore assembly

The inner kinetochore refers to a group of proteins that are adjacent to the centromeric chromatin. It contains the histone H3 variant CENP-A that is assembled into centromeric nucleosomes and remains well defined throughout the cell cycle (Black et al., 2004; Cheeseman and Desai 2008). Additionally, a group of 16 proteins (CENPs-C, -H, -I, -K through -U, -W, and -X) known as the constitutive centromere-associated network (CCAN) belongs to the inner kinetochore, remains there throughout the cell cycle, and is required for kinetochore assembly in mitosis (Hori et al., 2008; Okada et al., 2006; Cheeseman and Desai, 2008; Screpanti et al., 2011). In budding yeast and *Drosophila melanogaster* CENP-A is necessary and sufficient for kinetochore assembly (Heun et al., 2006). The specific requirements for kinetochore specification and assembly in mammalian cells have not been well defined. What is known, however, is that the kinetochore assembles in an 'inside out' manner. The CCAN and inner kinetochore components recruit proteins that reside in the outer kinetochore and are required for direct microtubule binding. In this way the inner kinetochore can be considered a platform on which the outer kinetochore, and microtubule binding sites, are assembled.

In mammalian cells CENP-A is not sufficient to define the site of kinetochore assembly. Overexpression of CENP-A leads to incorporation of the histone protein into nucleosomes throughout chromosome arms, but ectopic kinetochore assembly does not occur (Van Hooser et al., 2001; Gascoigne et al., 2011). It has been shown that the requirement for CENP-A can be bypassed in

cells, and ectopic kinetochores can be assembled, when other downstream members of the CCAN are directly tethered to the chromatin (Gascoigne et al., 2011). In vitro, kinetochores can be assembled on chromatin templates containing CENP-A and can support microtubule binding and mitotic checkpoint function. Interestingly, beads containing histone H3 were unable to promote kinetochore assembly and microtubule binding (Guse et al., 2011). Additionally, depletion of CENP-A is lethal in human cells and cells lacking CENP-A fail to maintain a functional kinetochore (Black et al., 2007). Taken together these data suggest that CENP-A, although not sufficient, is required for kinetochore assembly likely as the most upstream component in kinetochore assembly.

Protein members of the CCAN can be divided into subgroups, some of which bind CENP-A directly, and others that are required for downstream recruitment of CCAN members and ultimately for assembly of the microtubule binding site at the outer kinetochore (Santaguida and Musacchio 2009). Although the hierarchical nature of kinetochore assembly dictates that nearly all CENPs must be in place for appropriate kinetochore assembly and function, here the focus will be on CENPs that have been shown to have a direct role recruiting outer kinetochore proteins.

CENP-C binds CENP-A, is a core component of centromeric chromatin, and is required for kinetochore function (Tanaka et al., 2009). The C-terminal domain of CENP-C directs centromere localization while a conserved portion of the N-terminus recruits proteins that are considered the core microtubule binding network at the outer kinetochore (Przewloka et al., 2011; Screpanti et al., 2011).

Additionally, CENP-C works coordinately with CENP-T/W to recruit the MIS12 complex, the KNL1 complex, and the NDC80 complex to the outer kinetochore. CENP-C and CENP-T/W are thought to be recruited independently to centromeres and together these data suggest that assembly of the outer kinetochore may not be strictly linear (Gascoigne et al., 2011). Interestingly, it has been shown that CENP-T/W and another CCAN member, CENP-S/X, each contain histone folds. Together these proteins form a heterotetrameric supercomplex (CENP-T/W/S/X) that can supercoil DNA, similar to a canonical nucleosome. Inhibition of CENP-T/W/S/X tetramer formation or reduction of its DNA binding ability severely compromises kinetochore formation in vertebrate cells (Nishino et al., 2012). Finally, studies in chicken and human cells have shown that CENP-H/I/K, in cooperation with the outer kinetochore protein KNL1, function downstream of CENP-A and -C to direct recruitment of the outer kinetochore NDC80 complex. (Cheeseman et al., 2008). Taken together it seems that CENP-C acts as a conserved link between the centromere and kinetochore and in cooperation with CENP-T/W/S/X forms a platform for kinetochore assembly.

The outer kinetochore is a more dynamic region consisting of proteins that are recruited and turned over in response to microtubules or specific phases of mitosis (Cheeseman and Desai 2008). Some proteins at the outer kinetochore prevent entry into anaphase, specifically by generating a diffusible, inhibitory signal at the kinetochore. These proteins are part of the SAC, which is essentially a safety mechanism that helps to prevent aneuploidy by preventing cells from

attempting to segregate chromosomes before correct kinetochore-microtubule attachments have been achieved (Baker et al., 2007; Maresca et al., 2010). Briefly, two key proteins that have been identified as final effectors of SAC signaling from the kinetochore are Mad2 and BubR1, which function to inhibit the anaphase promoting complex/cyclosome (APC/C). The APC/C is an E3 ubiquitin ligase that targets cyclin B and securin for degradation, leading to anaphase entry (King et al., 1995; Sudakin et al., 1995; Peters, 2006). When recruited to unattached kinetochores, Mad2 undergoes a conformational change, allowing it to bind to Cdc20, the activating subunit of the APC/C (Sudakin et al., 2001). Mad2 promotes binding of BubR1 to Cdc20, resulting in inhibition of Cdc20 and the generation of a soluble 'wait anaphase' signal (Kulukian et al., 2009; Malureanu et al., 2009). As kinetochores gain attachments to microtubules, inhibition of Cdc20 subsides, allowing Cdc20 to interact with and activate the APC/C, ultimately leading to anaphase entry and chromosome segregation (Shah and Cleveland 2000; Musacchio and Hardwick 2002).

### 1.4 The KMN Network

A critical function of the outer kinetochore is to directly bind microtubules and regulate kinetochore-microtubule attachments (Santaguida and Musacchio 2009). Many proteins have been implicated as having roles in these processes, however, here the focus will be on a conserved subset of proteins that have been implicated as generating the core microtubule binding sites at the outer kinetochore.

In vivo studies have been monumental in defining which kinetochore proteins, when mutated or deleted, result in microtubule attachment defects. Coupled with in vitro analyses, we now have a clear idea of which proteins directly bind microtubules and comprise the core microtubule binding site in cells. The KMN network (KNL1, MIS12, and NDC80) is conserved in eukaryotes and is required for kinetochore-microtubule attachment in a variety of organisms (Kline-Smith et al., 2005) (Figure 1.5). It consists of 10 proteins further organized into 3 complexes: the KNL1 complex (KNL1 and Zwint-1), MIS12 complex (Mis12, Dsn1, Nnf1, and Nsl1), and the NDC80 complex (Ndc80/Hec1, Nuf2, Spc24, and Spc25) (Cheeseman et al., 2006; Cheeseman and Desai 2008; DeLuca and Musacchio 2011). There is evidence to suggest that this network of proteins plays a role in directing kinetochore assembly, generating and regulating kinetochore-microtubule attachments, and controlling progression through mitosis (Cheeseman et al., 2008; DeLuca et al, 2003; DeLuca et al., 2006; Liu et al., 2010; DeLuca et al., 2011). Although proteins within this network have varied tasks during kinetochore-microtubule attachment, it has been made abundantly clear that the KMN network comprises the core microtubule attachment site at the outer kinetochore.

***KNL1*** **–** Originally identified in *C. elegans* using RNAi genomic approaches, KNL1 has been characterized in vertebrate cells as an important player for recruitment of a subset of outer kinetochore proteins and may also play a role in microtubule binding (Desai et al., 2003; Cheeseman et al., 2008). Making assessments of direct binding between KNL1 and other kinetochore

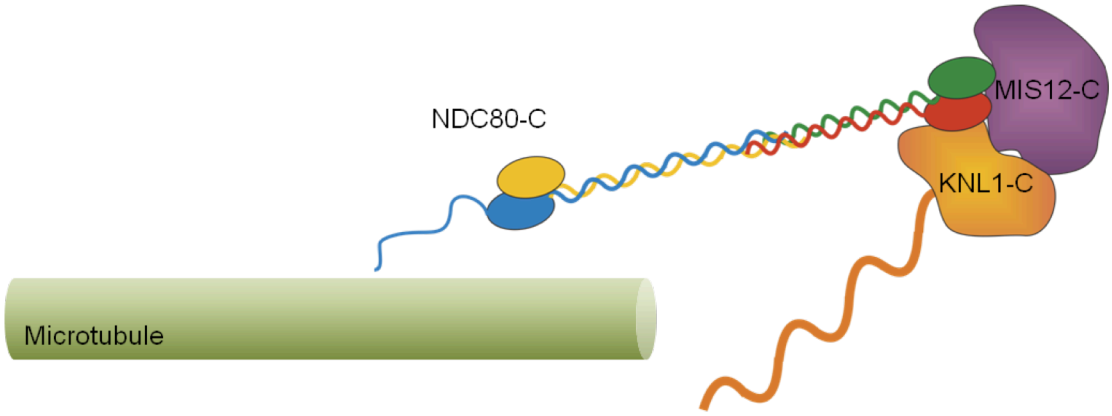


**Figure 1.5. The KMN network.** A schematic of the KMN network showing the relative positions and predicted interactions between protein complexes. This 10-member supercomplex of is comprised of the MIS12 complex (MIS12-C; Mis12, Dsn1, Nnf1, and Nsl1), the KNL1 complex (KNL1-C; KNL1 and Zwint-1), and the NDC80 complex (NDC80-C; Hec1, Nuf2, Spc24, Spc25). MIS12-C acts to anchor the KMN network to the kinetochore, and in coordination with KNL1-C forms a receptor for NDC80-C.

proteins has proven difficult because the large size of KNL1 (~260kDa) precludes its recombinant expression and purification (Cheeseman et al., 2006; Welburn et al., 2010). By immunofluorescence assays in human and chicken cells it has been shown that KNL1 localizes to the kinetochore throughout mitosis and depletion of KNL1 by siRNA leads to defects in chromosome alignment and segregation (Cheeseman et al., 2008). Although it has been demonstrated using in vitro microtubule binding assays that KNL1 has a weak affinity for microtubules, it was also shown that KNL1 acts synergistically with the NDC80 complex to bind microtubules and the KNL1 depletion phenotype is much less severe than in cells depleted of the NDC80 complex (Cheeseman et al., 2006). These data suggest that KNL1 does not serve as the primary microtubule binding component at the outer kinetochore but is still important for the generation of stable kinetochore-microtubule attachments. KNL1 does play a large role in recruiting many proteins to the outer kinetochore, but it does not reduce centromeric localization of CENPs-A and -C, suggesting that KNL1 functions downstream of the CCAN (Cheeseman et al., 2008). The localization of protein phosphatase 1 (PP1) is dependent on KNL1 and binding sites for the SAC proteins Bub1 and BubR1 have been mapped to the N-terminus of KNL1. Mutations to the motifs that mediate recruitment of these proteins by KNL1 disrupted kinetochore-microtubule attachment in cells, further suggesting that the KNL1 depletion phenotype may be an indirect effect due to lack of recruitment of proteins that are required for kinetochore-microtubule attachment, rather than a direct affect of KNL1 being a microtubule binding component at the outer

kinetochore (Liu et al., 2010; Kiyomitsu et al., 2011). Taken together these data suggest that the role of KNL1 at the kinetochore may be that of a structural scaffold protein that acts as a hub to efficiently recruit proteins that are required for direct microtubule binding as well as proteins that serve as regulators of kinetochore-microtubule attachment. With this idea in mind, the limited microtubule binding capacity of KNL1 may allow it to act as a sensor of microtubule attachment to facilitate a role in the SAC.

***MIS12*** **–** The MIS12 complex has been shown to have a structural role for kinetochore integrity. The MIS12 complex has a relative position at the kinetochore that is coincident with CENP-A, inward from both the KNL1 and the NDC80 complexes and does not have any microtubule binding affinity (Goshima et al., 2003; Obuse et al., 2004; Cheeseman et al., 2006; Kline et al., 2006; Wan et al., 2009). Depletion of MIS12 complex proteins results in a reduction of some CCAN members at the inner kinetochore. It has also been clearly demonstrated that the MIS12 complex is required for recruitment of the KNL1 and NDC80 complexes to the kinetochore in cells, consistent with direct binding between the MIS12 complex and the Spc24/Spc25 subunit of the NDC80 complex shown in vitro (Goshima et al., 2003; Cheeseman et al., 2006; Kline et al., 2006; Cheeseman et al., 2008; Petrovic et al., 2010). Cells depleted of MIS12 complex components have defects in chromosome alignment and segregation, likely due to a lack of the NDC80 complex at the outer kinetochore (Kline et al., 2006). Biochemically, MIS12 interacts with KNL1 and together these complexes can then facilitate binding to the NDC80 complex. Additionally, MIS12 has been

shown to directly bind CENP-C, further supporting the idea that MIS12 is a scaffolding protein and functions as part of the direct link between the inner and outer kinetochore (Przewloka et al., 2011; Screpanti et al., 2011). Taken together these data suggest that MIS12 acts as an anchor to correctly position the core microtubule binding proteins at the outer kinetochore and functions coordinately with KNL1 to form a receptor for the NDC80 complex (Cheeseman et al., 2006).

***NDC80*** **–** Perhaps the most well studied member of the KMN network is the heterotetrameric NDC80 complex, comprised of Ndc80/Hec1, Nuf2, Spc24, and Spc25 (Figure 1.6A). Data from in vivo and in vitro studies led to the idea that the NDC80 complex is the principal microtubule binding component of the KMN network. In vitro, the NDC80 complex has been shown to bind microtubules (Cheeseman et al., 2006; Wei et al., 2007; Powers et al., 2009) and in vivo studies in which components of the NDC80 complex have been depleted or mutated result in cells that are unable to mediate stable kinetochore-microtubule attachments (DeLuca et al., 2002; Martin-Lluesma et al., 2002; DeLuca et al., 2005; Guimaraes et al., 2008; Miller et al., 2008; Sundin et al., 2011; Tooley et al., 2011). The physical properties of the NDC80 complex support the idea that it is the direct link between microtubules and kinetochores. At ~60nm in length, it is long enough to span the distance between the inner kinetochore and outer kinetochore. The NDC80 complex is positioned such that the C-terminal globular domains of Spc24 and Spc25 can effectively anchor the complex to the kinetochore while the N-terminal portion of the Hec1/Nuf2 dimer is

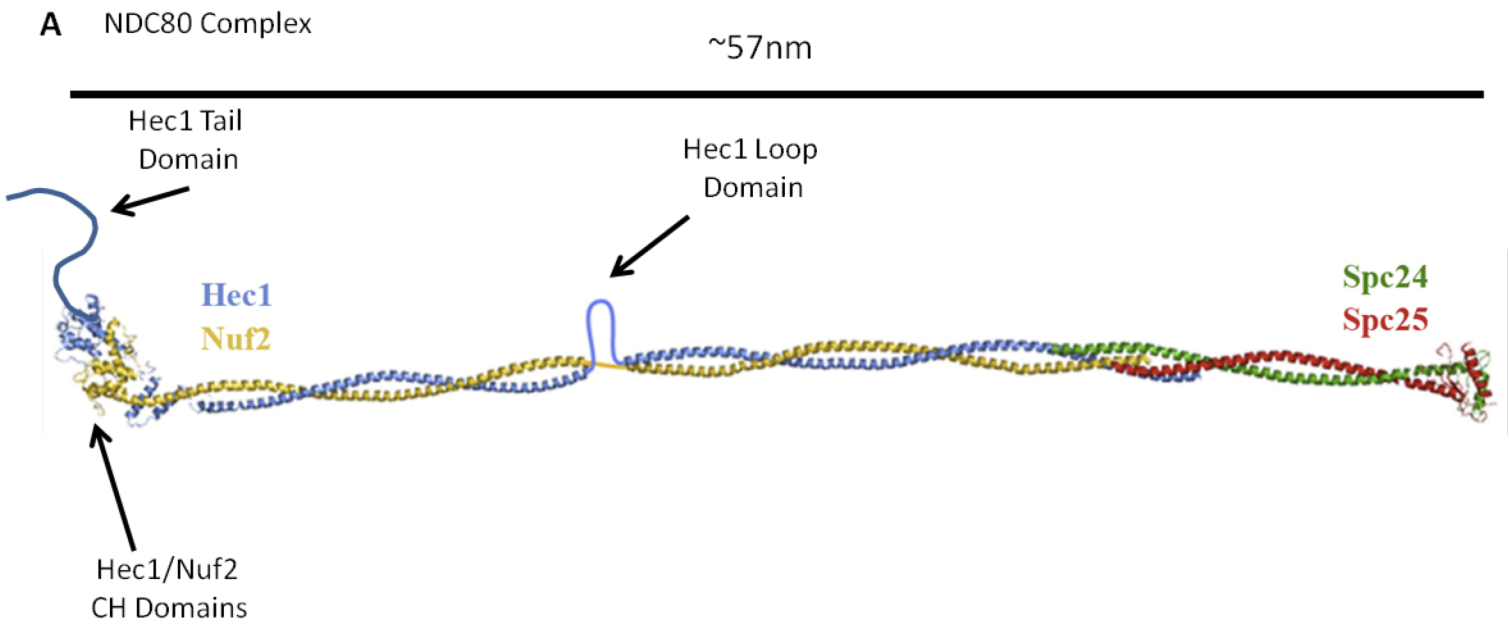
A
NDC80 Complex
~57nm
Hec1 Tail Domain
Hec1 Loop Domain
Hec1
Nuf2
Spc24
Spc25
Hec1/Nuf2 CH Domains

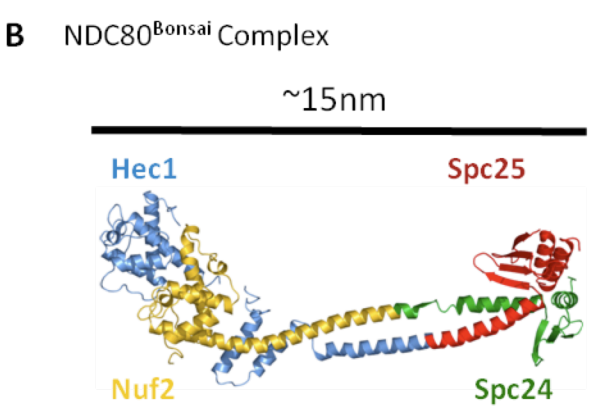
B
NDC80Bonsai Complex
~15nm
Hec1
Spc25
Nuf2
Spc24

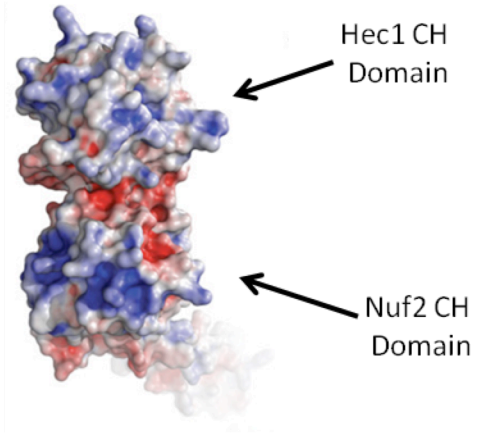
C
Hec1 CH Domain
Nuf2 CH Domain

**Figure 1.6. Structural features of the NDC80 complex. A)** A representation of the NDC80 complex showing the overall rod-like shape of the complex. The C-terminal globular domains of Spc24/Spc25 lie proximal to the chromosome and anchor the complex at the kinetochore. The N-terminal CH domains of Hec1/Nuf2 are poised at the outer kinetochore for interactions with microtubules. Extending off of the CH domain of Hec1 is an 80 amino acid "tail" domain. There are no structural data for this domain as it is predicted to be unstructured. Approximately 16nm from the Hec1 CH domain is a region of the coiled-coil that is unpaired with Nuf2. This region spans 40 amino acids in humans and is referred to as the "loop" domain. **B)** X-ray crystal tructure of the $NDC80^{Bonsai}$ complex, a truncated version of the NDC80 complex made from two chimeric proteins. The Hec1 tail domain is not present in this structure and the Hec1 loop domain has been truncated (Modified from Ciferri et al., 2008). **C)** Surface model of the Hec1/Nuf2 CH domains from $NDC80^{Bonsai}$ complex showing the electrostatic potential of the putative microtubule binding surface. Within each of the two CH domains there is a prominent positively charged ridge that has been proposed to make direct interactions with the negatively charged C-terminal tubulin tails (Modified from Ciferri et al., 2008).

poised for direct interactions with microtubules (Wei et al., 2005; DeLuca et al., 2005; Cheeseman et al., 2006). Additionally, biochemical analyses of the NDC80 complex have revealed that it can diffuse along microtubules, track with depolymerizing microtubule ends, and attaches to microtubules stably enough to pull a cargo in vitro (McIntosh, et al., 2008; Powers et al., 2009).

Structural studies have shown that the NDC80 complex has a pair of CH (calponin homology) domains at the N-terminus that reside within the globular domains of Hec1 and Nuf2, which are poised for interactions with microtubules. Originally identified as actin binding motifs, CH domains have more recently been implicated in microtubule binding (Slep and Vale 2007). It has been proposed that the tandem CH domains of the Hec1/Nuf2 dimer interfaced the microtubule lattice as has been seen in the microtubule plus-end binding protein EB1 (end-binding protein 1). X-ray crystal structure data from a truncated form of the NDC80 complex ($NDC80^{Bonsai}$) revealed that the CH domains of Hec1 and Nuf2 each have a positively-charged ridge that could potentially mediate electrostatic interactions with the negatively charged tubulin tails (Ciferri et al., 2008) (Figure 1.6, B and C). This model is supported by in vitro studies showing that charge reversal mutations within the positively charged ridge in either Hec1 or Nuf2 significantly reduce the microtubule binding affinity of the NDC80 complex (Ciferri et al., 2008).

Within the Hec1 protein there is a portion of the coiled doimain that is unpaired with Nuf2 and forms what has been named the ‘loop’ domain (Maiolica et al., 2007) (Figure1.6A). The loop is conserved from yeast to humans and in

humans the loop domain is approximately 40 amino acids and is predicted to be a β-sheet perhaps involved protein-protein interactions (Hsu et al., 2011; Maure et al., 2011). In both budding and fission yeasts, cells expressing Hec1 mutants in which the sequence of the loop domain has been deleted or mutated are unable to make stable kinetochore-microtubule attachments (Hsu et al., 2011; Maure et al., 2011). The mechanism differs between budding and fission yeast as the loop domain is required for recruitment of the Dam1 complex in budding yeast and the microtubule stabilizing protein Dis1/TOG in fission yeast (Hsu et al., 2011; Maure et al., 2011). These data suggest that the loop domain of Hec1 functions to recruit accessory proteins to the kinetochore and that the conserved loop motif may have a role in kinetochore-microtubule attachment in vertebrate cells, as well.

Extending from the N-terminus of Hec1 is an 80 amino acid “tail” domain that is highly positively charged, predicted to be unstructured, and is required for microtubule binding in vivo and in vitro (Ciferri et al., 2008; Guimaraes et al., 2008; Miller et al., 2008) (Figure 1.6A). It has been proposed that kinetochore-microtubule binding may be mediated by electrostatic interactions between the negatively charged C-terminal tubulin tails, or ‘E-hooks’, and the positively charged Hec1 tail (DeLuca et al., 2006). In support of this, in vitro microtubule binding assays using a purified “tail-less” Hec1 protein or microtubules treated with subtilisin, a protease that selectively cleaves the E-hooks from tubulin subunits, show a 100-fold reduction in microtubule binding affinity (Ciferri et al., 2008). In addition to potentially mediating direct contacts with microtubules,

another role for the Hec1 tail is the regulation of the kinetochore-microtubule attachments by phosphorylation of this domain by the mitotic kinase Aurora B (discussed in detail below) (Cheeseman et al., 2006; DeLuca et al., 2006; Ciferri et al., 2008; DeLuca et al., 2011).

Taken together, the data point to an organization of the KMN network that uses MIS12 as an anchor and direct link to the inner kinetochore. KNL1 is likely part of the physical scaffold of the outer kinetochore and acts as a center for protein recruitment to facilitate kinetochore-microtubule attachment, regulation of attachments, and anaphase entry. Together the KNL1 and the MIS12 complexes serve as a receptor for the NDC80 complex, which has multiple domains required for kinetochore-microtubule attachment and functions in both initiating and regulating microtubule binding.

### 1.5 Dam1/DASH

Many protein components of the kinetochore are conserved from yeast to humans. A notable exception is the 10-member Dam1/DASH complex, which is proposed to form rings around microtubules to couple microtubule depolymerization to chromosome movements. In budding yeast the 10 subunit Dam1/DASH complex has been identified as an important component of the mitotic spindle that is also required for accurate chromosome segregation (Hoffman et al., 1998; Jones et al., 1999; Cheeseman et al., 2001a; Cheeseman et al., 2001b; Janke et al., 2002; Enquist-Newman et al., 2001; De Wulf et al., 2003; Li et al., 2002). Biochemical analysis of the Dam1 complex revealed that it

can oligomerize into a ring shape around a microtubule and can move laterally on microtubules, track processively with depolymerizing microtubule ends, and attach strongly enough to microtubules to pull cargo in vitro (Miranda et al., 2005; Westermann et al., 2005; Westermann et al., 2006; Grishchuk et al., 2008). These data suggest an attractive mechanism of coupling dynamic microtubule plus ends to kinetochores. However, the presence of rings has yet to be shown in vivo (McIntosh 2005; Dong et al., 2007; McIntosh et al., 2008). Additionally, oligomers of the Dam1 complex that are not formed into rings are able to processively track microtubule tips suggesting that although ring formation is possible, it may not be the functional configuration the Dam1 complex in cells (Asbury et al., 2006; Franck et al., 2007; Gestaut et al., 2008). The discovery of Dam1 in yeast spurred a search for its homolog in mammalian cells. To date, a clear counterpart for the Dam1 complex has not been identified in vertebrates and it is possible that Dam1 is not required in cells that have kinetochores that bind multiple microtubules (Burrack et al., 2011; Thakur and Sanyal, 2011).

### 1.6 Other contributing factors

***Ska*** **–** The Ska complex (spindle and kinetochore associated complex) has been recently implicated in kinetochore-microtubule attachment. It is made of 3 proteins, Ska1, Ska2, and Ska3/Rama1 and has been shown to bind microtubules in vitro and track with depolymerizing microtubule tips (Hanisch et al., 2006; Daum et al., 2009; Welburn et al., 2009). In human cells, however, the depletion phenotype of this complex is ambiguous, and there is no cohesive

model on how the Ska complex functions in kinetochore-microtubule attachment. It has been proposed to play a direct role in microtubule binding at the outer kinetochore, relay microtubule attachment status to the SAC, and act as an oligomerization or processivity factor for other microtubule binding proteins (Hanisch et al., 2006; Daum et al., 2009; Welburn et al., 2009). It has also been suggested that the Ska complex binds to members of the KMN network to stabilize kinetochore-microtubule attachments. Interactions between the KMN network and the Ska complex are suggested to be antagonized by phosphorylation of Ska complex components by Aurora B kinase (Chan et al., 2012). Interestingly, the Ska complex is not found in fungi and it has been proposed that it may be the functional homolog of the Dam1 complex found in yeast (Welburn et al., 2009). Until all of the functions of the Ska complex are understood and characterized, however, it will be difficult to confidently make this assessment.

***MAPS*** **–** Microtubule dynamics are important for accurate chromosome segregation. Disruption of microtubule dynamics by addition of microtubule poisons, for example, leads to chromosome alignment and segregation defects (Jordan et al., 1992). A specialized class of MAPs (microtubule-associated proteins) called microtubule plus-end tracking proteins (+TIPs) is made of proteins that specifically accrue at microtubule plus-ends. These proteins are conserved in all eukaryotes and function to regulate microtubule dynamics (Akhmanova and Steinmetz, 2008). There are at least 15 families of +TIP proteins, classified by shared structural motifs. Nearly all microtubule +TIPs

influence microtubule dynamics, and together this network of proteins aids in the process of kinetochore-microtubule attachment. Some +TIPs directly affect microtubule dynamics, serving as microtubule polymerases or depolymerases. Others are required for the delivery or recruitment of additional +TIPs to the microtubule plus-end or are microtubule motor proteins. Importantly, a direct role for +TIPs in chromosome alignment has been demonstrated (Manning et al., 2010; Dujardin et al., 1998; Coquelle et al., 2002; Maiato et al., 2003). Disruption of microtubule dynamics ultimately results in a failure of cells to progress through mitosis accurately and has also been implicated in promoting CIN (chromosomal instability), both of which lead to disease states such as cancer (Bakhoum and Compton 2011).

### 1.7 Models for force generation at the microtubule attachment site

It is well known that microtubule polymerization and depolymerization are required for chromosome movements in mitosis (Inoue and Salmon, 1995; Maiato et al., 2004). Additionally, multiple in vitro studies have shown that the energy released by a depolymerizing microtubule is enough to move a cargo, and specifically, chromosomes (Koshland et al, 1988; Coue et al., 1991; Lombillo et al., 1995). How the kinetochore couples the force of depolymerizing microtubules with force generation, however, remains to be determined.

One model suggests that the coupling occurs through multiple weak binding sites on the microtubule lattice. This ‘sleeve’ model of force generation at the microtubule attachment site predicts that the microtubule binding

components at the outer kinetochore would have to be arranged in sleeves or channels in which microtubules could be inserted (Hill, 1985). In support of this, it has been shown that the NDC80 complex has a microtubule binding affinity in the low micromolar range, which would likely result in weak interactions with microtubules in cells (Cheeseman et al., 2008; Ciferri et al., 2008). Additionally, quantitative fluorescence microscopy studies suggest that there may be up to 22 NDC80 complexes per microtubule in human cells which could in turn form an array of binding sites for microtubules (Wan et al., 2009; Johnston et al., 2010). However, structural data do not support the idea of isolated sleeve-like microtubule binding sites (Dong et al., 2007).

An alternative to the sleeve model is one in which a ring-shaped coupler that encircles microtubules facilitates chromosome movements (Margolis and Wilson 1981). The discovery that the Dam1 complex can form rings around the outer circumference of microtubules and can bind strongly enough to be processive while carrying a cargo suggested that these rings could be pushed along the microtubule lattice by depolymerizing microtubule protofilaments to generate chromosome movements (Grishchuck et al., 2008). However, there is a lack of supporting evidence for this model as rings have not been observed at kinetochores in cells and non-ring oligomers of the Dam1 complex largely share the same microtubule binding properties as the ring conformation (Dong et al., 2007; McIntosh 2005; Asbury et al., 2006; McIntosh et al., 2008; Franck et al., 2007).

It has been proposed that thin fibrils may connect kinetochores to microtubules. These fibrils were observed in electron tomograms of mammalian cells extending outward ~60nm from the kinetochore to the flared plus ends of microtubules. The curvature of microtubule plus ends that were connected to fibrils was reduced as compared to microtubules that lacked fibrils, suggesting that the fibrils imposed a force against the depolymerizing microtubule protofilaments, thus changing their shape. These data led to the idea that kinetochore fibrils may be the couplers that harness the force produced by microtubule depolymerization to move chromosomes (McIntosh et al., 2008). Although other groups have identified a fibrous architechture to the outer kinetochore, the presence of distinct fibrils binding to microtubules has not been reported (Dong et al., 2007). Perhaps the most difficult part of this model to reconcile is that kinetochore fibrils were observed to bind to the luminal surface of microtubules. It was proposed that the fibrils may represent the NDC80 complex, however the NDC80 complex has been shown to bind the outer microtubule lattice (Wilson-Kubalek et al., 2008; Alushin et al., 2010). Additionally, the N-terminal portion of the NDC80 complex, known to mediate microtubule binding, has been mapped about 60nm exterior of the plus-ends of microtubule at metaphase, suggesting that the NDC80 complex binds the sides of the microtubule and not the tips, which is consistent with in vitro data (Cheeseman et al., 2006; Wilson-Kubalek et al., 2008; Wan et al., 2009; Alushin et al., 2010).

More recently, observations from electron tomography studies led to a model based on a fibrous network of proteins at the outer kinetochore. The model suggests that the outer kinetochore functions like a spider-web with the ability to bind microtubules approaching the kinetochore from a variety of angles with both end-on and lateral attachments. Furthermore, the meshwork of proteins were shown to be largely disorganized, regardless of microtubule attachment state, suggesting a lack of pre-defined microtubule binding sites as suggested by the 'sleeve' model (Dong et al., 2007; McEwen and Dong 2010). Support for the fibrous network model comes from structural data highlighting the rod-like shape of many outer kinetochore proteins as well as observations of a mesh-like structure at kinetochores in mammalian cells by EM (McEwen et al., 1998; Wei et al., 2005; Ciferri et al., 2005; DeLuca et al., 2005; Cheeseman et al., 2006). The fibrous network hypothesis does integrate two of the previous models by suggesting that the kinetochore is made of fibril-like proteins and that these fibrils can form an array of weak microtubule binding sites. It does not implicate kinetochore fibrils in direct microtubule binding, instead suggesting that they serve as connections between the inner and outer kinetochore (McEwen and Dong, 2010).

### 1.8 Regulating kinetochore-microtubule attachment strength

In addition to generating attachments to microtubules, the kinetochore must also serve as a regulator of the strength of these attachments. Early in mitosis chromosomes may be positioned near one of the spindle poles, where a

dense population of microtubules is anchored. Sister kinetochores may initially capture microtubules emanating from a single spindle pole (syntelic attachment) or one sister kinetochore may bind microtubules from both spindle poles (merotelic attachment). Although these erroneous binding events are common early in mitosis, their correction to a bi-oriented state (amphitelic attachment) in which sister kinetochore pairs bind microtubules from opposing spindle poles is critical for appropriate chromosome segregation (Figure 1.7). Furthermore, as chromosomes become bi-oriented, coordinated movements driven by microtubule polymerization and depolymerization cause kinetochores to oscillate at the spindle equator. Thus, the kinetochore must carry out multiple functions in the process of attaching to kinetochores and congressing chromosomes to the spindle equator for accurate segregation. The strength of kinetochore-microtubule attachments must be regulated and modified to facilitate these functions of the kinetochore. The mechanism of regulation of kinetochore-microtubule attachment strength has been clearly shown to be through phosphorylation of outer kinetochore components by the mitotic kinase Aurora B (ABK) (Cheeseman et al., 2006; DeLuca et al., 2006; Ciferri et al., 2008; Guimaraes et al., 2008; Miller et al., 2008; Welburn et al., 2010; DeLuca et al., 2011). Aurora B has several mitotic substrates including histone H3, CENP-A, MCAK (mitotic centromere-associated kinesin), and components of the KMN network (Cheeseman et al., 2006; DeLuca et al., 2006; Wang et al., 2010; Welburn et al., 2010; DeLuca et al., 2011). ABK has been implicated in a number of mitotic processes including microtubule dynamics, chromosome

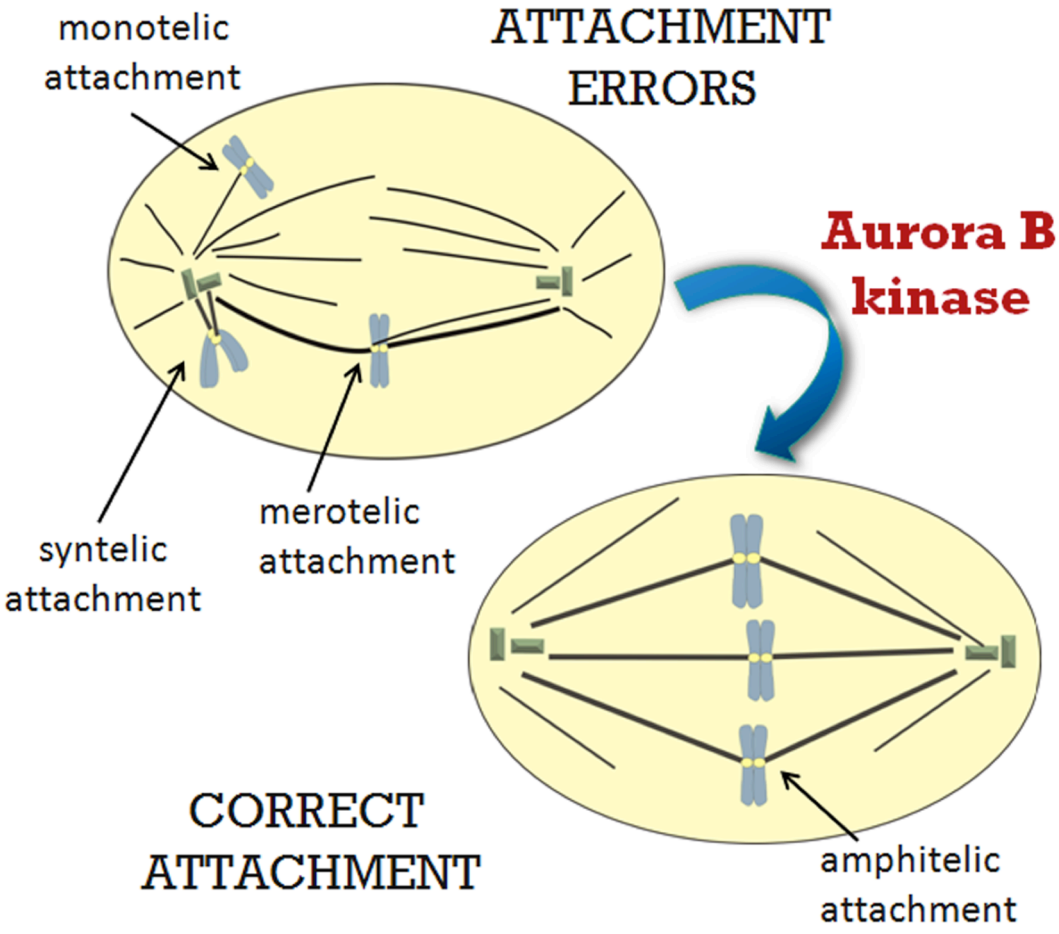


**Figure 1.7. Correction of erroneous kinetochore-microtubule attachments by Aurora B kinase.** Early in mitosis as the nuclear envelope breaks down some chromosomes can be positioned near a dense population of microtubules at a spindle pole. This can lead to both sister kinetochores on a chromosome capturing microtubules originating from only one spindle pole (syntelic attachment). Alternatively, chromosomes may have kinetochore attachments from only one spindle pole (monotelic attachment). Finally, one sister kinetochore may bind to microtubules from one spindle pole while the other sister binds microtubules from both spindle poles (merotelic attachment). Phosphorylation of outer kinetochore components by Aurora B kinase has been shown to increase microtubule turnover at the kinetochore and promote microtubule release, allowing the kinetochore to 'reset' and attempt to make correct attachments to microtubules, with each sister kinetochore binding microtubules from opposing spindle poles, leading to chromosome bi-orientation (amphitelic attachment).

alignment, and microtubule binding at the kinetochore, and is thus considered the 'master regulator' of kinetochore-microtubule attachment (Hauf et al., 2003; Cimini et al., 2006; Carmena and Earnshaw, 2003). Here the focus will be on how ABK acts to regulate the strength of kinetochore-microtubule attachments through phosphorylation of members of the KMN network.

The 80 amino acid tail domain of Hec1 is highly positively charged and has 9 putative ABK phosphorylation sites throughout its length. This domain has been shown to be phosphorylated by ABK in vitro and in vivo (Cheeseman et al., 2006; DeLuca et al., 2006; DeLuca et al., 2011). There are two models of how phosphorylation of the Hec1 tail regulates microtubule attachment strength (Figure 1.8). First, it is thought that the mechanism for regulating kinetochore-microtubule attachments is through disruption of direct electrostatic interactions between the positively charged Hec1 tail and the negatively charged tubulin E-hooks. In support of this, phosphorylation decreases the microtubule binding affinity of Hec1 in vitro and mammalian cells expressing Hec1 proteins with phospho-mimetic mutations (Ser/Thr → Asp) in the tail domain cannot generate stable kinetochore-microtubule attachments and fail to accurately segregate chromosomes (Ciferri et al., 2008; Guimaraes et al., 2008). Conversely, phospho-deficient mutants of Hec1 (Ser/Thr → Ala) support kinetochore-microtubule binding, but the interactions with microtubules appear hyper-stable and cells expressing these mutants do not properly align chromosomes and enter anaphase with unaligned chromosomes (DeLuca et al., 2006; DeLuca et al., 2011; Sundin et al., 2011). Another model suggests that the Hec1 tail

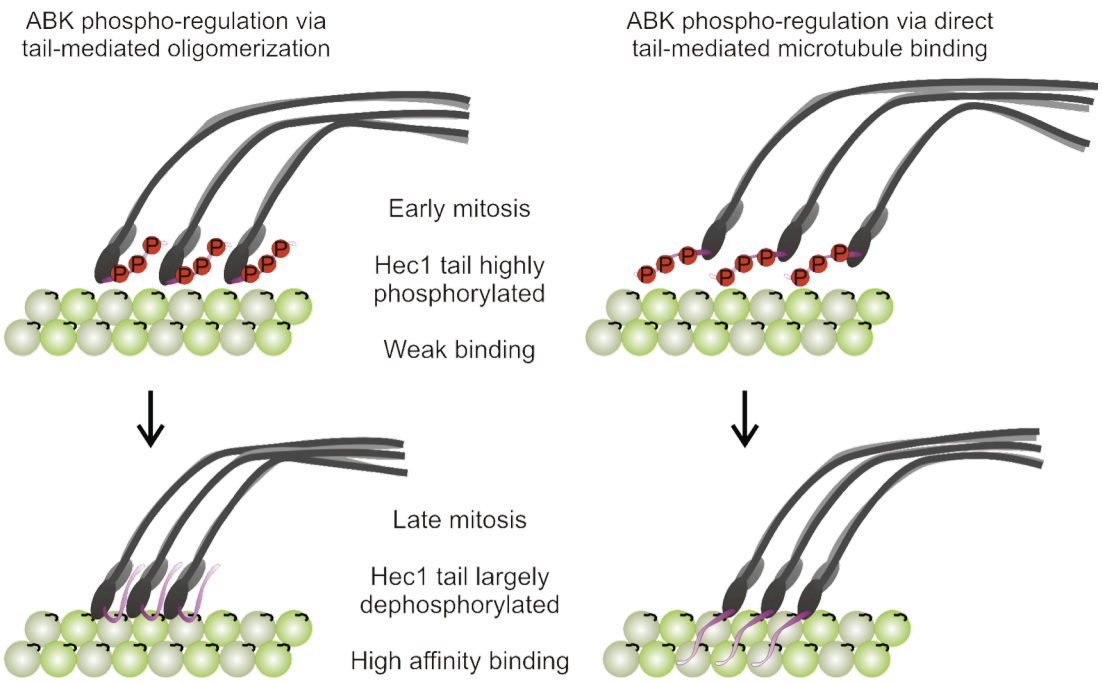


**Figure 1.8. Models of phospho-regulation of kinetochore-microtubule attachment by Aurora B kinase.** On the left is a model suggesting that high affinity binding of NDC80 complexes to microtubules is regulated by the oligomerization state of adjacent NDC80 complexes, which is regulated by Hec1 tail phosphorylation. On the right is a model suggesting that high-affinity binding of NDC80 complexes to microtubules is regulated by direct interactions of the Hec1 tail with tubulin E-hooks, which is regulated by tail phosphorylation (Hec1, dark gray; Nuf2, light gray; Hec1 tail, magenta) (Adapted from Sundin and DeLuca, 2010).

functions as an oligomerization factor for adjacent NDC80 complexes on the microtubule lattice. When the tail is highly phosphorylated, it has been suggested to reside between the N-terminal CH domains of neighboring NDC80 complexes, preventing oligomerization and tight binding to microtubules. As the tail becomes largely dephosphorylated, oligomerization of NDC80 complexes would then mediate stable binding to microtubules (Alushin et al., 2010). The data to support this model come from the cooperative nature of NDC80 complex-microtubule binding as well as electron micrographs of NDC80 complexes bound to microtubules in vitro showing a lack of clustering of NDC80 complexes when phospho-mimetic substitutions are introduced. These models of ABK-mediated phospho-regulation are not mutually exclusive as the tail domain is long enough to potentially make direct contacts to the microtubule lattice and also extend through the region between adjacent NDC80 complexes (Cheeseman et al., 2006; Alushin et al., 2010).

Although phosphorylation of Hec1 significantly reduces its microtubule binding affinity in vitro, it does not completely preclude binding of a reconstituted KMN network (Welburn et al., 2010). Additionally, it has been shown that the KNL1 and MIS12 complexes act in a synergistic manner with the NDC80 complex to facilitate microtubule binding, suggesting that other members of the KMN network may also contribute to ABK-mediated phospho-regulation of kinetochore-microtubule attachment (Cheeseman et al., 2006). Indeed, it has been demonstrated that ABK also phosphorylates the microtubule-binding domain of the KNL1 protein and the Dsn1 subunit of the MIS12 complex. Cells

expressing either KNL1 or Dsn1 phospho-mimetic mutants exhibited chromosome alignment defects, but the phenotypes were much less severe than cells expressing a phospho-mimetic Hec1 protein. Additionally, it was demonstrated phospho-mimetic substitutions to Hec1 reduced the binding affinity of the KMN network by 50% and that phospho-mimetic substitutions to all 3 subcomplexes of the KMN network abolished microtubule binding in vitro (Welburn et al., 2010). The mechanism of how KNL1 and Dsn1 contribute to kinetochore-microtubule attachment regulation, however, has not yet been resolved. Particularly surprising is the contribution of phosphorylated Dsn1 to the destabilization of microtubule attachments, as it has been shown that the MIS12 complex has no affinity for microtubules in vitro (Cheeseman et al., 2006). When different members of the KMN network are phosphorylated, the microtubule binding affinity of the entire supercomplex varies. It has been suggested that phosphorylation of KNL1 and Dsn1 serve to 'prime' the KMN network such that phosphorylation of the NDC80 complex would then result in a significant decrease in kinetochore-microtubule attachment stability (Welburn et al., 2010). It has also been shown that KNL1 recruits PP1 to kinetochores in an ABK-dependent manner. PP1 has been demonstrated to oppose ABK and act to stabilize kinetochore-microtubule attachments (Liu et al., 2010). These data suggest that although phosphorylation of Hec1 by ABK can modify the strength of kinetochore-microtubule interactions, phosphorylation of other components may be required to fully regulate kinetochore-microtubule attachment in cells.

## 1.9 Summary and conclusions

Progression through mitosis and accurate chromosome segregation are remarkable feats accomplished by cells. Kinetochores must capture and remain attached to microtubule plus ends that continue to polymerize and depolymerize at the attachment site. In addition, the strength of these attachments must be tightly regulated to ensure proper chromosome congression and segregation. The presence or absence of microtubules must also be monitored at each kinetochore for precise timing of anaphase entry. All of these processes culminate in chromosome congression at the spindle equator, and ultimately lead to accurate chromosome segregation into two new daughter cells.

Data and insight gathered from numerous studies of kinetochore structure and assembly have shown that there are distinct structural regions of the kinetochore that are recruited and assembled in a hierarchical manner. However, the data are leading to an emerging picture of the kinetochore that looks more like a network of proteins that interact fluidly from the inner kinetochore to the outer kinetochore rather than proteins that only function in sharply delineated regions.

Evidence is very strong showing that the core microtubule binding sites reside at the outer kinetochore and are formed by the KMN network. Although some microtubule binding affinity can be attributed to the KNL1 portion, it is very likely that the NDC80 complex represents the point of contact for direct microtubule binding. Additionally, regulation of kinetochore-microtubule

attachment strength occurs via the KMN network and most notably through the tail domain of the Hec1 protein of the NDC80 complex.

Although the NDC80 complex can be credited for microtubule binding and attachment regulation, how this complex contributes to these processes is not known. In particular, the NDC80 complex has distinct protein domains that have been implicated in these processes, though the molecular details are not clear in vertebrate cells. Here we set out to characterize the distinct domains of the NDC80 complex and determine how each contributes to kinetochore-microtubule attachment and regulation of these attachments. Using an siRNA (small interfering RNA)-mediated silence and rescue system in mammalian cells we are able to show in Chapter III that the CH domains of the NDC80 complex proteins Hec1 and Nuf2 have distinct functions in kinetochore-microtubule attachment in that the Hec1 CH domain likely makes direct contacts with the microtubule lattice while the Nuf2 CH domain does not. In Chapter IV we characterize the loop domain of Hec1 and its contributions to microtubule binding and show that although it does not likely make direct contacts with the microtubule lattice it is absolutely required for attaining stable kinetochore-microtubule attachments to support chromosome alignment, SAC silencing, and mitotic progression. In Chapter V we use in vivo, in vitro, and in silico methods to characterize the Hec1 tail domain with specific focus on how incremental phosphorylation of this domain by ABK facilitates varied functions of the kinetochore through mitosis. Taken together our data highlight the diverse functions of a single component of the

kinetochore and the importance of the NDC80 complex in the process of kinetochore-microtubule attachment.

# CHAPTER II

## Materials and methods

### 2.1 Cell culture

#### 2.1.1 HeLa cells

Cells were cultured in Dulbecco's modified Eagle's medium (DMEM) (Invitrogen) supplemented with 10% fetal bovine serum (FBS) (Atlanta Biologics) and 1% antibiotic/antimycotic solution at 37°C in 5% $CO_2$. Cells were cultured at 50% confluency 24 hours prior to transfection on acid-washed glass coverslips for immunofluorescence or on glass-bottomed dishes for live cell imaging (MatTek).

#### 2.1.2 PtK1 cells

Cells were cultured as outlined above except using F-12 medium (Invitrogen) supplemented with 10% FBS (Atlanta Biologics) and 1% antibiotic/antimycotic solution at 37°C in 5% $CO_2$.

### 2.2 siRNA and transfection

#### 2.2.1 HeLa cells

Small, interfering RNAs (siRNAs) against human Nuf2 (DeLuca et al. 2002) and human Hec1 (5' – AACCCTGGGTCGTGTCAGGAA – 3') were

purchased from Qiagen. Both siRNAs were tagged with a 3' Cy5 label. For siRNA transfection, 6 µl Oligofectamine (Invitrogen) was added to 48 µl OptiMem (Invitrogen) and the tube was flicked regularly for 5 minutes. To this, 8 µl of 20 µM siRNA and 200 µl of OptiMem were added and incubated for 30 minutes with periodic flicking of the tube. After incubation, the siRNA solution was added to 1ml OptiMem + 10% FBS and added to cells on coverslips in 6-well dishes or in glass bottom dishes. 24 hours post-transfection 1ml OptiMem + 10% FBS was added to the cells; cells were assayed at 48 hours post-transfection. For silence and rescue experiments, cells were transfected using FuGene6 (Roche) 24 hours after transfection using siRNA. For these experiments, 4 µl FuGene6 and 96 µl OptiMem were incubated for 5 minutes with regular flicking of the tube and 1 µg plasmid DNA was added and incubated for 30 minutes with periodic flicking of the tube. The DNA solution was added to 1ml OptiMem + 10% FBS and added to cells that had been previously transfected with siRNA. Cells were assayed 24 hours following DNA transfection.

### 2.2.2 PtK1 cells

An siRNA directed to PtK1 Hec1 (Guimaraes et al., 2008) was purchased from Qiagen. For all experiments 8 µl of 20uM siRNA were used. All transfection in PtK1 cells was carried out via electroporation as described below.

## 2.3 Electroporation

### 2.3.1 HeLa cells

For live cell imaging experiments, a combination of lipid-based transfection and electroporation using an Amaxa Nucleofector II apparatus (Lonza, Germany) was used. Cells were seeded in T25 flasks and grown to 50% confluency. Cells were transfected with Nuf2 or Hec1 siRNA using Oligofectamine (as described above). Eight hr post-transfection, cells were trypsinized and counted using a hemocytometer to ensure that $10^6$ cells were used for each reaction. Cells were harvested and pelleted by centrifugation. The cell pellet was resuspended in 100 µl of Solution L (Lonza) per $10^6$ cells. DNA constructs to be transfected were aliquotted at appropriate volumes to yield 8 µg per transfection into Eppendorf tubes. To each tube, 100 µl of cell suspension was added; the mixture was then added to an electroporation cuvette (Lonza). Cells were electroporated using program number V-001 and plated onto acid washed coverslips or into glass bottomed dishes in OptiMem + 10% FBS. Cells were analyzed 24 h post-electroporation.

### 2.3.2 PtK1 cells

All transfection with PtK1 cells was carried out using electroporation by the Amaxa Nucleofector II apparatus (Lonza, Germany). Cells were trypsinized and counted using a hemocytometer to ensure that $10^6$ cells were used for each reaction. Cells were harvested and pelleted by centrifugation. The cell pellet was

resuspended in 100μl of Solution R (Lonza) per $10^6$ cells. 8 μl of 20 μM siRNA and 4 μg of DNA constructs to be transfected were aliquotted into Eppendorf tubes. To each tube, 100 μl of cell suspension was added; the mixture was then added to an electroporation cuvette (Lonza). Cells were electroporated using program number T-020 and plated onto acid washed coverslips or into glass bottomed dishes in OptiMem + 10% FBS. Cells were analyzed 48 h post-electroporation.

### 2.4 Immunofluorescence and image acquisition

#### 2.4.1 HeLa cells

Cells were initially fixed for 10 seconds in 4% paraformaldehyde (pre-heated to 37°C) followed by a 5 minute permeabilization in fresh PHEM buffer (60 mM PIPES, 25 mM HEPES, 10 mM EGTA, 2 mM MgCl2, pH 7.0) + 0.5% Triton-X 100 at 37°C. Cells were then fixed for 20 minutes at room temperature in 4% paraformaldehyde (solution pre-heated to 37°C) in PHEM buffer and rinsed in PHEM + 0.1% Triton-X 100 for 15 minutes. To block non-specific antibody binding, 10% boiled donkey serum (BDS) was added to the cells and left to incubate for 60 minutes at room temperature. For cold-induced depolymerization assays, cells on coverslips were incubated in ice-cold DMEM + 10% FBS for 15 minutes on ice then prepared for immunofluorescence as described. Antibodies were prepared in 5% BDS and used at the following concentrations: Hec1 (9G3) at 1:1000 (GeneTex), ACA (anti-centromere antibody) at 1:300 (Antibodies, Inc.), α-tubulin at 1:200 (Sigma), α-Ska1 at 1:3000, α-Rama1 at 1:3000, α-KNL1 at

1:500 (Ska1, Rama1, and KNL1 antibodies were generous gifts from Dr. Iain Cheeseman), α-CLASP1 at 1:1000 (a generous gift from Dr. Helder Maiato), α-ZW10 at 1:500 (Abcam), and α-CENP-E at 1:500 (Abcam). Secondary antibodies conjugated to Cy5, Alexa488, or Rhodamine RedX (Jackson ImmunoResearch) were used at a dilution of 1:300. Primary antibodies were incubated overnight at 4°C, then coverslips were washed for 15 minutes in PHEM + 0.1% Triton-X 100 and rinsed with PHEM. Secondary antibodies were applied for 45 minutes at room temperature. Coverslips were washed for 15 minutes in PHEM + 0.1% Triton-X 100, counterstained with DAPI and mounted in an antifade solution containing 90% glycerol and 0.5% *N*-propyl gallate. Cells were chosen for analysis if they were both Cy5 (siRNA) postive and GFP (Nuf2 or Hec1-GFP fusion protein) positive. All microscopy was performed using a DeltaVision PersonalDV Imaging System (Applied Precision) equipped with a Photometrics CoolSnap HQ2 camera (Roper Scientific) and a 60x/1.42NA Planapochromat DIC oil immersion lens (Olympus). For fixed cell immunofluorescence experiments, 40 Z-stacks at 0.2 μm intervals were acquired through each cell. For time-lapse microscopy Leibovitz's L-15 medium without phenol red supplemented with 10% FBS and 4.5g/L glucose was added to live cells cultured in glass bottomed dishes (MatTek). A Precision Control WeatherStation was used throughout time-lapse imaging to maintain stage temperature at 37°C. A single Z-plane was imaged using a 60x/1.42NA Planapochromat DIC oil immersion lens (Olympus) every 4 minutes for up to 5 hours.

### 2.4.2 PtK1 cells

For measuring tubulin fluorescence, cells were rinsed with warm PHEM buffer and permeabilized for 5 min on ice with cold PHEM + 0.5% Triton-X 100. Cells were rinsed with cold PHEM + 0.5% Triton-X 100 and fixed for 3 min at RT with ice-cold methanol + 5 mM EGTA; cells were then transferred to -20°C for 20 min. Cells were rinsed with PHEM + 0.5% Triton-X 100 and permeabilized in PHEM + 0.5% Triton-X 100 for 5 min at RT. Coverslips were rinsed with PHEM and blocked for 1 hour at RT in 10% BDS. Primary antibodies were prepared in 5% BDS; mouse $\alpha$-alpha tubulin (Sigma) 1:200 and human $\alpha$-ACA 1:300 (Antibodies, Inc.). Primary antibodies were incubated for at least 1 hour at RT then overnight at 4°C. Coverslips were then washed for 15 minutes in PHEM + 0.1% Triton-X 100 and rinsed with PHEM. Secondary antibodies were applied for 45 minutes at room temperature; secondary antibodies conjugated to Cy5, Alexa488, or Rhodamine RedX (Jackson ImmunoResearch) were used at a dilution of 1:300. Coverslips were washed for 15 minutes in PHEM + 0.1% Triton-X 100, counterstained with DAPI and mounted in an antifade solution containing 90% glycerol and 0.5% *N*-propyl gallate. Cells were chosen and imaged as described for HeLa cells in section 2.4.3. For fixed cell immunofluorescence experiments, 55 Z-stacks at 0.2 μm intervals were acquired through each cell. For time-lapse microscopy Leibovitz's L-15 medium without phenol red supplemented with 10% FBS and 4.5 g/L glucose was added to live cells cultured in glass bottomed dishes (MatTek). For time-lapse imaging monastrol washout assays, cells were treated with 10μM monastrol (Tocris

Biologicals) for 2 hours and washed into filming media containing 10 μm MG132 (Tocris Biologicals). A Precision Control WeatherStation was used throughout time-lapse imaging to maintain stage temperature at 37°C. Five Z-planes at 1.0 μm intervals were imaged using a 60x/1.42NA Planapochromat DIC oil immersion lens (Olympus) every minute for up to 2 hours.

For live-cell imaging of kinetochore oscillations, stage temperature was maintained at 37°C with a Precision Control WeatherStation. Fluorescence images of GFP-Hec1-expressing cells were acquired with a 60x/1.42NA DIC Planapochromat oil immersion lens (Olympus) every 3 sec for 10 min. At each time point, 3 Z-stacks were collected at 0.5 μm intervals. Cells that were positive for both GFP-fusion protein and Cy5-labeled siRNA were chosen for analysis. Cells were chosen for analysis based on both positive GFP-fusion protein expression and Cy5-labeled siRNA transfection. Z-stacks from each time point were combined through a maximum projection function in the SoftWorx image analysis program. All measurements were made on kinetochores located within the middle of the spindle. Kinetochore movements were tracked using Metamorph software.

### 2.4.3 TIRF microscopy imaging of NDC80$^{Bonsai}$-GFP

For fluorescence imaging, coverslips were cleaned and silanized as described in Varga et al., 2006 with minor modifications. The coverslip surface was coated with anti-tubulin antibodies (Serotec, clone TU-20), then blocked with 1% Pluronic F-127 (Sigma), and then taxol-stabilized microtubules were

introduced. Imaging buffer was Brinkley buffer 1980 (BRB80; 80 mM PIPES pH 6.8, 1 mM MgCl2, 1 mM EGTA) containing 0.5 mg/ml casein, 4 mg/ml BSA and 2 mM DTT, 0.1 mg/ml glucose oxidase, 68 µg/ml catalase, 20 mM glucose and 0.5% 2-mercaptoethanol. All observations were made at 32°C.

Observations of single NDC80$^{Bonsai}$-GFP complexes were made using a Nikon Eclipse-Ti inverted microscope equipped with CFI APO 100x Nikon-TIRF NA1.49 objective and iXon3 camera (Andor Technology). In order to enable the specialized "Fast Kinetics" acquisition mode of the Andor iXon3 camera, it was additionally equipped with OptoMask (CAIRN) to accurately shield light from falling on the region of the sensor outside of the image sub-area. Frame size was 220 x 120 pixels. A 488nm diode laser (Coherent, 100mW max) set to 20 mW was used to excite the fluorescence. Images were acquired at 100 fps (exposure time 10ms). Acquisition was 200 sec.

For microtubule-affinity experiments, NDC80$^{Bonsai}$-GFP protein solution was flowed into the chamber for 4 minutes, which was sufficient to achieve steady-state decoration of NDC80$^{Bonsai}$-GFP of microtubules. Data were acquired in the presence of flowing imaging buffer. The iXon3 camera was used with the following settings: 1 MHz, 16-bit sensor readout mode, no EM gain, conventional gain 5.0x, frame size 256 x 256 pixels, exposure time 200 ms. The Optomask was not used. Laser beam intensity was set to 10% of maximum. For each field, a 2 second stream of stacks was captured (10 frames). For each concentration of NDC80$^{Bonsai}$-GFP, 10-12 different fields with microtubules were captured. In the same way, images were acquired using a range of NDC80$^{Bonsai}$-GFP

concentrations, starting with the lowest protein concentration. The same imaging chamber was used for no longer than 1.5 hours. All measurements were carried out at 32°C.

### 2.5 Data analysis

#### 2.5.1 Fluorescence intensity measurements

Kinetochore fluorescence intensity was measured from non-deconvolved TIFF (tagged image file format) image Z-stacks. Using Metamorph software, a pseudo color heat map was digitally applied to each image. Two boxes were generated, one with dimensions of 9 x 9 pixels, the other 13 x 13 pixels. Both boxes were centered over a single kinetochore. The focal plane corresponding to the brightest kinetochore fluorescence intensity was chosen visually by using the heat map. Total integrated fluorescence counts were measured for both the 9 x 9 pixel and 13 x 13 pixel regions and transferred to Microsoft Excel. The measured fluorescence intensity for the 9 x 9 region contains both kinetochore fluorescence and background fluorescence of the immediately surrounding area. The background fluorescence was calculated by subtracting the integrated intensity of the 9 x 9 pixel region from the integrated intensity values of the corresponding 13 x 13 pixel region. The result was scaled in proportion to the area of the 9 x 9 pixel region, and then subtracted from the integrated fluorescence intensity value of the 9 x 9 pixel region. The resulting value should be the fluorescence intensity of the measured kinetochore (Hoffman et al., 2001).

Ratiometric analyses were used to quantitate the presence of Hec1 or Nuf2 after siRNA depletion, and also to determine the levels of Mad1 present at kinetochores. The method described above was used to measure the fluorescence intensity of anti-centromere antibody, which recognizes CENPs-A, -B, and -C, proteins that remain stably associated with centromeric chromatin throughout mitosis. The fluorescence intensity of kinetochores stained with antibodies directed at proteins of interest was also measured. The calculated kinetochore fluorescence intensity value from the protein of interest was divided by the calculated kinetochore fluorescence intensity value of the anti-centromere antibody. Approximately 10 kinetochores per cell were measured, and average kinetochore fluorescence intensity was calculated for each cell. Then, an average across cells was calculated for each experimental condition.

For quantification of tubulin bundle fluorescence intensity in PtK1 cells, image Z-stacks were deconvolved and converted to TIFFs. Fluorescence intensity was measured using MetaMorph software. As described in Cimini et al., 2003, a computer-generated region with dimensions of 5 x 5 pixels was centered on a microtubule fiber, at the position where the microtubule meets the kinetochore. The integrated intensity of the 5 x 5 pixel region was measured and transferred to Microsoft Excel. The 5 x 5 pixel region was then moved directly above the microtubule and the integrated intensity was measured and likewise directly below the microtubule. The measurements taken above and below the microtubule were used as background intensity measurements. The average of

the two background intensity measurements was subtracted from the average value from the measured integrated intensity of the microtubule bundle.

### 2.5.2 Quantification of spindle pole separation rates

Time-lapse images of PtK1 cells were used to determine the rate of spindle pole separation after treatment with monastrol. Using the distance measure tool in SoftWorx software, the distance between the spindle poles was measured at each time point. The first 6-10 time points were plotted as a function of time and the slope of the line was calculated using Microsoft Excel to determine the rate of spindle pole separation. The rates from 10 cells were calculated for each condition and reported as an average.

## 2.6 In vitro data analysis

### 2.6.1 Analysis of single molecules of NDC80$^{Bonsai}$-GFP

These methods, and those in sections 2.6.2, 2.6.3, 2.6.4, 2.6.5, and 2.6.6, were carried out by Anatoly Zaytsev as part of our collaboration with Ekaterina Grishchuk's laboratory at the University of Pennsylvania. To ensure that individual NDC80$^{Bonsai}$-GFP complexes were measured for single molecule experiments, we measured the integrated intensity of the NDC80$^{Bonsai}$-GFP spots in a circular area 500 nm (5 pixels) in diameter, then normalized this value to the intensity of a single GFP fluorophore, as described in Grishchuk et al., 2008. Microscope and camera settings were identical to settings used in single-molecule experiments. Additionally, a custom-written program (Mathematica;

Wolfram Research) was used, which selected the maximum integral intensity of a circular region with a diameter of 5 pixels for each time frame. The same analysis was applied to the region adjacent to selected microtubules and results were used as the background fluorescence measurement. This approach gives the estimation that more than 95% of all NCDC80$^{Bonsai}$-GFP complexes were single complexes.

### 2.6.2 Analysis of single molecule diffusion data

The positions of microtubules were determined from experimental data in ImageJ (NIH) using an average-projection. Using MetaMorph 7.7 (Molecular Devices) kymographs were made (width of selection line 6 pixels). Kymographs were analyzed in custom written software in Mathematica 8.0 (Wolfram Research). Rectangular regions were manually selected on kymographs. The size of the frame along the spatial axis was selected such that it was large enough to contain all trajectories of a single NDC80$^{Bonsai}$-GFP complex, but did not contain any trajectories of other NDC80$^{Bonsai}$-GFP complexes. The size of the frame along the time axis was selected to contain the maximum number of frames of analyzed trajectory but was no shorter than 10 frames (100 ms). Next, for all selected trajectories, the position of an NDC80$^{Bonsai}$-GFP complex was determined for each time point using a Gaussian fit of the fluorescence intensity as the peak position.

### 2.6.3 Analysis of single molecule dissociation rate

For each kymograph, all landing events were manually selected by clicking to the landing point and to the detaching point. Only events longer than two time-frames were analyzed (residency time ≥30 ms). The duration of each event was plotted as a histogram for wild-type or mutant NDC80$^{Bonsai}$-GFP complexes. Histograms were fitted with an exponential curve excluding initial decline. Residency time (τ) was determined from exponential fit. Dissociation rate ($k_{off}$) is inverted residency time.

In order to measure the photobleaching rate of NDC80$^{Bonsai}$-GFP, 50nM of protein was incubated in imaging buffer for a 10 min in a chamber without microtubules and without blocking agent. Soluble protein was then washed out in order to exclude any exchange of NDC80$^{Bonsai}$-GFP complexes on the coverslip surface with the soluble protein pool. Time-lapse stacks were acquired with the same microscope and camera settings used in all experiments. The average pixel intensity was plotted as a function of time and fit with exponential function. The observed lifetimes of NDC80$^{Bonsai}$-GFP complexes on microtubules were corrected for the effects of photobleaching as described in Helenius et al., 2006.

### 2.6.4 Analysis of single molecule association rate

The association rate for individual NDC80$^{Bonsai}$-GFP complexes was determined using the total number of landing events on the microtubule during a period of time and dividing by the length of the microtubule, duration of

observation, and the concentration of NDC80$^{Bonsai}$-GFP. The total number of landing events was determined from the histogram of residency time distribution.

### 2.6.5 Analysis of TIRF-based microtubule affinity measurements.

For analysis of TIRF-based binding data, custom software was written in ImageJ (NIH). Ten frames for each imaged field were averaged together. Individual microtubules were selected using a line with a width of 16 pixels. Along each row across the selected line, the maximum fluorescence intensity was recorded and plotted as a function of the coordinate along the microtubule. Fluorescence intensity of the microtubule was identified as the average value from this graph. For each concentration, at least 40 microtubules were analyzed and averaged.

### 2.6.6 Mathematical model description.

Calculations were carried out using custom-written software in Object Pascal in Delphi programming environment (Anatoly Zaytsev).

## 2.7 Protein expression and purification

For NDC80$^{Bonsai}$-GFP, DNA constructs encoding for Hec1-Spc25 and Nuf2-Spc24 chimeras were cloned into a dicistronic protein expression vector, pGEX6P-2rbs. GFP was fused to the C-terminus of Spc24, and GST was fused to the N-terminus of Nuf2. Ndc80$^{Bonsai}$-GFP was transformed in BL21(DE3) *E. coli* and cells were grown at 37°C until the $OD_{600}$ = 0.45–0.6. Protein expression was

induced with 400 μM IPTG for 12–16 hr at 18°C. Cells were harvested by centrifugation at 4000 x g. Bacterial pellets were resuspended in 30 mL lysis buffer per liter of bacterial cell culture (25 mM Tris-HCl, pH 7.6, 300 mM NaCl, 1 mM DTT, 1 mM EDTA, and two Complete Protease Inhibitor Cocktail Tablets [Roche]). Lysates were sonicated and cleared by centrifugation at 40,000 rpm for 45–60 min in a Beckman 70 Ti rotor. Supernatants were incubated with 3 mL of glutathione-s-transferase coated beads. After at least 4hr at 4°C, beads were washed with 3 x 20 mL of lysis buffer. To cleave $NDC80^{Bonsai}$-GFP from beads, cleavage buffer was added to the resin (50 mM Tris-HCl, pH 7.6, 150 mM NaCl, 1 mM DTT, 1 mM EDTA) with 10 units of PreScission protease (GE Healthcare). Resin was incubated and rocked overnight at 4°C. Supernatent was harvested by centrifugation and protein was purified using a Superdex 200 size exclusion chromatography (SEC) column (GE Healthcare). Column was equilibrated with Superdex lysis buffer (25 mM Tris-HCl, pH 7.6, 300 mM NaCl, 1 mM EDTA, and 5% glycerol). Fractions were collected and those containing the $NDC80^{Bonsai}$-GFP complex were combined and concentrated. Mutant complexes were expressed and purified in the same manner (Ciferri et al., 2008).

Prior to use for TIRF microscopy assays, protein was dialyzed to exchange high salt buffer (25 mM Tris pH7.6, 300 mM NaCl, 1 mM EDTA, 20% glycerol, 1 mM DTT) for BRB80 buffer (pH 6.8). Dialysis column pore size was 10 kDa (Sigma-Aldrich D9062), loaded 100 μl of purified $NDC80^{Bonsai}$-GFP and dialyzed for 3 hr at 4°C. After dialysis, protein solution was airfuged at 28 psi for 12 min in order to remove any protein aggregates (Anatoly Zaytsev).

# CHAPTER III

## The NDC80 complex proteins Nuf2 and Hec1 make distinct contributions to kinetochore-microtubule attachment in mitosis

Lynsie J. R. Sundin, Geoffrey J. Guimaraes, and Jennifer G. DeLuca. (2011).

Mol. Biol. Cell. **22**, 759-768.

My contribution to the work in this chapter includes the optimization of the in vivo silence and rescue protocol for Nuf2. I also designed and carried out the experiments and analyzed the data presented in this chapter.

### 3.1 Introduction

At the onset of mitosis in vertebrate cells, the stable interphase microtubule network is converted into a bipolar spindle made up of short, dynamic microtubules. An essential function of these spindle microtubules is to capture mitotic chromosomes by attaching to a large protein structure, called the kinetochore, built at sites of centromeric heterochromatin. In many cases, the initial attachment between microtubules and kinetochores is along the length of a microtubule, and these lateral attachments must eventually be replaced by end-on attachments, where the plus-ends of spindle microtubules are embedded in the kinetochore. When both sister kinetochores of a mitotic chromosome are

attached in this manner, forces can be generated for directed chromosome movement and to silence the spindle assembly checkpoint.

The formation of stable, end-on kinetochore-microtubule connections depends on the kinetochore-associated NDC80 complex (Wigge and Kilmartin, 2001; DeLuca et al., 2002; Martin-Lluesma et al., 2002; McCleland et al., 2004), which is a member of the conserved KMN network, containing also KNL1 and the Mis12 complex (Cheeseman et al., 2006). The NDC80 complex is a long, dumb-bell shaped hetero-tetramer built from the individual proteins Spc24, Spc25, Nuf2, and Hec1 (also referred to as Ndc80). The C-termini of Spc24 and Spc25 anchor the complex into the kinetochore, while N-terminal domains of Nuf2 and Hec1 reside exterior to Spc24 and Spc25, poised to interact with the plus-ends of spindle microtubules (DeLuca et al., 2006; Wan et al., 2009). Both KNL1 and the NDC80 complex are able to bind microtubules *in vitro*, however, depletion of KNL1 from cultured cells results in less severe kinetochore-microtubule attachment defects than does depletion of NDC80 complex components (Cheeseman et al., 2008). This has led to the idea that the NDC80 complex, aided by other factors including KNL1, serves as the primary contact between kinetochores and microtubules in cells.

Structural studies of the N-terminus of Hec1 (Wei et al., 2007) and of a modified NDC80 complex ($NDC80^{Bonsai}$) truncated of much of its coiled-coil domain (Ciferri et al., 2008), revealed that portions of the N-termini of both Hec1 and Nuf2 fold into calponin homology (CH) domains, motifs well-known for mediating binding to actin, and in fewer cases, to microtubules (Gimona et al.,

2002; Slep and Vale, 2007). The N-terminus of Hec1 contains an additional motif that precedes the CH domain, referred to as the tail domain. This domain is highly basic and positively-charged, and in humans is about 80 amino acids in length. Unfortunately, there are no structural data for this motif, which is predicted to be flexible and disordered (Wei et al., 2007; Ciferri et al., 2008; Guimaraes et al., 2008). The Hec1 tail, however, is required for the efficient formation of stable kinetochore-microtubule attachments in cells (Guimaraes et al., 2008; Miller et al., 2008), and its removal results in a significant decrease in binding affinity of N-terminal Hec1 fragments or purified $NDC80^{Bonsai}$ complexes for microtubules *in vitro* (Wei et al., 2007; Ciferri et al., 2008). The Hec1 tail is also likely involved in regulation of kinetochore-microtubule attachment stability, as multiple sites within this domain are phosphorylated *in vitro* by Aurora B kinase, which has been widely implicated in correcting kinetochore-microtubule attachment errors in mitosis by increasing kinetochore-microtubule turnover (Ditchfield et al., 2003; Hauf et al., 2003; Lampson and Kapoor, 2005; Cimini et al., 2006; Pinsky et al., 2005; Biggins and Murray, 2001; Tanaka et al., 2002). This is supported by the finding that phosphorylation of the Hec1 tail domain by a purified Aurora kinase *in vitro* results in decreased binding affinity of the NDC80 complex for microtubules (Cheeseman et al., 2006). Furthermore, *in vivo* studies have shown that the phosphorylation state of the Hec1 tail domain affects the stability of kinetochore-microtubule attachments. Specifically, expression of a non-phosphorylatable Hec1 tail domain mutant in cells results in hyper-stable kinetochore-microtubule attachments (DeLuca et al., 2006), whereas expression

of phospho-mimetic versions of Hec1 in cells results in unstable kinetochore-microtubule attachments (Guimaraes et al., 2008; Welburn et al., 2010).

Given the ability of CH domains to confer microtubule binding in known microtubule associated proteins (Hayashi and Ikura, 2003; Dougherty et al., 2005), it has been predicted that the ability of the NDC80 complex to mediate kinetochore-microtubule attachment in cells is largely facilitated by the Hec1 and Nuf2 CH domains. Structural data in combination with sequence analysis from various species reveals a conserved face of the Hec1-Nuf2 CH domain pair that is highly positively charged (Ciferri et al., 2008). Charge reversal mutations (Lys to Glu) of even single amino acids within this conserved face in either Hec1 or Nuf2 resulted in a loss of high affinity binding of NDC80 complexes to microtubules *in vitro* (Ciferri et al., 2008). These findings have led to the prediction that both the Hec1 and Nuf2 CH domains are essential for kinetochore-microtubule attachment in cells. Two recent cryo-electron microscopy studies, however, have suggested that for microtubules decorated with recombinant NDC80 complexes *in vitro*, the CH domain of Hec1 directly interfaces the microtubule lattice, while the Nuf2 CH domain may not (Wilson-Kubalek et al., 2008; Alushin et al., 2010). Using a gene silence and rescue approach in HeLa cells, we investigated the respective contributions of the Hec1 and Nuf2 CH domains in the formation of kinetochore-microtubule attachments *in vivo*.

## 3.2 Results

### 3.2.1 The Hec1 CH domain is required for chromosome alignment and stable kinetochore-microtubule attachment in cells.

Endogenous Hec1 was depleted from HeLa cells using fluorescently-labeled siRNAs directed to the 5' untranslated region of human Hec1 (Supplemental Figure 3.1), and either wild-type (WT) Hec1-GFP or mutant versions of Hec1-GFP were subsequently expressed. For all rescue experiments, kinetochore fluorescence intensities of the GFP-fusion proteins were quantified, and only those cells whose average kinetochore fluorescence intensities fell into a defined experimental range were used (Supplemental Figure 3.2). Cells were fixed and assayed for their ability to align chromosomes at the spindle equator (Figure 3.1, A and B). Only cells that formed bipolar spindles were scored, and cells containing multipolar spindles were excluded. For each rescue experiment, the percentage of cells with multipolar spindles varied, but in all cases was under 25% (Supplemental Figure 3.3). Cells depleted of Hec1, as expected, failed to properly congress their chromosomes (Figure 3.1A), and 92% of transfected cells contained mostly unaligned chromosomes (defined as having no recognizable metaphase plate or a recognizable plate with >10 unaligned chromosomes). Cell populations rescued with wild-type (WT) Hec1-GFP, however, contained cells in all phases of mitosis, with 59% cells exhibiting mostly aligned chromosomes (defined as having ≤4 chromosomes off a well-defined metaphase plate), 8% of cells exhibiting partially aligned chromosomes (defined as having 5-10 chromosomes off a metaphase plate), and 33% exhibiting mostly unaligned

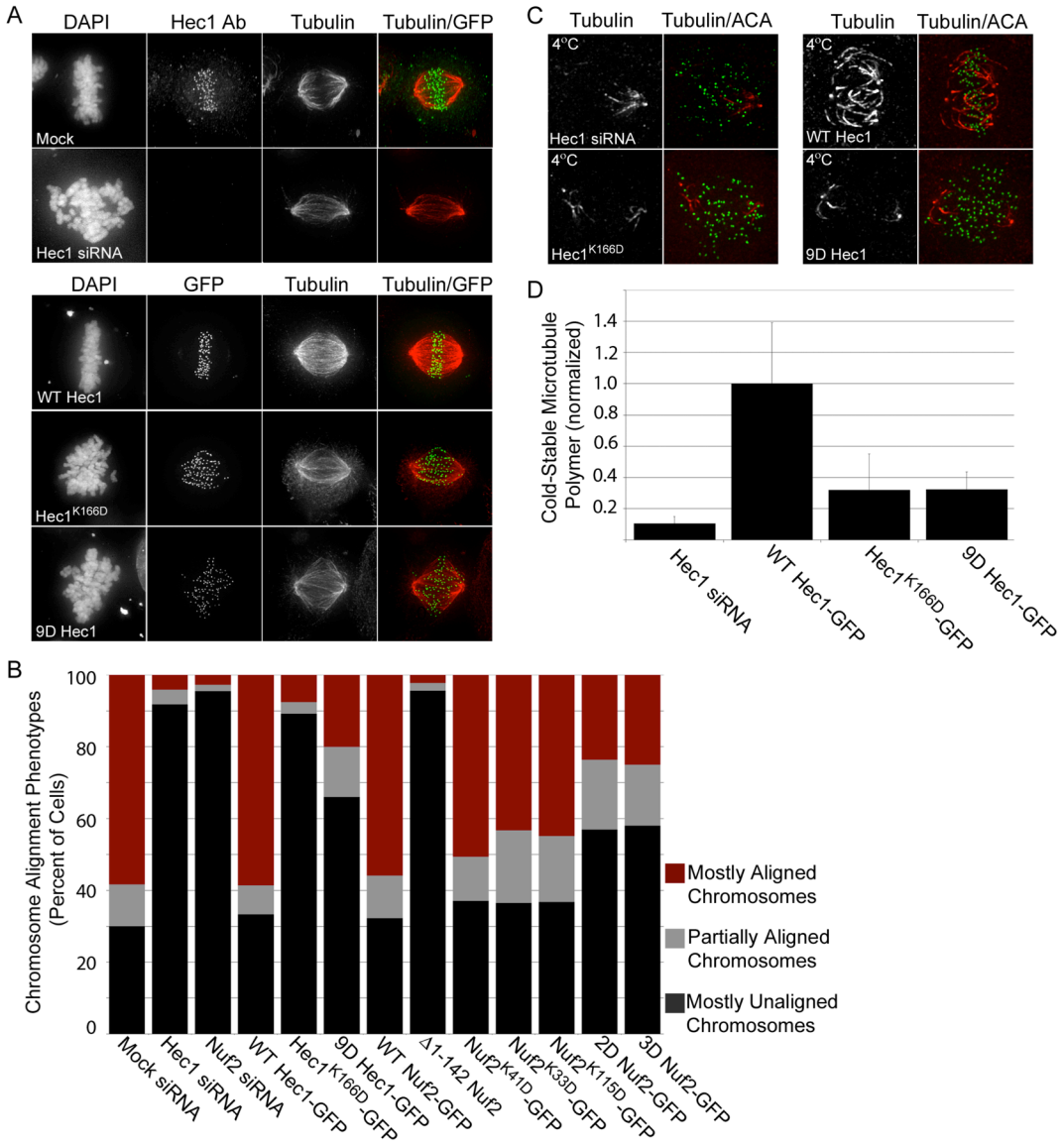
A
DAPI
Hec1 Ab
Tubulin
Tubulin/GFP
Mock
Hec1 siRNA
DAPI
GFP
Tubulin
Tubulin/GFP
WT Hec1
Hec1K166D
9D Hec1
C
Tubulin
Tubulin/ACA
4°C
Hec1 siRNA
Hec1K166D
WT Hec1
9D Hec1
D
Cold-Stable Microtubule Polymer (normalized)
1.4
1.2
1.0
0.8
0.6
0.4
0.2
Hec1 siRNA
WT Hec1-GFP
Hec1K166D -GFP
9D Hec1-GFP
B
Chromosome Alignment Phenotypes (Percent of Cells)
100
80
60
40
20
0
Mostly Aligned Chromosomes
Partially Aligned Chromosomes
Mostly Unaligned Chromosomes
Mock siRNA
Hec1 siRNA
Nuf2 siRNA
WT Hec1-GFP
Hec1K166D -GFP
9D Hec1-GFP
WT Nuf2-GFP
Δ1-142 Nuf2
Nuf2K41D -GFP
Nuf2K33D -GFP
Nuf2K115D -GFP
2D Nuf2-GFP
3D Nuf2-GFP

**Figure 3.1. Stable kinetochore-microtubule attachment depends on the charged face of the Hec1 CH domain. A)** Immunofluorescence images showing HeLa cells depleted of Hec1 and rescued with various mutant versions. The upper panels show a control cell and a cell depleted of endogenous Hec1. The lower panels show cells depleted of endogenous Hec1 and rescued with either WT Hec1 or a Hec1 mutant fused to GFP. **B)** Quantification of chromosome alignment phenotypes in cells depleted of Hec1 or Nuf2 and cells rescued with Hec1 or Nuf2 GFP-fusions. Cells with mostly aligned chromosomes (red) exhibited less than 5 chromosomes off of a well-formed metaphase plate, cells with partially aligned chromosomes (gray) exhibited 5-10 chromosomes off of a metaphase plate, and cells with mostly unaligned chromosomes (black) exhibited either no chromosome alignment or more than 10 chromosomes off of a metaphase plate. For each condition, at least 90 cells were scored. **C)** Images of cells subjected to a cold-induced microtubule-depolymerization assay and immunostained with tubulin and ACA antibodies (recognizing CENP-A, -B, and –C). Cells depleted of Hec1 and cells depleted of Hec1 and rescued with either WT or mutant GFP fusions are shown. **D)** Quantification of microtubule fluorescence intensity after cold-induced microtubule depolymerization. For each condition, spindles from at least 10 cells were measured.

chromosomes (Figure 3.1B). To address the role of the Hec1 CH domain in kinetochore-microtubule attachment, we generated a charge reversal (positive to negative) point mutation within the conserved face of the CH domain at amino acid 166 from Lys to Asp (Hec1$^{K166D}$). This residue was chosen based on X-ray structures of the Hec1 CH domain (Wei et al., 2007; Ciferri et al., 2008) and the previous finding that a charge reversal mutation at this site decreased binding affinity of the NDC80 complex for microtubules by 54-fold *in vitro* (Ciferri et al., 2008). Hec1$^{K166D}$-GFP failed to rescue the chromosome alignment defect in Hec1-depleted cells, and 89% of transfected cells exhibited mostly unaligned chromosomes (Figure 3.1, A and B). To determine if stable kinetochore-microtubule attachments were able to form, cells were subjected to a cold-induced microtubule depolymerization assay. In this assay, most non-kinetochore microtubules are depolymerized, while microtubules embedded by their plus-ends into kinetochores are selectively stabilized. Cells rescued with WT Hec1-GFP retained abundant kinetochore fibers, while those rescued with Hec1$^{K166D}$-GFP did not (Figure 3.1C). Quantification revealed a 68% decrease in cold-stable microtubule polymer in cells rescued with Hec1$^{K166D}$-GFP when compared to cells rescued with WT Hec1-GFP, which was similar to the decrease measured in cells depleted of Hec1 (Figure 3.1D). These results indicate that the charged surface of the Hec1 CH domain is required for the formation of stable kinetochore-microtubule attachments in HeLa cells.

It has been previously reported that the N-terminal tail domain of Hec1 is required for the generation of stable kinetochore-microtubule attachments in cells

(Guimaraes et al., 2008; Miller et al., 2008). Furthermore, cultured cells expressing Hec1 mutants in which multiple amino acids within the tail were mutated to mimic phosphorylation (Ser or Thr to Asp) failed to form stable kinetochore-microtubule attachments (Guimaraes et al., 2008; Welburn et al., 2010). To compare the phenotypes of HeLa cells rescued with a CH domain mutant versus a tail domain mutant, we rescued Hec1-depleted HeLa cells with 9D Hec1-GFP, a mutant in which 9 amino acids (Ser or Thr) within the tail were mutated to Asp to mimic phosphorylation. As expected, cells expressing 9D Hec1-GFP exhibited defects in aligning their chromosomes (Figure 3.1A); 66% cells exhibited mostly unaligned chromosomes, 14% of cells exhibited partially aligned chromosomes, and 20% exhibited mostly aligned chromosomes (Figure 3.1B). Although these cells exhibited a clear defect in chromosome alignment, we noted that a small population could achieve chromosome alignment. To determine if stable kinetochore-microtubules were able to form in cells rescued with 9D Hec1-GFP, we carried out a cold-induced microtubule depolymerization assay. Cells rescued with 9D Hec1-GFP did not retain high levels of microtubule polymer after incubation in ice-cold media (Figure 3.1, C and D), suggesting that kinetochore-microtubule attachment was indeed impaired. These results demonstrate that both the tail and CH domain of Hec1 are important for the formation of stable kinetochore-microtubule attachments in HeLa cells, but disruption of the CH domain results in somewhat more severe defects.

To determine the fate of cells rescued with Hec1 mutants, we performed live cell imaging of HeLa cells transiently transfected with mCherry-Histone H2B

to visualize chromosomes. Each cell included in the analysis was confirmed to have been transfected with Hec1 siRNA (detected by Cy5 fluorescence). For all live-cell time-lapse imaging experiments, the GFP fluorescence intensity at kinetochores was quantified, and only those cells whose average kinetochore fluorescence intensities fell into a defined experimental range were used (Supplemental Figure 3.4). The majority of cells depleted of endogenous Hec1 and rescued with WT Hec1 -GFP formed metaphase plates and entered anaphase with aligned chromosomes (Figure 3.2; Supplemental Movie 3.1). The average time from nuclear envelope breakdown to anaphase onset was 31 ± 5 min. By contrast, 17 of 18 cells rescued with $Hec1^{K166D}$-GFP failed to align their chromosomes and arrested in a prometaphase-like state for >5 hr (Figure 3.2; Supplemental Movie 3.2). Cells rescued with the phospho-mimetic tail domain mutant 9D Hec1 -GFP also experienced severe defects in chromosome segregation (Figure 3.2). Specifically, of 16 cells filmed, 13 failed to align chromosomes and remained arrested in a prometaphase-like state for >5 hr (Figure 3.2; Supplemental Movie 3.3). Results from these experiments demonstrate that both the tail and CH domains of Hec1 are required for normal chromosome alignment and timely progression through mitosis.

### 3.2.2 The Nuf2 CH domain is required for timely progression through mitosis

We next investigated the role of the Nuf2 CH domain in chromosome alignment and kinetochore-microtubule attachment using the silence and rescue

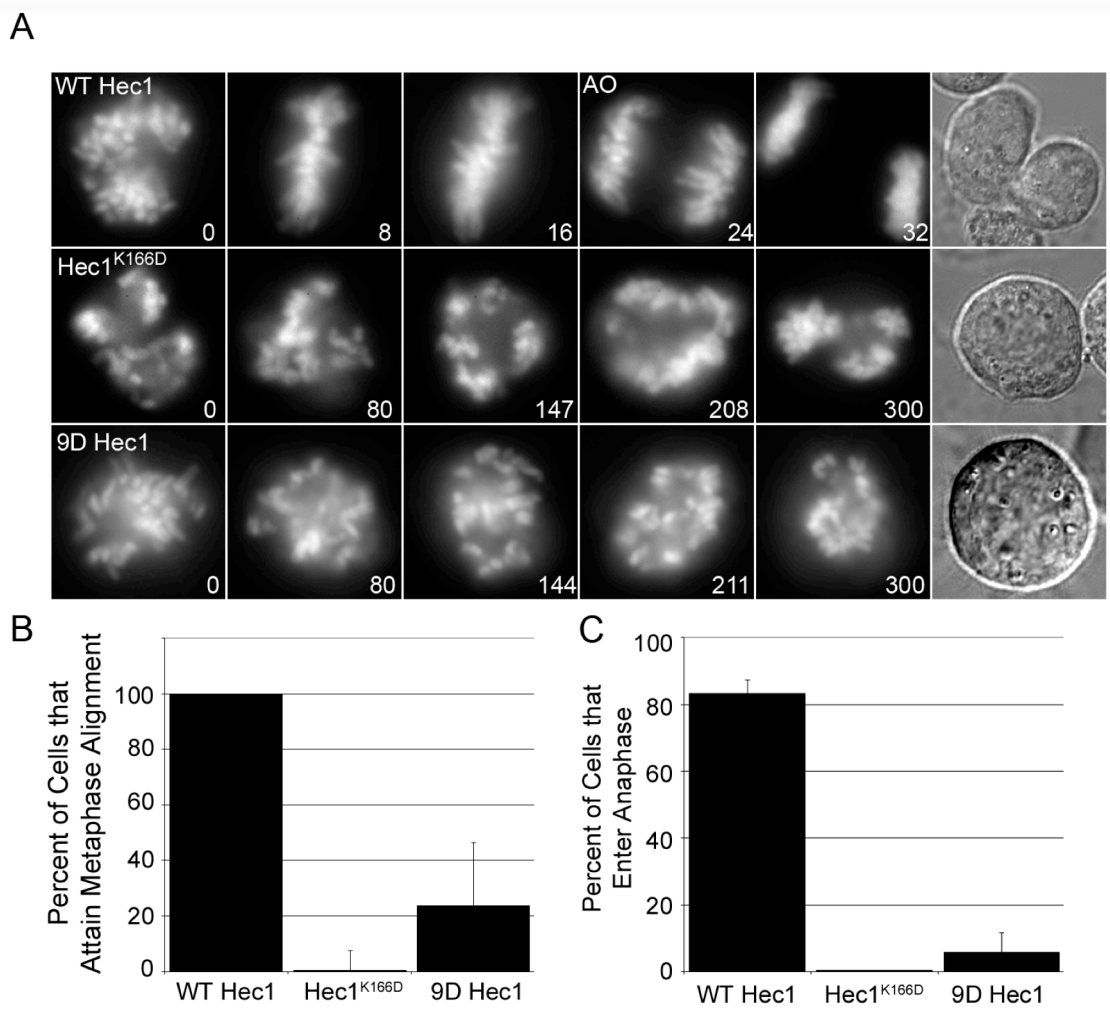


**Figure 3.2. Cells rescued with a Hec1 CH domain charge reversal mutant arrest in mitosis with unaligned chromosomes. A)** Still images from time-lapse acquisitions of HeLa cells depleted of endogenous Hec1 and rescued with either WT Hec1-GFP or various Hec1 mutants fused to GFP. Anaphase onset (AO) is indicated for cells that enter anaphase. The DIC image shows the time-point corresponding to the final mCherry image. **B)** Quantification of metaphase plate formation during live cell imaging. Bar graph represents the percent of cells that attained metaphase alignment at some point during time-lapse imaging. **C)** Quantification of anaphase entry during live cell imaging. Bar graph represents the percent of cells that entered anaphase during time-lapse imaging. All cells were filmed for 5 hr except those rescued with WT Hec1, which were filmed for 2 hr. Error bars in **(B)** and **(C)** represent standard deviation across at least 2 independent experiments. The n values for each experiment are as follows: WT Hec1: 12 cells; Hec1$^{K166D}$: 18 cells; 9D Hec1: 17 cells.

system described above for Hec1. As expected, HeLa cells depleted of Nuf2, which results in a concomitant depletion of Hec1 (Hori et al., 2003; DeLuca et al., 2003), failed to align their chromosomes, and 95% of cells exhibited mostly unaligned chromosomes (Figures 3.1B and 3.3A). Expression of WT Nuf2-GFP in Nuf2-depleted cells rescued the chromosome alignment defect; 56% of cells exhibited mostly aligned chromosomes, 12% of cells exhibited partially aligned chromosomes, and 32% exhibited mostly unaligned chromosomes. By contrast, cells rescued with a Nuf2 mutant deleted of its entire CH domain (Δ1-142 Nuf2) fused to GFP, failed to restore normal chromosome alignment, and 96% of cells expressing Δ1-142 Nuf2-GFP exhibited mostly unaligned chromosomes (Figures 3.1B and 3.3A). We reasoned that this may not be an appropriate approach to specifically test the role of the Nuf2 CH domain in mitotic functions, as removal of the entire domain likely affects the structure or positioning of the remaining Hec1 N-terminus. To more precisely address the role of the Nuf2 CH domain in kinetochore-microtubule attachment, we generated a single charge reversal mutation in the conserved, positively charged face of the CH domain (Ciferri et al., 2008), similar to the strategy used for Hec1. We mutated Lys115 to Asp ($Nuf2^{K115D}$), due to the previous finding that a charge reversal mutation at this site reduced the affinity of NDC80 complexes for microtubules *in vitro* by 46-fold (Ciferri et al., 2008). Surprisingly, cells rescued with $Nuf2^{K115D}$-GFP were able to align their chromosomes nearly as well as those cells rescued with WT Nuf2-GFP (Figures 3.1B and 3.3A). We next generated single charge reversal mutations at Lys33 and at Lys41, which also reside within the conserved face of

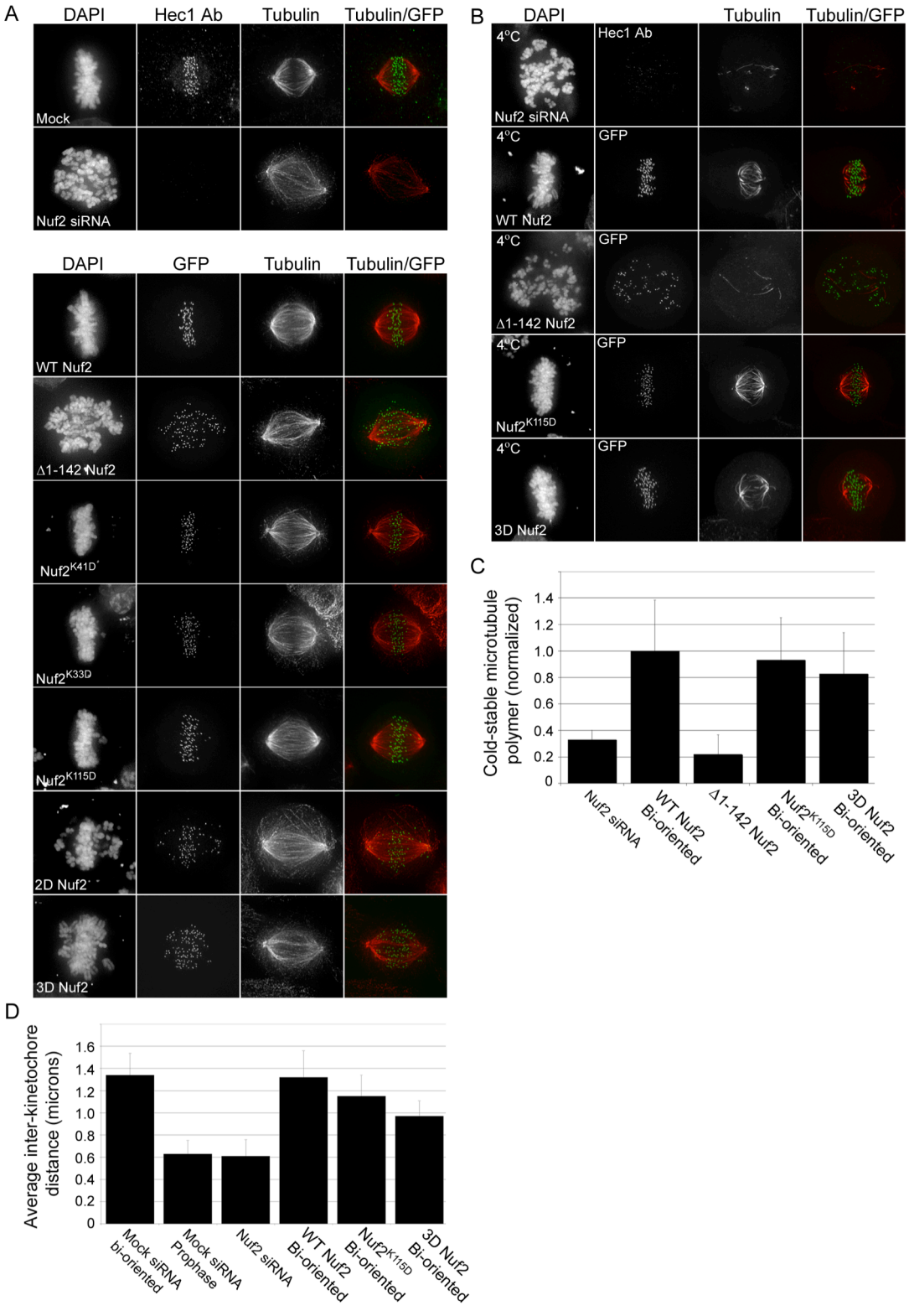
A
DAPI
Hec1 Ab
Tubulin
Tubulin/GFP
Mock
Nuf2 siRNA
DAPI
GFP
Tubulin
Tubulin/GFP
WT Nuf2
Δ1-142 Nuf2
Nuf2K41D
Nuf2K33D
Nuf2K115D
2D Nuf2
3D Nuf2
B
DAPI
Tubulin
Tubulin/GFP
4°C
Hec1 Ab
Nuf2 siRNA
GFP
WT Nuf2
Δ1-142 Nuf2
Nuf2K115D
3D Nuf2
C
Cold-stable microtubule polymer (normalized)
0
0.2
0.4
0.6
0.8
1.0
1.2
1.4
Nuf2 siRNA
WT Nuf2 Bi-oriented
Δ1-142 Nuf2
Nuf2K115D Bi-oriented
3D Nuf2 Bi-oriented
D
Average inter-kinetochore distance (microns)
0
0.2
0.4
0.6
0.8
1.0
1.2
1.4
1.6
Mock siRNA bi-oriented
Mock siRNA Prophase
Nuf2 siRNA
WT Nuf2 Bi-oriented
Nuf2K115D Bi-oriented
3D Nuf2 Bi-oriented

**Figure 3.3. The charged face of the Nuf2 CH domain is not required for the formation of stable kinetochore-microtubule attachments. A)** Immunofluorescence images showing HeLa cells depleted of Nuf2 and rescued with various mutant versions. The upper panels show a control cell and a cell depleted of endogenous Nuf2 stained with Hec1 and tubulin antibodies. The lower panels show cells depleted of endogenous Nuf2 and rescued with either WT Nuf2 or a Nuf2 mutant fused to GFP. For the 2D Nuf2 mutant, 2 Lys to Asp substitutions were made at amino acid positions 33 and 41; the 3D Nuf2 mutant contains 3 Lys to Asp substitutions at amino acid positions 33, 41, and 115. **B)** Images of cells subjected to a cold-induced microtubule-depolymerization assay and immunostained with tubulin antibodies, DAPI and, in Nuf2-depleted cells, Hec1 antibodies. Cells depleted of Nuf2 alone and cells depleted of Nuf2 and rescued with either WT or mutant GFP fusions are shown. **C)** Quantification of microtubule fluorescence intensity after cold-induced microtubule depolymerization. For each condition, spindles from at least 10 cells were measured. **D)** Quantification of inter-kinetochore distances, which were measured from GFP-centroid to GFP-centroid in cells rescued with Nuf2-GFP fusion proteins. In cells depleted of Nuf2, inter-kinetochore distances were measured from ACA-centroid to ACA-centroid. For cells depleted of endogenous Nuf2 and rescued with GFP-fusions, kinetochores from bi-oriented chromosomes were measured.

the Nuf2 CH domain. Cells depleted of endogenous Nuf2 and rescued with either $Nuf2^{K33D}$ or $Nuf2^{K41D}$ were also able to align their chromosomes nearly as well as cells rescued with WT Nuf2-GFP, indicating that single amino acid charge reversal mutations within the Nuf2 CH domain are not sufficient to disrupt chromosome alignment.

To more severely disrupt the charged face of the Nuf2 CH domain, we generated mutants in which two or three of the Lys residues were mutated to Asp, termed 2D Nuf2-GFP (Lys33 and Lys41 mutated to Asp) and 3D Nuf2-GFP (Lys33, Lys41, and Lys115 mutated to Asp). In each case, the ability to align chromosomes was impaired when compared to the mutants containing a single amino acid change. Specifically, in cells rescued with 2D Nuf2-GFP or 3D Nuf2-GFP, only ~25% of the fixed cells scored were able to align their chromosomes, compared to ~40% for any of the single charge reversal mutants (Figures 3.1B and 3.3A). Of note, the chromosome alignment phenotypes for cells expressing the 2D or 3D Nuf2 CH domain mutants were significantly less severe than in cells expressing a single Hec1 charge reversal mutation. Due to this, we tested whether the kinetochore-microtubule attachments in cells rescued with Nuf2 CH domain mutants with partially aligned or mostly aligned chromosomes were stable. We first quantified the level of cold-stable microtubule polymer in these cells and found that those rescued with a mutant containing a single amino acid change ($Nuf2^{K115D}$-GFP) or with three amino acid changes (3D Nuf2-GFP) retained near-wild-type levels of cold-stable microtubule polymer (Figure 3.3, B and C). To further assess kinetochore-microtubule attachment stability, we

measured the distances between sister kinetochores on bi-oriented chromosomes. The average inter-kinetochore distance for sister kinetochores on bi-oriented chromosomes in cells rescued with WT Nuf2-GFP was 1.34 ± 0.24 μm (compared to 0.63 ± 0.15 μm in prophase, at "rest length"). By contrast, the average inter-kinetochore distance of sister pairs of bi-oriented chromosomes in cells rescued with Nuf2$^{K115D}$-GFP was 1.15 ± 0.19 μm, and 0.97 ± 0.14 μm in cells rescued with 3D Nuf2-GFP (Figure 3.3D). Both the 14% and 28% reduction in inter-kinetochore distances for Nuf2$^{K115D}$-GFP and 3D Nuf2-GFP, respectively, over WT Nuf2-GFP are statistically significant ($p < 0.0001$), indicating that mutation of the conserved face of the Nuf2 CH domain results in a defect in generating wild-type kinetochore tension on bi-oriented chromosomes.

To determine the fate of cells rescued with Nuf2-GFP fusion proteins, we followed Nuf2-depleted cells rescued with WT Nuf2-GFP or mutant versions of Nuf2-GFP via time-lapse microscopy. Cells depleted of endogenous Nuf2 and rescued with WT Nuf2-GFP properly aligned chromosomes at the spindle equator and entered anaphase in an average of 40 ± 8min (Figure 3.4; Supplemental Movie 3.4). As predicted from our fixed cell analysis, cells rescued with Δ1-142 Nuf2-GFP failed to align chromosomes at the spindle equator and all cells imaged arrested for >5 hr in a prometaphase-like state (Figure 3.4; Supplemental Movie 3.5). By contrast, most cells rescued with the single Lys to Asp mutations (Nuf2$^{K115D}$-GFP, Nuf2$^{K33D}$-GFP, and Nuf2$^{K41D}$-GFP) were able to align their chromosomes and generate metaphase plates (Figure 3.4; Supplemental Movies 3.6-3.8, respectively). In many cases, alignment was

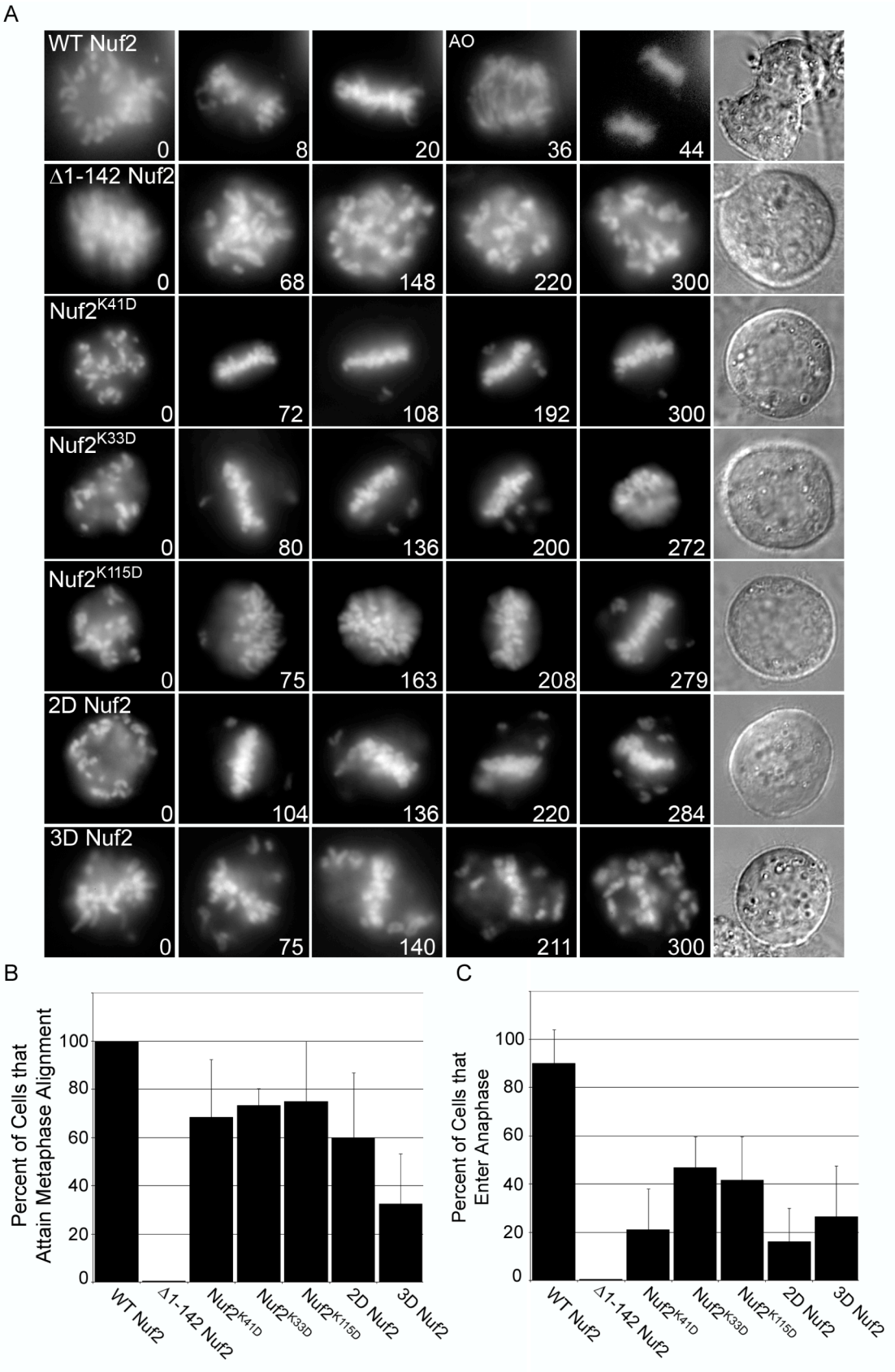
A
WT Nuf2
0
8
20
AO
36
44
Δ1-142 Nuf2
0
68
148
220
300
Nuf2K41D
0
72
108
192
300
Nuf2K33D
0
80
136
200
272
Nuf2K115D
0
75
163
208
279
2D Nuf2
0
104
136
220
284
3D Nuf2
0
75
140
211
300
B
Percent of Cells that Attain Metaphase Alignment
0
20
40
60
80
100
WT Nuf2
Δ1-142 Nuf2
Nuf2K41D
Nuf2K33D
Nuf2K115D
2D Nuf2
3D Nuf2
C
Percent of Cells that Enter Anaphase
0
20
40
60
80
100
WT Nuf2
Δ1-142 Nuf2
Nuf2K41D
Nuf2K33D
Nuf2K115D
2D Nuf2
3D Nuf2

**Figure 3.4. Cells rescued with Nuf2 CH domain charge reversal mutants arrest in mitosis with at least partially aligned chromosomes. A)** Still images from time-lapse acquisitions of HeLa cells depleted of endogenous Nuf2 and rescued with either WT Nuf2-GFP or Nuf2 mutants fused to GFP. Anaphase onset (AO) is indicated for cells that enter anaphase. The DIC image shows the time-point corresponding to the final mCherry image. **B)** Quantification of metaphase plate formation during live cell imaging. Bar graph represents the percent of cells that attained metaphase alignment at some point during time-lapse imaging. **C)** Quantification of anaphase entry during live cell imaging. Bar graph represents the percent of cells that entered anaphase during time-lapse imaging. All cells were filmed for 5 hr except those rescued with WT Nuf2, which were filmed for 2 hr. Error bars in **(B)** and **(C)** represent standard deviation across at least 2 independent experiments. The n values for each experiment are as follows: WT Nuf2: 10 cells; D1-142 Nuf2: 8 cells; $Nuf2^{K41D}$: 19 cells; $Nuf2^{K33D}$: 15 cells; $Nuf2^{K115D}$: 12 cells; 2D Nuf2: 25 cells; 3D Nuf2: 34 cells.

transient, with individual chromosomes leaving and returning to the spindle equator, or in some cases, the entire plate would disassemble and eventually reassemble. As observed in the fixed cell analysis, chromosome alignment defects were more severe in cells expressing 2D Nuf2-GFP and 3D Nuf2-GFP, but a significant population of the cells (60% and 32%, respectively) were able to align chromosomes at the spindle equator at some point during filming (Figure 3.4; Supplemental Movies 3.9 and 3.10). This is in contrast to cells depleted of Hec1 and rescued with the single charge reversal mutant, Hec1$^{K166D}$-GFP, where no chromosome alignment was observed (Figure 3.2).

Although cells rescued with the Nuf2 CH domain mutants were able to align their chromosomes (to varying degrees), they failed to enter anaphase in a timely manner. Specifically, only 42%, 47%, and 21% of cells rescued with the single charge reversal mutants Nuf2$^{K115D}$-GFP, Nuf2$^{K33D}$-GFP, or Nuf2$^{K41D}$-GFP (respectively) entered anaphase during the 5 hr of imaging. In addition, the cells that did enter anaphase did so with a delay of ~40 min when compared to cells rescued with WT Nuf2-GFP (data not shown). Similarly, only 16% and 26% of cells rescued with 2D Nuf2-GFP or 3D Nuf2-GFP, respectively, entered anaphase during the 5 hr time-lapse, and these cells did so with an average delay of ~90 min when compared to cells rescued with WT Nuf2-GFP (data not shown). Together, these results suggest that the Nuf2 CH domain is not absolutely required for formation of stable kinetochore-microtubule attachments, but is needed to generate wild-type tension across sister kinetochore pairs and for timely entry into anaphase.

### 3.2.3 Nuf2 CH domain mutants do not affect recruitment of kinetochore outer domain proteins

Due to the distinct phenotypes observed in cells rescued with Nuf2 CH domain mutants compared to those rescued with Hec1 mutants, we tested whether these cells were defective in recruiting kinetochore outer domain proteins. As expected, Hec1 was absent from kinetochores in Nuf2-depleted cells (Figure 3.5), but present on kinetochores in cells rescued with either WT Nuf2-GFP or 3D Nuf2-GFP. We next tested for the presence of Ska complex proteins, since similar defects to those observed in cells rescued with Nuf2$^{K115D}$-GFP or 3D Nuf2-GFP have been observed in cells depleted of Ska complex components (Hanisch et al., 2006; Gaitanos et al., 2009; Theis et al., 2009; Welburn et al., 2009; Raaijmakers et al., 2009; Daum et al., 2009). As previously demonstrated, Ska1 and Rama1/Ska3 were absent from kinetochores depleted of Nuf2 (Hanisch et al., 2006; Welburn et al., 2009; Raaijmakers et al., 2009) However, both Ska1 and Rama1/Ska3 were present at kinetochores in cells rescued with WT Nuf2-GFP or 3D Nuf2-GFP (Figure 3.5). The outer domain protein CLASP1, which was also absent from kinetochores in cells depleted of Nuf2, was present at kinetochores in cells rescued with WT Nuf2-GFP or 3D Nuf2-GFP (Figure 3.5). Similar results were found for ZW10, which was absent on kinetochores in cells depleted of Nuf2, but present at kinetochores in cells rescued with WT Nuf2-GFP or 3D Nuf2-GFP (Figure 3.5). Finally, CENP-E and KNL-1 were present at kinetochores in Nuf2-depleted cells and in cells rescued with WT Nuf2-GFP and 3D Nuf2-GFP (Figure 3.5). These results suggest that the defects observed in

A

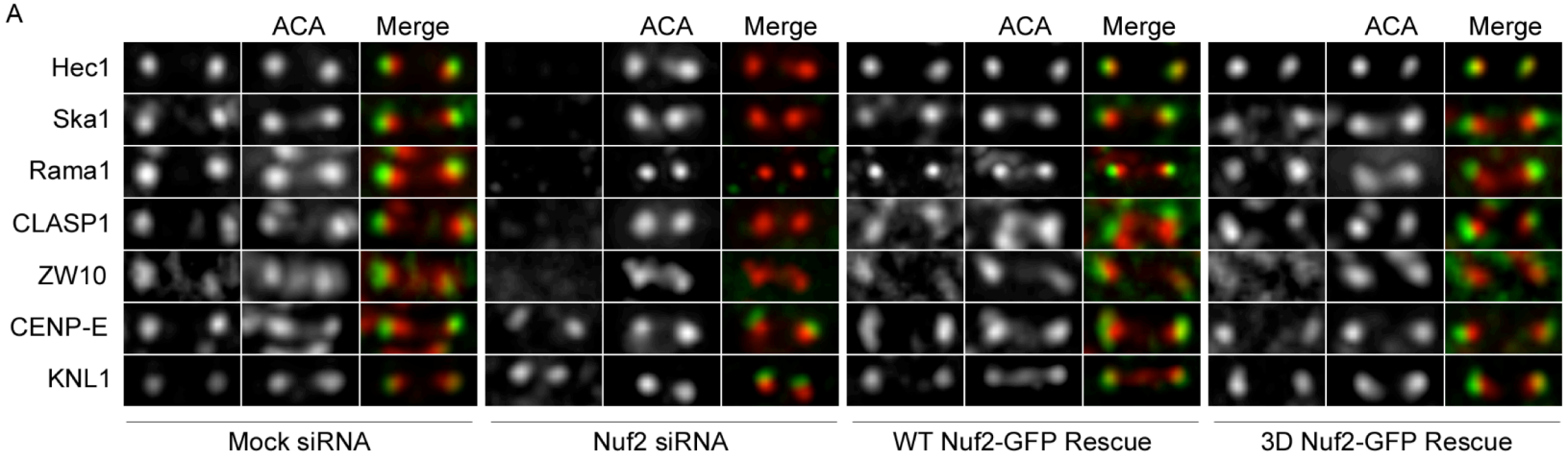


B

| | Mock siRNA | Nuf2 siRNA | WT Nuf2 Rescue | 3D Nuf2 Rescue |
|---|---|---|---|---|
| Hec1 | + | - | + | + |
| Ska1 | + | - | + | + |
| Rama1 | + | - | + | + |
| CLASP1 | + | - | + | + |
| ZW10 | + | - | + | + |
| CENP-E | + | + | + | + |
| KNL1 | + | + | + | + |

**Figure 3.5. Charge reversal mutations within the Nuf2 CH domain do not affect recruitment of outer kinetochore proteins. A)** Images showing single kinetochore pairs from control cells, Nuf2-depleted cells, cells rescued with WT Nuf2-GFP, and cells rescued with 3D Nuf2-GFP. For each series, the first panel shows immunostaining for the antibody listed on the far left. ACA staining is shown as well a merge of ACA staining with each test antibody. **B)** Chart summarizing immunofluorescence data shown in **(A).**

cells rescued with the Nuf2 CH domain mutants are not due impaired recruitment of kinetochore outer domain proteins.

### 3.2.4 Distinct roles for Nuf2 and Hec1 CH domains in kinetochore function

Phosphorylation of the Hec1 tail domain has been suggested to play an important role in the regulation of kinetochore-microtubule attachment (DeLuca et al., 2006; Cheeseman et al., 2006). Cells expressing non-phosphorylatable mutants of Hec1 form stable kinetochore-microtubule attachments, but exhibit an increased rate of attachment errors (DeLuca et al., 2006), suggesting that prevention of phosphorylation of the Hec1 tail results in the generation of hyper-stable kinetochore-microtubule attachments. We wanted to test if a non-phosphorylatable mutant of Hec1 could rescue the attachment defects observed in cells rescued with the Hec1 and Nuf2 CH domain mutants. We first time-lapse imaged HeLa cells depleted of endogenous Hec1 and rescued with 9A Hec1-GFP, a mutant version of Hec1 in which all 9 putative Aurora B kinase phosphorylation sites (Ser or Thr) were mutated to Ala to prevent phosphorylation. The majority of cells rescued with 9A Hec1-GFP were unable to completely align their chromosomes, but 19 of 20 cells filmed entered anaphase in an average of 75 ± 30 min after nuclear envelope breakdown with multiple lagging chromosomes (Figure 3.6; Supplemental Movie 3.11). Fixed cell analysis of cells rescued with 9A Hec1-GFP demonstrated that stable kinetochore-microtubule attachments were able to form, and inter-kinetochore distances of

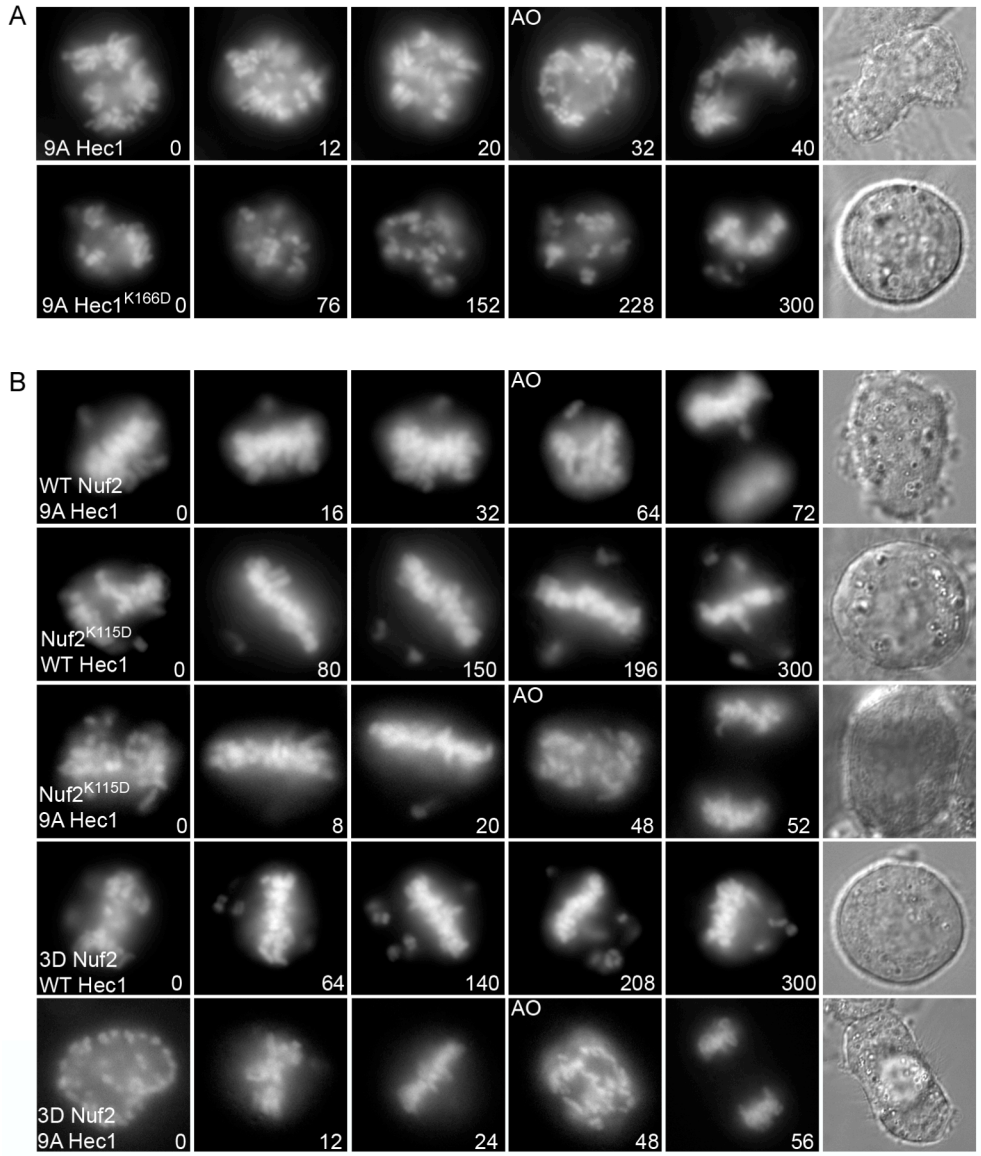
A
9A Hec1 0
12
20
AO
32
40
9A Hec1K166D 0
76
152
228
300
B
WT Nuf2
9A Hec1 0
16
32
AO
64
72
Nuf2K115D
WT Hec1 0
80
150
196
300
Nuf2K115D
9A Hec1 0
8
20
AO
48
52
3D Nuf2
WT Hec1 0
64
140
208
300
3D Nuf2
9A Hec1 0
12
24
AO
48
56
C
Percent of Cells that Enter Anaphase
0
20
40
60
80
100
9A Hec1
9A Hec1K166D
WT Nuf2 / 9A Hec1
Nuf2K115D / WT Hec1
Nuf2K115D / 9A Hec1
3D Nuf2 / WT Hec1
3D Nuf2 / 9A Hec1

**Figure 3.6. Expression of a non-phosphorylatable Hec1 tail domain overcomes the mitotic arrest observed in cells rescued with a Nuf2 CH domain charge reversal mutant, but not a Hec1 CH domain charge reversal mutant. A)** Still images from time-lapse acquisitions of HeLa cells depleted of endogenous Hec1 and rescued with either 9A Hec1-GFP or 9A Hec1 $^{K166D}$-GFP. The DIC image shows the time-point corresponding to the final mCherry image. **B)** Still images from time-lapse acquisitions of HeLa cells depleted of endogenous Nuf2 and Hec1 using siRNAs targeted to both Nuf2 and Hec1 genes, and rescued with either WT Nuf2-GFP or a mutant Nuf2-GFP containing Lys to Asp mutations in the CH domain, and either WT Hec1- or 9A Hec1-GFP. Anaphase onset (AO) is indicated for cells that enter anaphase in **(A)** and **(B)**. **C)** Quantification of anaphase entry during live cell imaging. Bar graph represents the percent of cells that entered anaphase during time-lapse imaging. All cells were filmed for 5 hr. Error bars represent standard deviation across at least 2 independent experiments. The n values for each experiment are as follows: 9A Hec1: 20 cells; 9A Hec1$^{K166D}$: 18 cells; WT Nuf2/9A Hec1: 28 cells; Nuf2$^{K115D}$/ WT Hec1: 20 cells; Nuf2$^{K115D}$/9A Hec1: 19 cells; 3D Nuf2/WT Hec1: 29 cells; 3D Nuf2/9A Hec1: 39 cells.

sister kinetochore pairs on bi-oriented chromosomes were increased from those measured in wild-type metaphase cells (data not shown).

We next designed a 9A Hec1$^{K166D}$-GFP mutant and used this to rescue cells depleted of endogenous Hec1. The non-phosphorylatable Hec1 tail failed to rescue the attachment defect resulting from the K166D mutation, and cells remained arrested in mitosis rather than entering anaphase as did the cells rescued with 9A Hec1-GFP (Figure 3.6; Supplemental Movie 3.12). To determine if the non-phosphorylatable Hec1 tail could compensate for the defects observed in cells rescued with the Nuf2 CH domain mutants, we carried out double silence and rescue experiments, in which siRNAs directed to the sequences of both Nuf2 and Hec1 were transfected into HeLa cells, and cells were subsequently rescued with Nuf2$^{K115D}$-GFP and either WT Hec1 or 9A Hec1. As shown in Figure 6, time lapse imaging reveals that cells rescued with Nuf2$^{K115D}$-GFP and WT Hec1 exhibited a phenotype similar to that of cells rescued with Nuf2$^{K115D}$-GFP alone, and the majority of cells arrested in mitosis for > 5 h (Figure 3.6; Supplemental Movie 3.14). By contrast, most cells rescued with Nuf2$^{K115D}$-GFP and 9A Hec1 did not arrest (16 of 19 cells), but instead, initiated anaphase in an average of 55 ± 34 min (Figure 3.6; Supplemental Movie 3.15). Not unexpectedly, many cells exhibited one or multiple lagging chromosomes in anaphase (data not shown). Similar results were observed in cells depleted of Nuf2 and Hec1 and rescued with 3D Nuf2-GFP and 9A Hec1. Here, an increased number of cells (44%) entered anaphase when compared to cells depleted of Nuf2 and Hec1 and rescued with 3D Nuf2-GFP and WT Hec1 (14%) (Figure 3.6; Supplemental

Movies 3.16 and 3.17). Similar to cells rescued with Nuf2$^{K115D}$-GFP and 9A Hec1, we often observed lagging chromosomes in cells rescued with 3D Nuf2-GFP and 9A Hec1 that entered anaphase. These results suggest that the Nuf2 CH domain is not absolutely required for the formation of tension-generating, end-on kinetochore-microtubule attachments, and attachments generated through the Hec1 CH domain and Hec1 tail domain can provide sufficient stable kinetochore-microtubule attachments to silence the spindle assembly checkpoint.

### 3.3 Discussion

We find that mutating a single Lys residue within the CH domain of Hec1 (Lys 166 to Asp) severely perturbs kinetochore-microtubule attachment stability *in vivo*. This is not surprising, since recombinantly expressed, purified NDC80$^{Bonsai}$ complexes containing a charge reversal mutation at this residue have been shown to bind microtubules *in vitro* with 54-fold less affinity than WT NDC80$^{Bonsai}$ complexes (Ciferri et al., 2008). We also demonstrated that a non-phosphorylatable Hec1 tail-domain mutant, which has been previously shown to induce hyper-stable kinetochore-microtubule attachments (DeLuca et al., 2006), was not able to rescue the Hec1$^{K166D}$ phenotype, further suggesting that the CH domain of Hec1 is absolutely essential for high affinity kinetochore-microtubule binding. In contrast, we found that mutating single Lys residues in the CH domain of Nuf2 had a significantly less severe effect on the formation of stable kinetochore-microtubule attachments. The same mutations, however, resulted in a decrease in binding affinity of purified NDC80$^{Bonsai}$ complexes *in vitro*.

Specifically, a charge reversal mutation at Lys115 decreased the microtubule binding affinity 46-fold, while mutations at Lys33 and Lys41 resulted in a 9-fold and 6-fold decrease in affinity, respectively (Ciferri et al., 2008). In our study, cells expressing Nuf2 CH domain charge reversal mutants were able to generate stable kinetochore-microtubule attachments, and exhibited only a partial loss of inter-kinetochore tension and cold-stable microtubule polymer. Furthermore, the partial loss of kinetochore-microtubule attachment stability could be overcome by co-expression of a non-phosphorylatable Hec1 tail domain mutant. Our results support a model in which the Hec1 protein interfaces the microtubule lattice to generate high affinity kinetochore-microtubule attachments, while the Nuf2 protein does not.

Our results are consistent with two recently published studies that generated models of the NDC80 complex-microtubule interface based on reconstructions of cryo-elecctron microscopy data fit to the crystal structures of tubulin and the CH domains of Hec1 and Nuf2 (Wilson-Kubalek et al., 2008; Alushin et al., 2010). These models suggest that the interface between the microtubule lattice and the NDC80 complex is made up of only a small region within the Hec1 CH domain, and this region includes Lys at position 166. In both reconstructed models, the Nuf2 CH domain does not interface the microtubule, but faces away from the lattice (Wilson-Kubalek et al., 2008; Alushin et al., 2010). The Nuf2 Lys residues that were mutated in our study (Lys33, Lys41, and Lys115) lie within the face of the Nuf2 CH domain that faces away from the

microtubule lattice according to both of these studies, which may explain the difference in severity between the Hec1 and Nuf2 CH domain mutants.

Although the Nuf2 CH domain is not likely required for direct microtubule binding, cells expressing Nuf2 CH domain mutants do experience mitotic defects. Specifically, sister kinetochores fail to generate wild-type inter-kinetochore tension and cells arrest in mitosis with aligned or partially aligned chromosomes. One possibility is that the Nuf2 CH domain serves to recruit outer kinetochore proteins known to function at the kinetochore-microtubule interface. To address this, we tested the localization of outer kinetochore proteins known to be important in kinetochore-microtubule attachment. Of the proteins investigated, which included Ska1, Rama1, CLASP1, ZW10, CENP-E, and KNL1, all localized to kinetochores in cells expressing the 3D Nuf2 CH domain mutant. This suggests that lack of protein recruitment is not likely responsible for the observed phenotypes, however, it is possible that the Nuf2 CH domain recruits an outer kinetochore protein required for the generation of wild-type inter-kinetochore tension that was not tested.

A second possibility is that the Nuf2 CH domain plays a role in properly oligomerizing NDC80 complexes at the kinetochore or tethering NDC80 complexes to one another so that optimal tension-generating kinetochore-microtubule associations can be formed. It has been demonstrated *in vitro* that NDC80 complex binding to microtubules is cooperative, and oligomerization of complexes is required for high affinity binding (Cheeseman et al., 2006; Powers et al., 2009, Ciferri et al., 2008; Alushin et al., 2010). If the Nuf2 CH domain is

required for such oligomerization, it could provide an explanation for the phenotype severity differences observed between *in vitro* and *in vivo* experiments with Nuf2 CH domain charge reversal mutants. The defects in cells may be less severe because the kinetochore serves to position NDC80 complexes into a specific geometry in relation to the microtubule lattice, reducing the need for explicit oligomerization of NDC80 complexes to facilitate kinetochore-microtubule binding. As kinetochore-microtubule attachments become stabilized during metaphase, however, oligomerization of adjacent NDC80 complexes may be critical for the generation of wild-type levels of inter-kinetochore tension. For NDC80 complex-microtubule binding studies carried out *in vitro,* the complexes are not specifically arranged and concentrated by a structure such as the kinetochore, therefore the requirement for domains that facilitate oligomerization may be more stringent. Because of this, mutation of such domains would likely result in a significant loss in high-affinity microtubule binding.

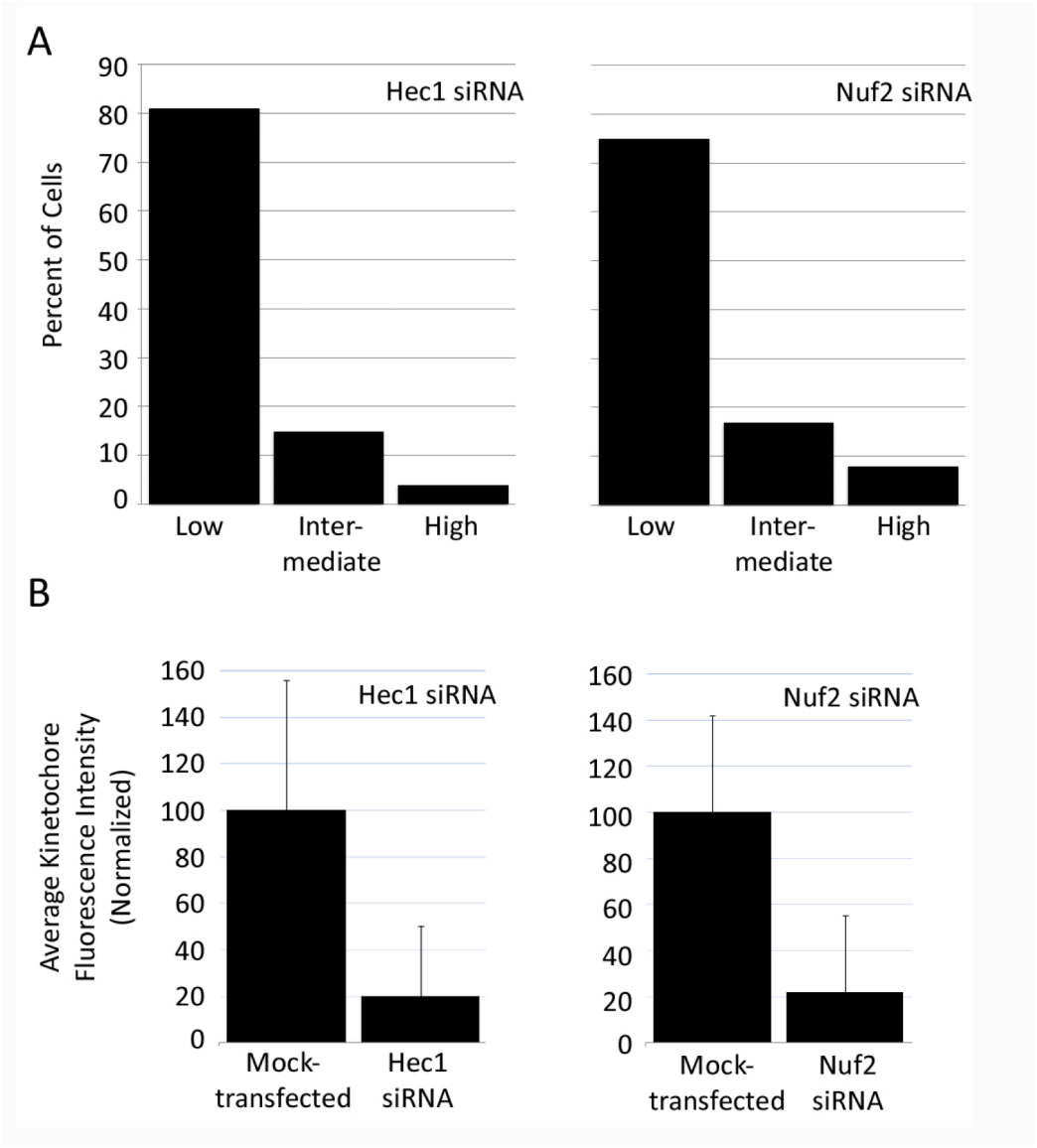


**Supplemental Figure 3.1. Quantification of Hec1 and Nuf2 depletion.** HeLa cells were transfected with either Hec1 or Nuf2 siRNAs directly labeled with Cy5, fixed, and processed for immunofluorescence as described in the Materials and Methods section. **A)** To gauge the penetrance of depletion, Cy5-positive cells were categorized by their overall level of protein depletion at kinetochores. For both Hec1 and Nuf2 siRNA-transfections, cells that had no detectable Hec1 at kinetochores were scored as “low,” cells that had wild-type or near wild-type levels of Hec1 at kinetochores were scored as “high,” and those with an intermediate level of Hec1 at kinetochores were scored as “intermediate.” For each transfection, >100 cells were scored. **B)** To determine the average level of Hec1 remaining at kinetochore after siRNA transfection, kinetochore fluorescence intensity of Hec1 was quantified in mock-transfected cells and Cy5-positive siRNA-transfected cells using MetaMorph software.

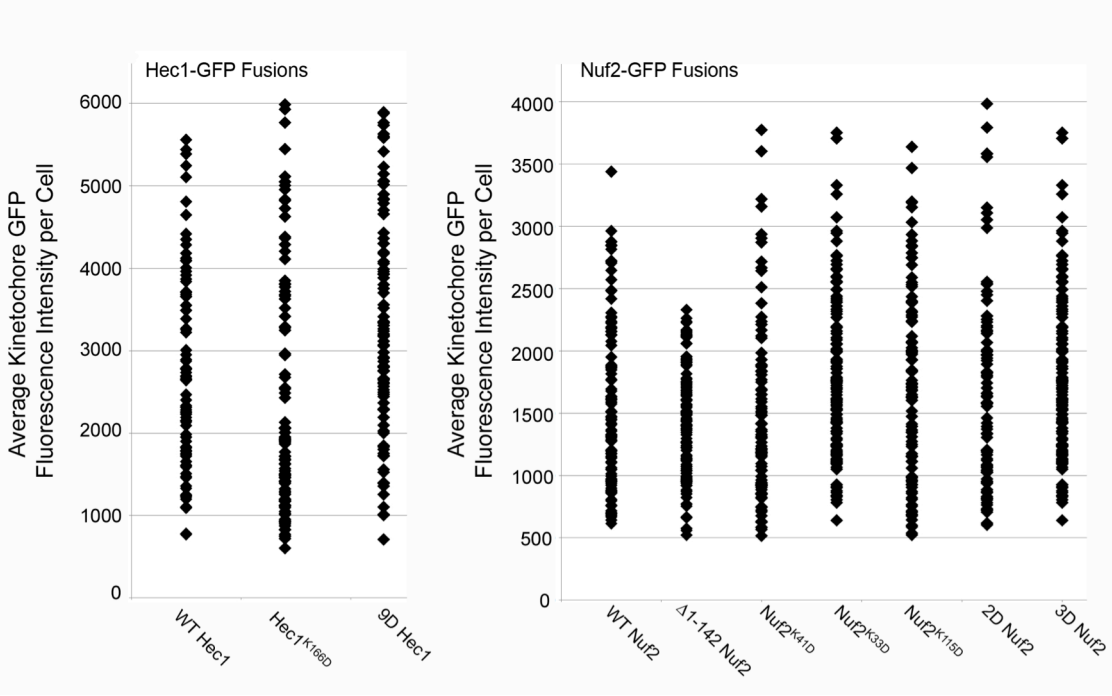


**Supplemental Figure 3.2. Quantification of GFP fluorescence intensity in fixed cells expressing rescue fusion proteins.** Cells were transfected with Hec1 or Nuf2 Cy5-labeled siRNAs and the indicated GFP fusion was subsequently expressed (described in Materials and Methods). For each rescue, GFP fluorescence intensity at kinetochores was quantified for every cell, and the average intensity per cell is shown in the graphs. For Hec1 rescue experiments, only cells whose average GFP fluorescence intensity at kinetochores fell between 600 and 6000 counts were included for phenotype analysis. For Nuf2 rescue experiments, only cells whose average GFP fluorescence intensity at kinetochores fell between 500 and 4000 counts were included for phenotype analysis. From left to right on the graphs above, the following numbers of cells and kinetochores (respectively) were scored and used for analysis: WT Hec1: 91, 910; Hec1$^{K166D}$: 101, 1027; 9D Hec1: 104, 1017; WT Nuf2: 96, 1113; D1-142 Nuf2: 119, 1105; Nuf2$^{K41D}$: 96, 921; Nuf2$^{K33D}$: 93, 942 ; Nuf2$^{K115D}$: 99, 1040; 2D Nuf2: 95,1004; 3D Nuf2: 134, 1130.

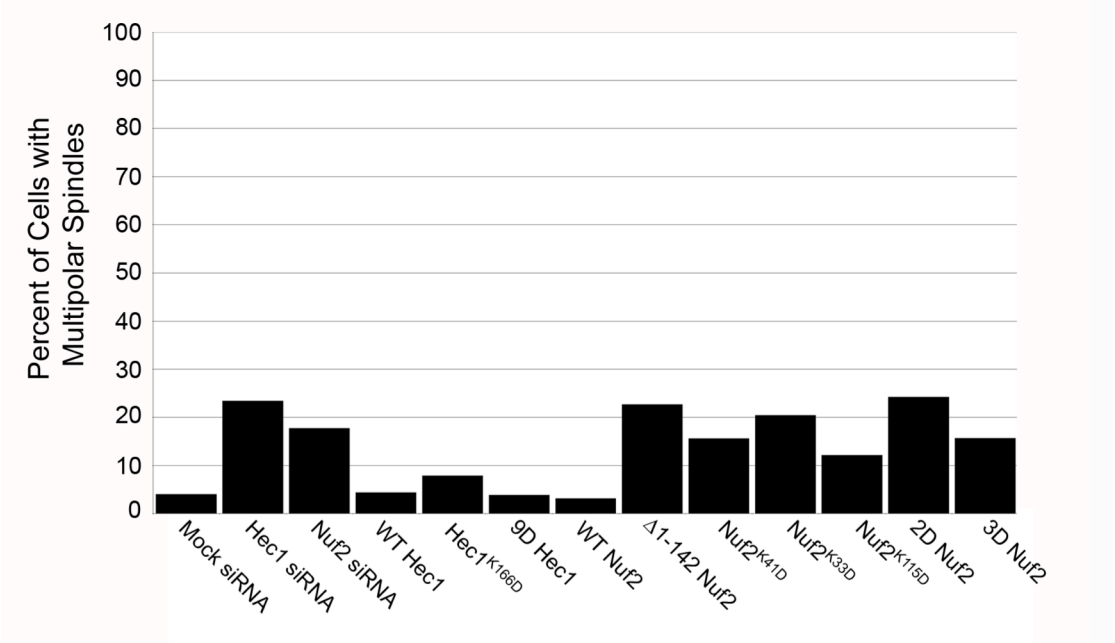


**Supplemental Figure3.3. Percent of cells with multipolar spindles.** Cells were mock-transfected, transfected with the indicated siRNA, or transfected with the indicated siRNA and subsequently rescued with the indicated GFP fusion. Cells were fixed and immunostained with anti-tubulin antibodies, and the percent of cells with multipolar spindles was scored (n>100 cells were analyzed for each condition).

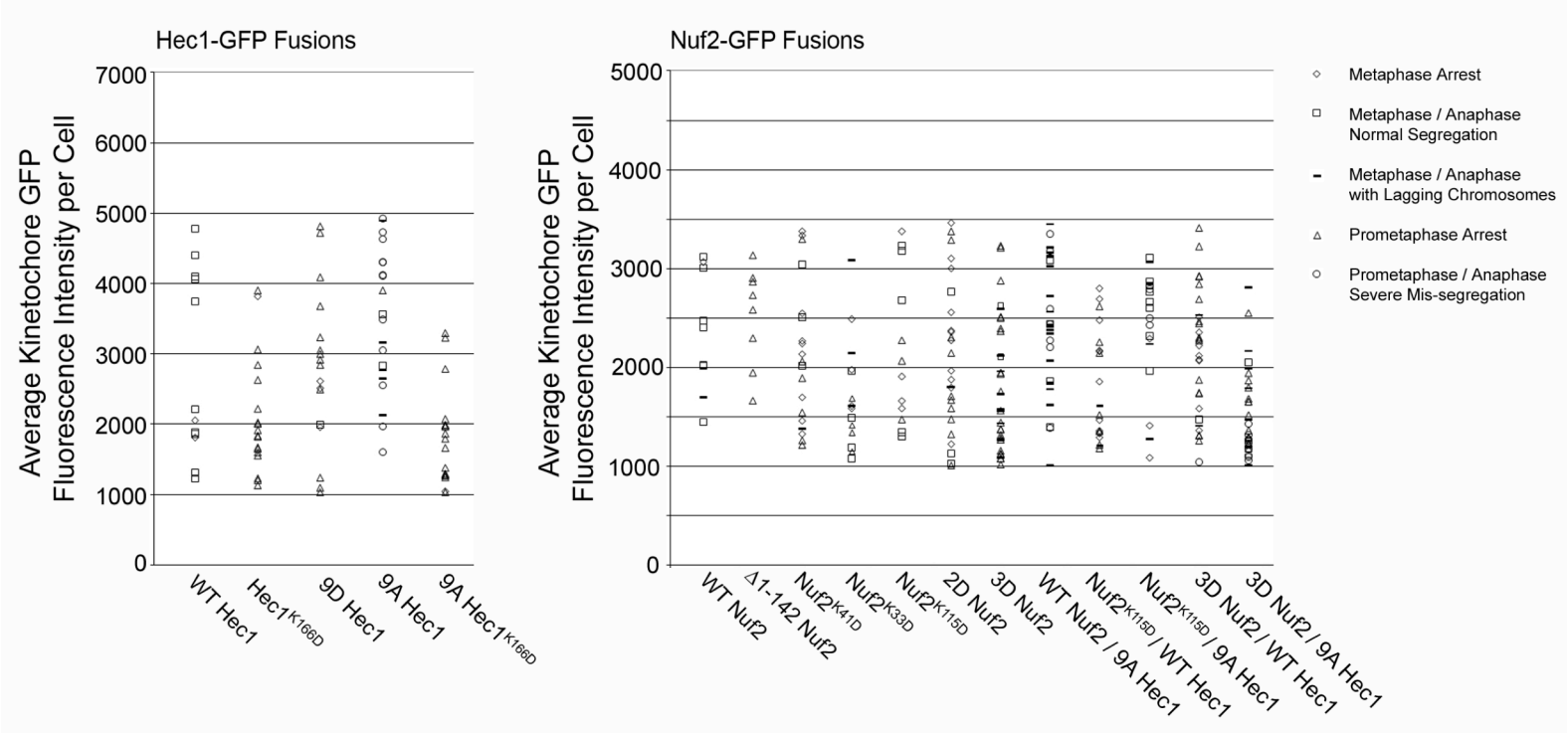
Hec1-GFP Fusions
Average Kinetochore GFP Fluorescence Intensity per Cell
7000
6000
5000
4000
3000
2000
1000
0
WT Hec1
Hec1K166D
9D Hec1
9A Hec1
9A Hec1K166D
Nuf2-GFP Fusions
Average Kinetochore GFP Fluorescence Intensity per Cell
5000
4000
3000
2000
1000
0
WT Nuf2
Δ1-142 Nuf2
Nuf2K41D
Nuf2K33D
Nuf2K115D
2D Nuf2
3D Nuf2
WT Nuf2 / 9A Hec1
Nuf2K115D / WT Hec1
Nuf2K115D / 9A Hec1
3D Nuf2 / WT Hec1
3D Nuf2 / 9A Hec1
Metaphase Arrest
Metaphase / Anaphase Normal Segregation
Metaphase / Anaphase with Lagging Chromosomes
Prometaphase Arrest
Prometaphase / Anaphase Severe Mis-segregation

**Supplemental Figure 3.4. Quantification of GFP fluorescence intensity in live cells expressing rescue fusion proteins.** Cells were transfected with Hec1 or Nuf2 Cy5-labeled siRNAs, the indicated GFP fusion was subsequently expressed, and cells were time-lapse imaged. For each rescue, GFP fluorescence intensity at kinetochores was quantified for every cell, and the average intensity per cell is shown in the graphs. For each time-lapse sequence, kinetochore fluorescence intensity measurements were taken from one of the first 5 frames of filming to ensure the measurements were not affected by photo-bleaching. For Hec1 rescue experiments, only cells whose average GFP fluorescence intensity at kinetochores fell between 1000 and 5000 counts were included for phenotype analysis. For Nuf2 rescue experiments, only cells whose average GFP fluorescence intensity at kinetochores fell between 1000 and 3500 counts were included for phenotype analysis. For each cell, the mitotic progression phenotype was scored, and these phenotypes are indicated on the graphs. Importantly, within the kinetochore fluorescence intensity ranges for the cells used for this study, we found no correlation between phenotype and GFP fluorescence intensity at kinetochores. The following numbers of cells and kinetochores were scored and used for analysis: WT Hec1: 12, 123 ; Hec1$^{K166D}$: 18, 160; 9D Hec1: 17, 197; 9A Hec1: 20, 205; 9A Hec1$^{K166D}$: 18, 200; WT Nuf2: 10, 127; D1-142 Nuf2: 8, 91; Nuf2$^{K41D}$: 19, 208; Nuf2$^{K33D}$: 15, 159; Nuf2$^{K115D}$: 12, 235; 2D Nuf2: 25, 346; 3D Nuf2: 34, 355; WT Nuf2/9A Hec1: 28, 272; Nuf2$^{K115D}$/ WT Hec1: 20, 167; Nuf2$^{K115D}$/9A Hec1: 19, 195; 3D Nuf2/WT Hec1: 29, 282; 3D Nuf2/9A Hec1: 39, 400.

# CHAPTER IV

## The loop domain of Hec1 is required for stable kinetochore-microtubule attachments in mitosis

My contribution to the work in this chapter includes carrying out the experiments, and data analysis and interpretation for the figures shown.

### 4.1 Introduction

Equal segregation of duplicated chromosomes is required for successful completion of mitosis. Driving this process are attachments between kinetochores and microtubules of the mitotic spindle. Central to forming and regulating kinetochore-microtubule attachments is the NDC80 complex, comprised of Hec1, Nuf2, Spc24, and Spc25 (DeLuca et al., 2006; Cheeseman et al., 2006). The structure of the NDC80 complex is that of a long rod, with the Spc24/Spc25 dimer on the C-terminal end, proximal to the chromatin and acting as an anchor for the entire complex. The N-terminal portion of the NDC80 complex is formed by the globular CH domains of the Hec1/Nuf2 dimer, which are poised for direct interactions with microtubules. Within the Hec1 protein there is a portion of the coiled domain that is unpaired with Nuf2 and forms what has been named the “loop” domain. In humans the loop domain is approximately 40 amino acids and is predicted to be a β-sheet perhaps involved protein-protein

interactions (Maiolica et al., 2007; Hsu et al., 2011; Maure et al., 2011). In both budding yeast and fission yeast, Hec1 mutants that had the loop domain deleted or mutated failed to support stable kinetochore-microtubule interactions (Hsu et al., 2011; Maure et al., 2011). The mechanism by which the loop domain functioned in generating stable kinetochore-microtubule attachments differed between organisms. In budding yeast, the loop domain is required for NDC80 complex-Dam1 interactions and for efficient loading of the Dam1 complex on kinetochores (Maure et al., 2011). In fission yeast the loop domain is required for recruitment of accessory proteins required for stable kinetochore-microtubule attachment (Hsu et al., 2011). In both budding yeast and fission yeast the SAC is active in the context of Hec1 loop domain mutants, halting mitotic progression (Hsu et al., 2011; Maure et al., 2011). These data support the idea that the loop domain of Hec1 may play a role in kinetochore-microtubule attachment in mammalian cells. To this end, we designed a Hec1 mutant in which the primary amino acid sequence of the loop domain had been completely changed. Using an siRNA-mediated silence and rescue system we assessed the ability of HeLa cells to generate stable kinetochore-microtubule attachments in fixed cells and also assayed the ability of cells expressing this mutant to progress through mitosis. Here we show that the loop domain of Hec1 is required to generate stable kinetochore-microtubule attachments to facilitate chromosome alignment and the progression of cells through mitosis. We also demonstrate that the Hec1 loop domain is required for the recruitment of Cdt1, a member of the origin of replication complex (ORC). Thus, the loop domain represents a distinct domain

within the Hec1 protein of the NDC80 complex that is required to form a fully functional microtubule binding site at the outer kinetochore. These data also indicate a previously uncharacterized mitotic role for Cdt1.

## 4.2 Results

### 4.2.1 The loop domain of Hec1 is required for kinetochore-microtubule attachment in cells

HeLa cells were depleted of endogenous Hec1 by siRNA and rescued with either wild-type (WT) Hec1 or a mutant in which the sequence of the loop domain had been completely altered fused to GFP (Hec1 Loop$^{MUT}$-GFP) (Figure 4.1A). Cells were fixed and assayed for their ability to align chromosomes at the spindle equator. Cells rescued with Hec1 Loop$^{MUT}$-GFP were largely unable to align chromosomes at the metaphase plate (Figure 4.1, B and C). Cells were scored as “mostly unaligned” if there were >10 chromosomes off of the metaphase plate or if the cell lacked a well-defined metaphase plate. Cells in which 5-10 chromosomes were not aligned on a metaphase plate were scored as “partially aligned” while cells ≤4 chromosomes off of a metaphase plate were scored as “mostly aligned”. Over 70% of cells rescued with Hec1 Loop$^{MUT}$-GFP had mostly unaligned chromosomes, similar to cells depleted of Hec1 by siRNA, while the majority of cells rescued with WT Hec1-GFP had mostly aligned chromosomes (Figure 4.1, B and C). These data suggest that the loop domain is required for kinetochore-microtubule attachment to facilitate chromosome alignment.

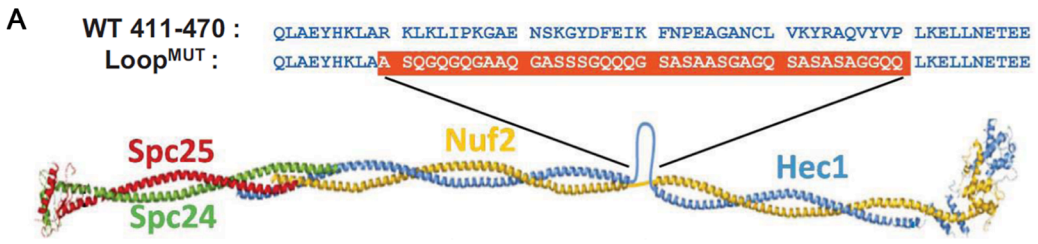
A
WT 411-470 :
Loop^MUT :
QLAEYHKLAR KLKLIPKGAE NSKGYDFEIK FNPEAGANCL VKYRAQVYVP LKELLNETEE
QLAEYHKLAA SQGQGQGAAQ GASSSGQQQG SASAASGAGQ SASASAGGQQ LKELLNETEE
Spc25
Spc24
Nuf2
Hec1

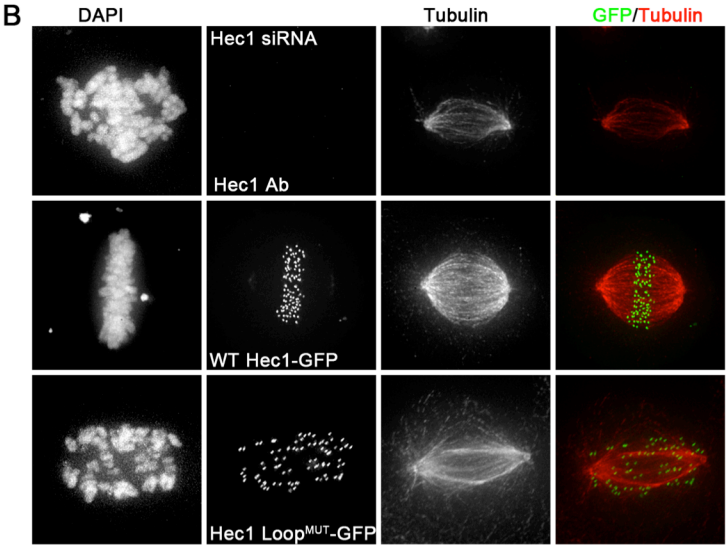
B
DAPI
Tubulin
GFP/Tubulin
Hec1 siRNA
Hec1 Ab
WT Hec1-GFP
Hec1 Loop^MUT-GFP

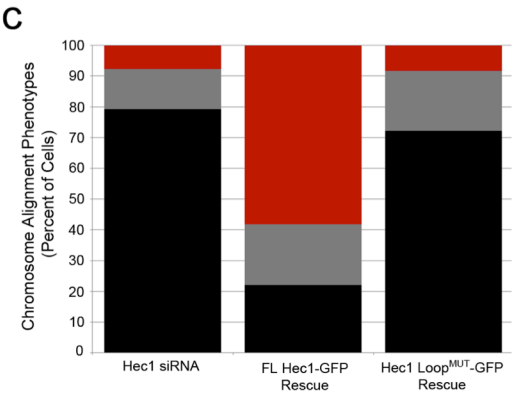
C
Chromosome Alignment Phenotypes (Percent of Cells)
100
90
80
70
60
50
40
30
20
10
0
Hec1 siRNA
FL Hec1-GFP Rescue
Hec1 Loop^MUT-GFP Rescue

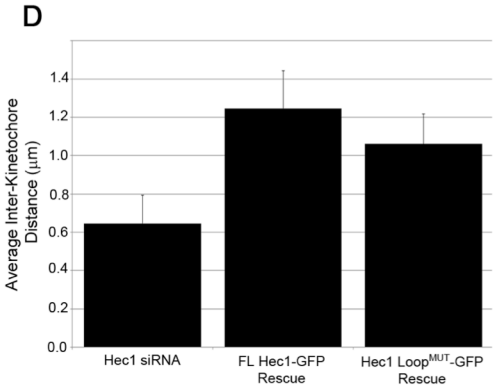
D
Average Inter-Kinetochore Distance (μm)
1.4
1.2
1.0
0.8
0.6
0.4
0.2
0.0
Hec1 siRNA
FL Hec1-GFP Rescue
Hec1 Loop^MUT-GFP Rescue

**Figure 4.1. The Hec1 loop domain is required for kinetochore-microtubule attachment in cells. A)** Schematic of Hec1 Loop$^{MUT}$, a mutant in which the entire primary sequence of the Hec1 loop domain has been altered. The position and length of the loop are retained (Adapted from Varma et al., in press). **B)** Immunofluoresence images showing HeLa cells that have been depleted of Hec1 by siRNA and rescued with either WT Hec1-GFP or Hec1 Loop$^{MUT}$-GFP. **C)** Quantification of chromosome alignment phenotypes in cells depleted of Hec1 and cells rescued with WT Hec1-GFP or Hec1 Loop$^{MUT}$-GFP. Cells with mostly aligned chromosomes (red) had <5 chromosomes off of a well-formed metaphase plate, cells with partially aligned chromosomes (gray) had 5-10 chromosomes off of a metaphase plate, and cells with mostly unaligned chromosomes (black) had >10 chromosomes off of a metaphase plate or lacked any chromosome alignment. **D)** Quantification of average interkinetochore distances measured in cells depleted of Hec1 or cells depleted of Hec1 and rescued with either WT Hec1-GFP or Hec1 Loop$^{MUT}$-GFP. Interkinetochore distances were measured from GFP centroid to GFP centroid in cells rescued with GFP-fusion proteins or from ACA centroid to ACA centroid in cells depleted of Hec1. Interkinetochore distances were measured on bioriented kinetochore pairs in cells rescued with Hec1-GFP fusion proteins.

Next, we measured inter-kinetochore distances to monitor microtubule attachment status in cells rescued with WT or mutant Hec1. As sister kinetochore pairs gain attachments to microtubules from opposing spindle poles, tension is exerted, increasing the distance between sister kinetochores. Thus, the inter-kinetochore distance can be measured as readout for microtubule attachment to the kinetochore. Cells rescued with WT-Hec1-GFP had an average inter-kinetochore distance of 1.25 (± 0.15μm) at metaphase. Cells rescued with Hec1 Loop$^{MUT}$-GFP had a reduced inter-kinetochore distance (1.06± 0.16μm) when compared to cells rescued with WT Hec1-GFP, but greater than that of cells depleted of Hec1 (0.65 ± 0.15μm) (Figure 4.1D). These data indicate that the loop domain of Hec1 is required for generating kinetochore-microtubule attachments that can produce wild-type levels of tension across sister kinetochore pairs.

### 4.2.2 The Hec1 loop domain is required for progression through mitosis and anaphase entry

Although the chromosome alignment phenotype in cells rescued with Hec1 Loop$^{MUT}$-GFP was severe, there was a population of cells that had partially or mostly aligned chromosomes. To assess the stability of kinetochore-microtubule attachments in cells that reached metaphase or a metaphase-like phase, cells were subjected to ice cold buffer prior to fixation. Microtubules that are attached to kinetochores are more resistant to cold treatment than microtubules that have not established connections with kinetochores (Salmon

and Begg, 1980). Cells rescued with Hec1 Loop$^{MUT}$-GFP had a ~50% reduction in cold-stable microtubules in metaphase-like cells when compared to metaphase cells rescued with WT Hec1-GFP, suggesting a reduction in the stability in kinetochore-microtubule attachments in these cells (Figure 4.2, A and B).

Because of the reduction in the average inter-kinetochore distance and kinetochore-microtubule attachment stability in cells rescued with Hec1 Loop$^{MUT}$-GFP, we wanted to ask if these cells could enter anaphase. To this end, cells were depleted of endogenous Hec1 and rescued with either WT Hec1-GFP or Hec1 Loop$^{MUT}$-GFP and co-transfected with mCherry-histone H2B to follow chromosomes. Time-lapse imaging of living cells revealed that the large majority of cells (12/13) rescued with WT Hec1-GFP entered anaphase in average of 42 ± 21min (Figure 4.2C, upper panel). All cells rescued with Hec1 Loop$^{MUT}$-GFP (29/29) arrested in mitosis for at least 5 hours, of which 86% arrested in prometaphase and a small population (14%) arrested in a metaphase-like state (Figure 4.2C, lower panel).

To assess the nature of the mitotic arrest observed in cells rescued with Hec1 Loop$^{MUT}$-GFP, we assayed for the presence of the SAC protein Mad1 at kinetochores. The SAC acts as a surveillance system to prevent premature anaphase entry, thus avoiding chromosome missegregation. Mad1 is present at kinetochores that lack microtubule attachments and is largely absent from kinetochores at metaphase (Campbell et al., 2001). Compared to cells rescued with WT Hec1-GFP there was a 4.5-fold increase the in amount of Mad1 at kinetochores in cells rescued with Hec1 Loop$^{MUT}$-GFP (Figure 4.2, D and E;

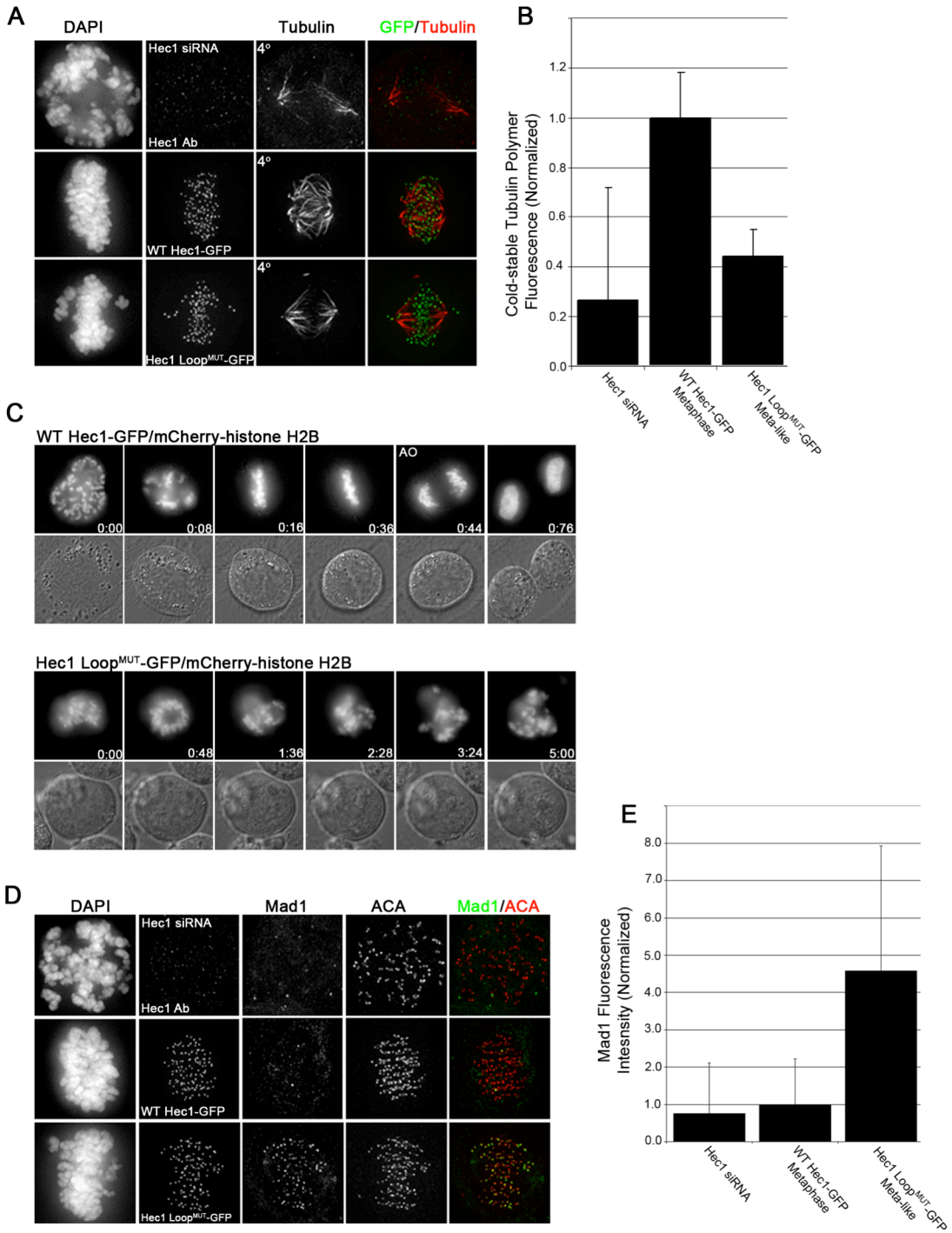
A
DAPI
Tubulin
GFP/Tubulin
Hec1 siRNA
Hec1 Ab
4°
WT Hec1-GFP
Hec1 Loop^MUT-GFP
B
Cold-stable Tubulin Polymer Fluorescence (Normalized)
0.0
0.2
0.4
0.6
0.8
1.0
1.2
Hec1 siRNA
WT Hec1-GFP Metaphase
Hec1 Loop^MUT-GFP Meta-like
C
WT Hec1-GFP/mCherry-histone H2B
0:00
0:08
0:16
0:36
AO
0:44
0:76
Hec1 Loop^MUT-GFP/mCherry-histone H2B
0:00
0:48
1:36
2:28
3:24
5:00
D
DAPI
Mad1
ACA
Mad1/ACA
Hec1 siRNA
Hec1 Ab
WT Hec1-GFP
Hec1 Loop^MUT-GFP
E
Mad1 Fluorescence Intesnsity (Normalized)
0.0
1.0
2.0
3.0
4.0
5.0
6.0
7.0
8.0
Hec1 siRNA
WT Hec1-GFP Metaphase
Hec1 Loop^MUT-GFP Meta-like

**Figure 4.2. The Hec1 loop domain is required for stable kinetochore-microtubule attachments and mitotic progression. A)** Immunofluorescence images of cells subjected to a cold-induced microtubule-depolymerization assay. **B)** Quantification of cold-stable microtubule polymer remaining in the mitotic spindle after cold treatment. Values are represented as relative numbers; all conditions normalized to cells depleted of Hec1 and rescued with WT Hec1-GFP. **C)** Still images from time-lapse acquisitions of HeLa cells depleted of Hec1 and rescued with either WT Hec1-GFP or Hec1 Loop$^{MUT}$-GFP. Cells were co-transfected with mCherry-histone H2B to follow chromosomes during imaging. Time shown as hr:min. Anaphase onset (AO) is indicated for cells that enter anaphase. The DIC image corresponds to the same time point shown in the mCherry image. **D)** Immunofluorescence images of cells depleted of Hec1 and cells depleted of Hec1 and rescued with WT Hec1-GFP or Hec1 Loop$^{MUT}$-GFP and stained for the SAC protein Mad1 in cells with bioriented chromosomes. **E)** Quantification of Mad1 fluorescence intensity at kinetochores represented as a value normalized to cells rescued with WT Hec1-GFP.

Table 4.1). These data indicate that the SAC is active in cells rescued with Hec1 Loop$^{MUT}$-GFP even as they reach a metaphase-like state, suggesting that disruption of the loop domain does not inhibit Mad1-dependent SAC signaling from the kinetochore.

### 4.2.3 The Hec1 loop domain is required for recruitment of Cdt1 to the kinetochore

Our data suggest that the loop domain of Hec1 is required for the process of kinetochore-microtubule attachment and mitotic progression. Previous studies in both budding and fission yeasts showed that the loop domain of Hec1 is required for recruitment of proteins that are needed for the generation of stable kinetochore-microtubule attachments (Hsu et al., 2011; Maure et al., 2011). Thus, we next asked if the loop domain of Hec1 affected the recruitment of proteins also required for stable kinetochore-microtubule attachment. We found that Ska complex components were present at kinetochores in cells rescued with either WT Hec1-GFP or Hec1 Loop$^{MUT}$-GFP. Similarly, ZW10 and KNL1 were each present at kinetochores in cells rescued with either WT Hec1-GFP or Hec1 Loop$^{MUT}$-GFP (Table 4.1). In collaboration with the Salmon and Cook groups at the University of North Carolina Chapel Hill, we found that Cdt1, a protein required for DNA replication origin licensing, fails to localize to kinetochores expressing Hec1 Loop$^{MUT}$-GFP, but localizes with WT Hec1 to kinetochores in cells (Varma et al., in press). Furthermore, depletion of Cdt1 largely recapitulates the phenotype in cells rescued with Hec1 Loop$^{MUT}$-GFP (Machida et

**Table 4.1 The Hec1 loop domain is required for Cdt1 recruitment to kinetochores.** The presence or absence of proteins at kinetochores was assessed by immunofluorescence in cells depleted of Hec1 and rescued with WT Hec1-GFP or Hec1 Loop$^{MUT}$-GFP.

| Protein | WT Hec1-GFP | Hec1 Loop$^{MUT}$-GFP |
|---|---|---|
| Ska3 (meta) | + | + |
| ZW10 | + | + |
| KNL1 | + | + |
| Mad1 (meta) | - | + |
| Cdt1 | + | - |

al., 2005; Sclafani and Holzen, 2007; Varma et al., in press). These data suggest that the loop domain of Hec1 is required for recruitment of Cdt1 to kinetochores during mitosis. Our data also demonstrate a previously unknown mitosis-specific role for Cdt1 in kinetochore-microtubule attachment.

### 4.3 Discussion

Here we have identified and characterized the Hec1 loop domain, a 40 amino acid interruption in the coiled-coil that is unpaired with Nuf2. The presence and position of the loop is conserved from yeast to humans, but the function of this domain has remained undefined, particularly at vertebrate kinetochores. Cells depleted of Hec1 and rescued with Hec1 Loop$^{MUT}$-GFP are unable to generate stable kinetochore-microtubule attachments as demonstrated by chromosome alignment and inter-kinetochore distance measurements. Furthermore, time-lapse imaging of living cells showed that all cells rescued with this mutant arrest in mitosis and fail to enter anaphase. The nature of the mitotic arrest in cells rescued with Hec1 Loop$^{MUT}$-GFP is likely due to an active SAC and the presence of significantly increased levels of Mad1 at kinetochores as compared to cells rescued with WT Hec1-GFP. Finally, Cdt1 recruitment to the kinetochore is dependent on the Hec1 loop domain and depletion of Cdt1 from cells largely phenocopies cells rescued with Hec1 Loop$^{MUT\text{-}GFP}$. Together these data suggest that the loop domain of Hec1 is required for recruiting Cdt1 to the kinetochore to facilitate the generation of stable kinetochore-microtubule

attachments that can sustain wild-type levels of tension to promote mitotic progression.

The severe kinetochore-microtubule attachment defects caused by Hec1 Loop$^{MUT}$ are somewhat surprising considering that a truncated form of the NDC80 complex that lacks the loop domain can bind microtubules in vitro (Ciferri et al., 2008). Recent studies in yeast, however, have demonstrated that the Hec1 loop domain is required for recruitment of the Dam1 complex in budding yeast or Dis1/TOG in fission yeast (Hsu et al., 2011; Maure et al., 2011). Although the primary sequence of the loop domain is not conserved from yeast to humans our data suggest that the loop domain may be functionally conserved to act as a hub for protein-protein interactions to facilitate kinetochore-microtubule attachment.

The mechanism behind Cdt1-dependent microtubule attachment stability may be to confer an extended structure to the NDC80 complex. At kinetochores that completely lack microtubule attachments, the average separation between the N- and C-terminal ends of the NCD80 complex is ~19nm in both controls and cells that lack Cdt1 (Wan et al., 2009; Varma et al., in press). In control metaphase cells, this distance increases to 42nm, but the NDC80 complex only achieves partial extension (~29nm) in cells depleted of Cdt1. The loop domain resides ~16nm from the CH domain of Hec1, which has been shown to be required for kinetochore-microtubule attachments and is thought to make direct contacts with the microtubule lattice (Wilson-Kubalek et al., 2008; Alushin et al., 2010; Sundin et al., 2011; Tooley et al., 2011). However, the plus-end of a kinetochore-microtubule extends over 60nm beyond the N-terminus of Hec1,

which puts the loop domain in the proximity of the microtubule wall (Wan et al., 2009). We propose a model of microtubule binding in which Cdt1 physically links the Hec1 loop to microtubules directly or to a microtubule-associated protein to stabilize the extended conformation of the NDC80 complex and enhance microtubule binding (Varma et al., in press).

The dual function of Cdt1 in DNA replication licensing and kinetochore-microtubule attachment may represent a mechanism to coordinate chromosome duplication with chromosome segregation, processes that much each be tightly regulated. Aberrant regulation of Cdt1 has the potential to affect both DNA replication licensing and mitosis. Overexpression of Cdt1 or Hec1 is known to promote genome instability and aneuploidy, which are hallmarks of most cancers and birth defects (Arentson et al., 2002; Diaz-Rodriguez et al., 2008; Tatsumi et al., 2006; Liontos et al., 2007). Here we have demonstrated a partnership between Hec1 and Cdt1 in generating stable kinetochore-microtubule attachments, which not only highlights a previously unknown mitotic function of Cdt1, but perhaps also elucidates a mechanism for genome preservation.

# CHAPTER V

## Incremental phosphorylation of the Hec1 tail domain regulates kinetochore-microtubule attachment strength

My contribution to the work in this chapter includes the design and optimization of the acquisition and analysis of the spindle pole separation rate data. Additionally, I have been involved with interpreting all of the data presented here and have contributed to experimental design for both the in vivo and in vitro assays.

### 5.1 Introduction

Cell division is driven by kinetochore-microtubule attachment, a dynamic process during which the plus ends of microtubules are captured by microtubule-binding components at the outer kinetochore. Microtubules that are bound to kinetochores continue to polymerize and depolymerize at their plus-ends, providing the force by which chromosomes are moved during mitosis. This requires that binding events between kinetochores and microtubules be strong enough to harness the forces generated by dynamic microtubules, yet labile enough to promote movement of the kinetochore along the microtubule lattice and to correct inappropriate attachments.

It is common early in mitosis for kinetochores to make incorrect attachments to microtubules resulting in monotelic, syntelic, or merotelic

attachments. It is imperative that these errors be corrected to allow kinetochores to 'reset' and attempt to make correct attachments to microtubules. Additionally, as chromosomes become bi-oriented and aligned at the metaphase plate, they oscillate across the spindle equator due to coordinated polymerization and depolymerization of microtubules attached to kinetochores.

Microtubule dynamics are thought to be vitally important for normal chromosome segregation, and are regulated by mitotic kinases such as Aurora B kinase (ABK). However, the mechanism of how the stability of kinetochore-microtubule attachments is regulated remains unknown. Several proteins have been implicated in regulating microtubule dynamics at the kinetochore, however the prevailing view is that direct regulation of kinetochore-microtubule attachment strength is through the NDC80 complex (Maiato et al., 2004; Stumpff et al., 2008). Two dimers, Spc24-Spc25 and Hec1-Nuf2, make up this highly elongated complex, which is anchored into the kinetochore by the Spc24-Spc25 moiety (Ciferri et al., 2005; DeLuca et al., 2006). Recent cryo-electron microscopy studies paired with X-ray crystallography demonstrated that the primary point of contact with microtubules resides within the Hec1 calponin homology (CH) domain, a known microtubule-binding motif (Ciferri et al., 2008; Wilson-Kubalek et al., 2008; Alushin et al., 2010). However, Hec1 also has an unstructured N-terminal 'tail', which is required for kinetochore-microtubule attachment in vivo and high affinity microtubule binding of NDC80 complexes in vitro (Wei et al., 2007; Ciferri et al., 2008; Guimaraes et al., 2008; Miller et al., 2008). This tail is a target for Aurora kinases in vitro and in vivo: its hyper-phosphorylation

destabilizes kinetochore-microtubule attachments and weakens binding of purified NDC80 complexes to microtubules, suggesting that Hec1 is a major target through which Aurora kinases regulate kinetochore-microtubule attachments (DeLuca et al., 2006; Cheeseman et al., 2006; Ciferri et al., 2008; Guimaraes et al., 2008; DeLuca et al., 2011). There are nine putative ABK phosphorylation sites that have been mapped in vitro along the length of the Hec1 tail, five of which have been confirmed in vivo (Cheeseman et al., 2006; DeLuca et al., 2011). How the Hec1 tail domain participates in microtubule binding and how this binding is phospho-regulated, however, remains debated. One idea is that phosphorylation acts as an on/off switch, toggling between full binding and full release. The evidence to support this comes from in vivo studies demonstrating that phospho-mimetic mutations to the Hec1 tail (Ser/Thr → Asp) inhibit kinetochore-microtubule attachments while a phospho-deficient mutant (Ser/Thr → Ala) results in hyper-stable attachments (Guimaraes et al., 2008; DeLuca et al, 2011). However, it has also been shown that cells expressing a non-phosphorylatable (phospho-deficient) Hec1 mutant cannot generate wild-type oscillations of kinetochores across the spindle equator (DeLuca et al., 2011). These data led to the hypothesis that phosphorylation of the Hec1 tail acts as a sensitive tuner of kinetochore-microtubule attachment stability rather than a simple toggle. Here we set out to test the idea that the regulation of the binding affinity between kinetochores and microtubules must be tightly regulated and finely tuned to support proper chromosome segregation. To this end, we have generated a series of Hec1 mutants containing phospho-mimetic

substitutions in a phospho-deficient background. Using this system we can prevent endogenous phosphorylation of the Hec1 tail domain and precisely control the number and position of residues that are mutated to mimic phosphorylated amino acids. Using an siRNA-mediated silence and rescue system, we assessed the kinetochore-microtubule attachment phenotype in PtK1 cells and characterized the microtubule binding properties of these Hec1 mutants in vitro. Additionally, we have used mathematical modeling to predict the stability of kinetochore-microtubule attachments in cells in response to Hec1 phosphorylation.

## 5.2 Results

### 5.2.1 A Hec1 mutant containing three phospho-mimetic substitutions enables error correction kinetics most similar to WT Hec1

Previous reports have indicated that Hec1 phosphorylation is required for microtubule release from the kinetochore and regulation of chromosome movements, supporting the hypothesis that phosphorylation of Hec1 is required to regulate attachment strength (DeLuca et al., 2011). To test this idea, we used an siRNA-mediated silence and rescue system in PtK1 cells. Cells were depleted of endogenous Hec1 and rescued with either WT or mutant Hec1 protein fused to GFP. Cells were rescued with a series of mutants in which one, two, three, or four ABK target sites were mutated to Asp (D) to mimic phosphorylation, while the remaining ABK sites were mutated to Ala (A) to prevent any endogenous phosphorylation (Figure 5.1). This system afforded

## In vivo

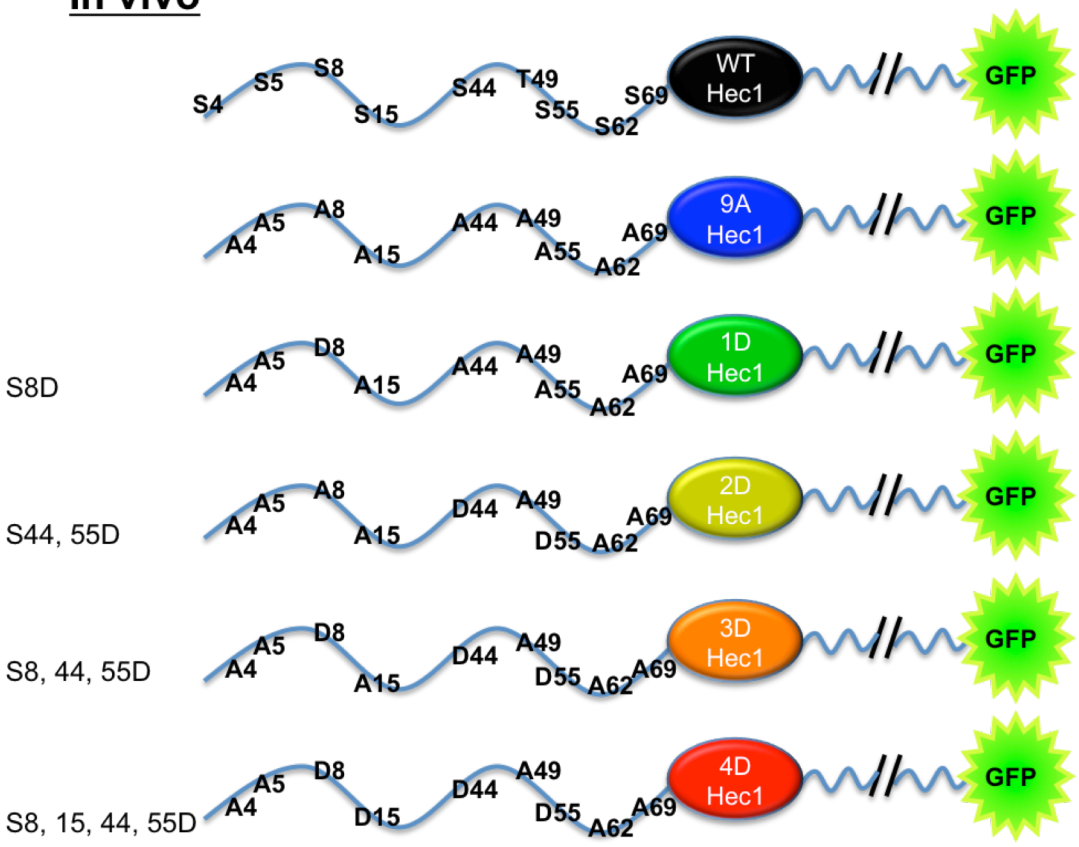


## In vitro

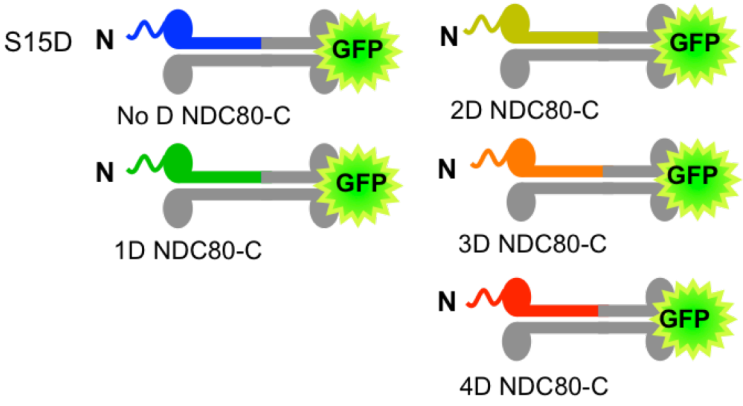

**Figure 5.1. Schematic of Hec1 and NDC80$^{Bonsai}$ constructs used for both in vivo and in vitro experiments.** The top panel shows each of the WT and Hec1 phospho-mimetic mutants used for the in vivo silence and rescue experiments. The relative positions of the nine Aurora B kinase phosphorylation sites within the N-terminal tail domain of Hec1 are shown. In each of the phospho-mutants used, the position of the phospho-mimetic (D) or phospho-deficient (A) substitutions are shown. The bottom panel shows a schematic of the NDC80$^{Bonsai}$-GFP complexes used for the in vitro experiments. The "N" shows the position of the N-terminus of Hec1. The remaining proteins of the NDC80$^{Bonsai}$-GFP complex (Nuf2, Spc24, and Spc25; all shown in gray) have not been mutagenized. The positions of the phospho-mimetic substitutions were the same for both the in vivo experiments and the in vitro analyses.

precise control of both the number and position of phospho-mimetic sites on the Hec1 tail.

We first wanted to ask how many phospho-mimetic mutations are required for efficient correction of erroneous kinetochore-microtubule attachments. Cells were treated with monastrol, a small molecule inhibitor of Eg5, a kinesin motor required for spindle pole separation early in mitosis. Upon entry into mitosis, monastrol-treated cells fail to separate their spindle poles, remain monopolar, and have an increased number of incorrect microtubule attachments to kinetochores. Upon monastrol washout, spindle poles begin to separate, but the rate of spindle bipolarization is dependent on the release of microtubules from kinetochores (DeLuca et al., 2011). Thus, we used the rate of spindle pole separation to assay the efficiency of error correction in cells. Using time-lapse images of live cells, we were able to measure the distance between spindle poles over time and calculate the rate of spindle pole separation in cells expressing either WT or phospho-mimetic Hec1 mutant proteins. All cells were co-transfected with mCherry-tubulin (Figure 5.2, A-D). Cells rescued with WT Hec1-GFP had an average rate of spindle pole separation of 0.83 ±0.29 μm/min, similar to cells that were transfected with mCherry-tubulin alone (0.82 ±0.26 μm/min). Cells expressing 9A-Hec1-GFP had an average spindle pole separation rate of 0.55 ±0.20 μm/min, which was 34% slower than the rate of spindle pole separation in cells expressing WT-Hec1-GFP. Interestingly, cells treated with the ABK inhibitor ZM447439 throughout imaging had an average rate of spindle pole separation of 0.53 ±0.24 μm/min, which was most similar to cells rescued with 9A

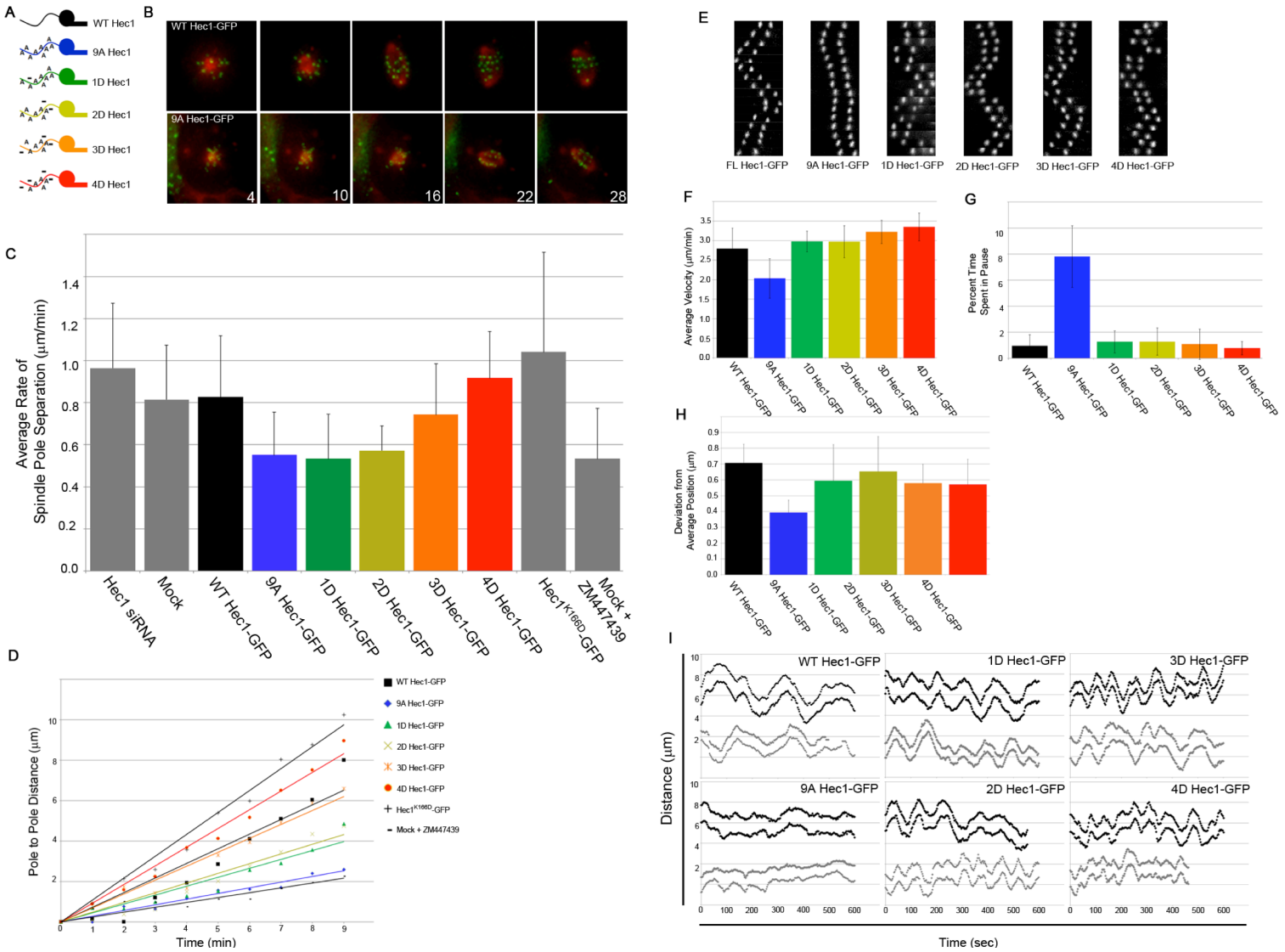
A
WT Hec1
9A Hec1
1D Hec1
2D Hec1
3D Hec1
4D Hec1
B
WT Hec1-GFP
9A Hec1-GFP
4
10
16
22
28
C
Average Rate of Spindle Pole Separation (μm/min)
Hec1 siRNA
Mock
WT Hec1-GFP
9A Hec1-GFP
1D Hec1-GFP
2D Hec1-GFP
3D Hec1-GFP
4D Hec1-GFP
Hec1K168D-GFP
Mock + ZM447439
D
Pole to Pole Distance (μm)
Time (min)
WT Hec1-GFP
9A Hec1-GFP
1D Hec1-GFP
2D Hec1-GFP
3D Hec1-GFP
4D Hec1-GFP
Hec1K168D-GFP
Mock + ZM447439
E
FL Hec1-GFP
9A Hec1-GFP
1D Hec1-GFP
2D Hec1-GFP
3D Hec1-GFP
4D Hec1-GFP
F
Average Velocity (μm/min)
G
Percent Time Spent in Pause
H
Deviation from Average Position (μm)
I
Distance (μm)
WT Hec1-GFP
1D Hec1-GFP
3D Hec1-GFP
9A Hec1-GFP
2D Hec1-GFP
4D Hec1-GFP
Time (sec)

**Figure 5.2. Incremental phoshphorylation of the Hec1 tail is required for distinct kinetochore functions. A**). Schematic representing the Hec1 phospho-mimetic mutants used for in vivo studies. For all "D" mutants, the remaining ABK phosphorylation sites were mutated to Ala. **B**) Representative still images from time-lapse movies of monastrol-treated PtK1 cells. Time shown in minutes post-monastrol washout. Green = Hec1-GFP; Red = mCherry-tubulin. **C**) Average rates of spindle pole separation were calculated by measuring the distance between spindle poles after monastrol washout from time-lapse movies of PtK1 expressing phospho-mimetic mutants of Hec1. **D**) Representative tracks from single cells showing the distance between spindle poles over time. Solid line is linear fit of first 9 timepoints, indicating the rate of spindle pole separation for a single cell. **E**) Kymographs of representative sister kinetochore pairs from cells depleted of endogenous Hec1 and rescued with indicated mutants. **F**) Quantification of average velocity of kinetochore movement in cells rescued with Hec1 mutants. Both pole-ward and away from the pole movements were measured. **G**) Quantification of percent time in pause. If a kinetochore did not move for two sequential time points (6 seconds), a kinetochore was scored as 'paused'. The percentage of time spent 'paused' was then calculated from the total time of the time-lapse image sequence. **H**) Quantification of deviation from average position of kinetochore pairs. **I)** Representative plot of sister kinetochore pairs oscillating over time. For each Hec1 mutant used, two sister kinetochore pairs are shown. In **C, F-H** errors bars represent standard deviation.

Hec1-GFP (Figure 5.2, C and D). We found that as the number of phospho-mimetic mutations in the Hec1 tail increased, the rate of spindle pole separation increased. A Hec1 tail domain with either 3 or 4 phospho-mimetic mutations resulted in cells with an average rate of spindle pole separation most similar to WT-Hec1-GFP, and overall the average rates of spindle pole separation changed stepwise with an increasing number of substitutions (Figure 5.2, C and D). These data suggest that the rate of spindle pole separation after monastrol treatment, and thus error correction efficiency by microtubule release from kinetochores, is dependent on phosphorylation of the Hec1 tail. These data also suggest that phosphorylation of Hec1 by ABK is the principal mechanism of microtubule attachment error correction during mitosis (Figure 5.2, C and D).

### 5.2.2 A Hec1 mutant with a single phospho-mimetic substitution facilitates wild-type oscaillations

As chromosomes become bioriented, kinetochores continue to oscillate across the spindle equator to facilitate chromosome alignment. We have demonstrated that error correction efficiency requires that 3-4 sites in the Hec1 tail be phosphorylated, however oscillatory movements of kinetochores along microtubules may require a tighter grip on microtubules such that kinetochores can move with dynamic microtubule plus ends without completely releasing the microtubule. We next asked how many phospho-mimetic substitutions on the Hec1 tail are required to recapitulate wild-type kinetochore oscillations. We measured the oscillation kinetics of cells rescued with WT-Hec1-GFP and found

that they oscillated normally, while cells rescued with 9A Hec1-GFP did not (DeLuca et al., 2011). Strikingly, we found that cells expressing a Hec1 mutant with just one phospho-mimetic substitution (1D Hec1-GFP) exhibited kinetochore oscillation movements most similar to cells expressing WT-Hec1-GFP (Figure 5.2, E-I). Representative kymographs and representative tracks of sister kinetochore pairs showed that a phospho-deficient Hec1 mutant (9A Hec1-GFP) did not exhibit kinetochore oscillations, consistent with previous data, while cells expressing 1D Hec1-GFP regained oscillatory movements (DeLuca et al., 2011; Figure 5.2, E and I). Measurements of the average velocity, percent time spent paused, and deviation from average position also showed that cells expressing 1D Hec1-GFP had oscillations most similar to cells rescued with WT Hec1-GFP (Figure 5.2, F-H). As the number of phospho-mimetic substitutions was increased, the kinetochore oscillations became erratic, similar to a Hec1 mutant that does not bind microtubules (4D Hec1-GFP) (Figure 5.2, E-I). These data suggest that the strength of kinetochore-microtubule attachments is sensitive to small changes in phosphorylation to the Hec1 tail. Furthermore, these data suggest that only a low level of phosphorylation (1 site) is required for appropriate kinetochore oscillations, while a greater level of phosphorylation (3-4 sites) is required for efficient error correction.

### 5.2.3 Phospho-mimetic substitutions disrupt interactions of individual NDC80 complexes with microtubules

It has been demonstrated that the Hec1 tail is required for microtubule binding in vivo and in vitro and that a phospho-mimetic Hec1 mutant cannot support stable kinetochore-microtubule attachment (Ciferri et al., 2008; Guimaraes et al., 2008; Miller et al., 2008). However, how the Hec1 tail mediates tight binding to microtubules is not known. One model suggests that the tail binds microtubules directly and phosphorylation disrupts electrostatic interactions between the positively charged Hec1 tail and the negatively charged tubulin E-hooks. Alternatively, it has been suggested that the tail domain is positioned between adjacent NDC80 complexes, with phosphorylation preventing oligomerization, thus preventing tight binding between the NDC80 complex and microtubules. To gain molecular insight into how phosphorylation of Hec1 affects microtubule binding, we used in vitro TIRF (total internal reflection fluorescence) microscopy assays to characterize how phospho-mimetic substitutions in the Hec1 tail domain affect the ability of individual NDC80 complexes to bind and diffuse along microtubules (Figure 5.3A). These experiments were carried out in collaboration with Ekaterina Grishchuk's laboratory at the University of Pennsylvania. We used the same system of introducing phosho-mimetic substitutions to the Hec1 tail as was carried out for the in vivo assays. For the in vitro assays, however, a truncated form of the NDC80 complex ($NDC80^{Bonsai}$) fused to GFP was recombinantly expressed and purified for use in the in vitro assays. $NDC80^{Bonsai}$ has a portion of the coiled-coil domain truncated, while the

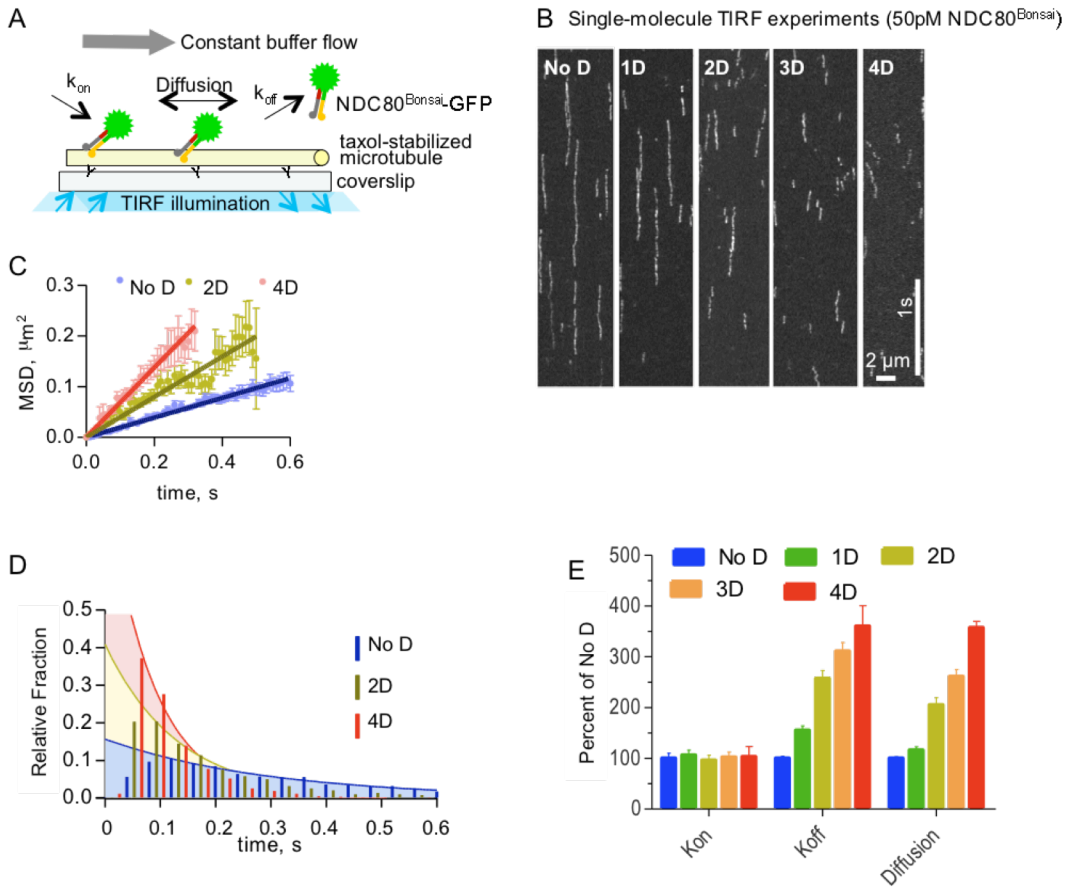


**Figure 5.3. Phospho-mimetic substitutions to the Hec1 tail disrupt NDC80 complex-MT interactions. A)** Schematic representation of our in vitro TIRF experiments. Taxol-stabilized microtubules were immobilized on the surface of a coverslip and purified NDC80$^{Bonsai}$ complexes containing WT or phospho-mimetic Hec1 proteins were flowed through the imaging chamber. **B)** Representative diffusion kymographs of single NDC80$^{Bonsai}$ – GFP complexes binding to microtubules. Stream acquisition with exposure time 10 ms. These data were used to determine association rate ($k_{on}$), residency time ($\tau$) and diffusion coefficient (D) as in JR Cooper et al., 2010. **C)** MSD (Mean Squared Displacement) plotted versus time for No D, 2D, and 4D NDC80$^{Bonsai}$-GFP mutants. Symbols are experimental data with SEM; lines are linear fit. Diffusion coefficient (D) is determined as a half of the slope for these curves. Values for other mutants lie between these curves. **D)** Histogram of lifetimes for No D and 4D NDC80$^{Bonsai}$-GFP mutants. Lines are exponential fit**. E)** Summary of single molecule parameters plotted as a percent of No D NDC80$^{Bonsai}$-GFP.

microtubule binding motifs have been left intact (Ciferri et al., 2008). Because there was no kinase in our in vitro experimental system, NDC80$^{Bonsai}$-GFP complexes containing a WT Hec1 protein will be referred to as No D NDC80$^{Bonsai}$ -GFP to reflect a complete lack of phosphorylation to this complex (Figure 5.1). Limiting concentrations of NDC80$^{Bonsai}$-GFP complexes were flowed over immobilized microtubules and were imaged using exposure times of 5-10msec to allow us to record the landings of individual NDC80$^{Bonsai}$ molecules on microtubules and their subsequent diffusion on the microtubule lattice (Figure 5.3B). Quantification of the brightness of the GFP-dots demonstrated that >90% of the recorded events corresponded to molecules with one GFP fluorophore, as expected for a single NDC80$^{Bonsai}$-GFP complex (Figure 5.4). Using this method we were able to determine the diffusion coefficient, residency time, and association and dissociation rate constants $k_{on}$ and $k_{off}$ for individual NDC80$^{Bonsai}$ complexes (Figure 5.3, Table 5.1).

From kymographs of individual NDC80$^{Bonsai}$ complexes binding to microtubules, the mean square displacement measurements were plotted and the diffusion coefficients were calculated (Figure 5.3, B and C). The diffusion coefficients of NDC80$^{Bonsai}$ varied from 0.1 to 1 $\mu m^2$/sec, with the diffusion coefficient of No D NDC80$^{Bonsai}$-GFP being ~0.1 $\mu m^2$/sec, consistent with previously reported values (Powers et al., 2009). The diffusion coefficient changed in response to the number of phospho-mimetic substitutions in NDC80$^{Bonsai}$-GFP, increasing in a stepwise manner (Figure 5.3, C and E). Using these single molecule data we also determined the residency times of No D and

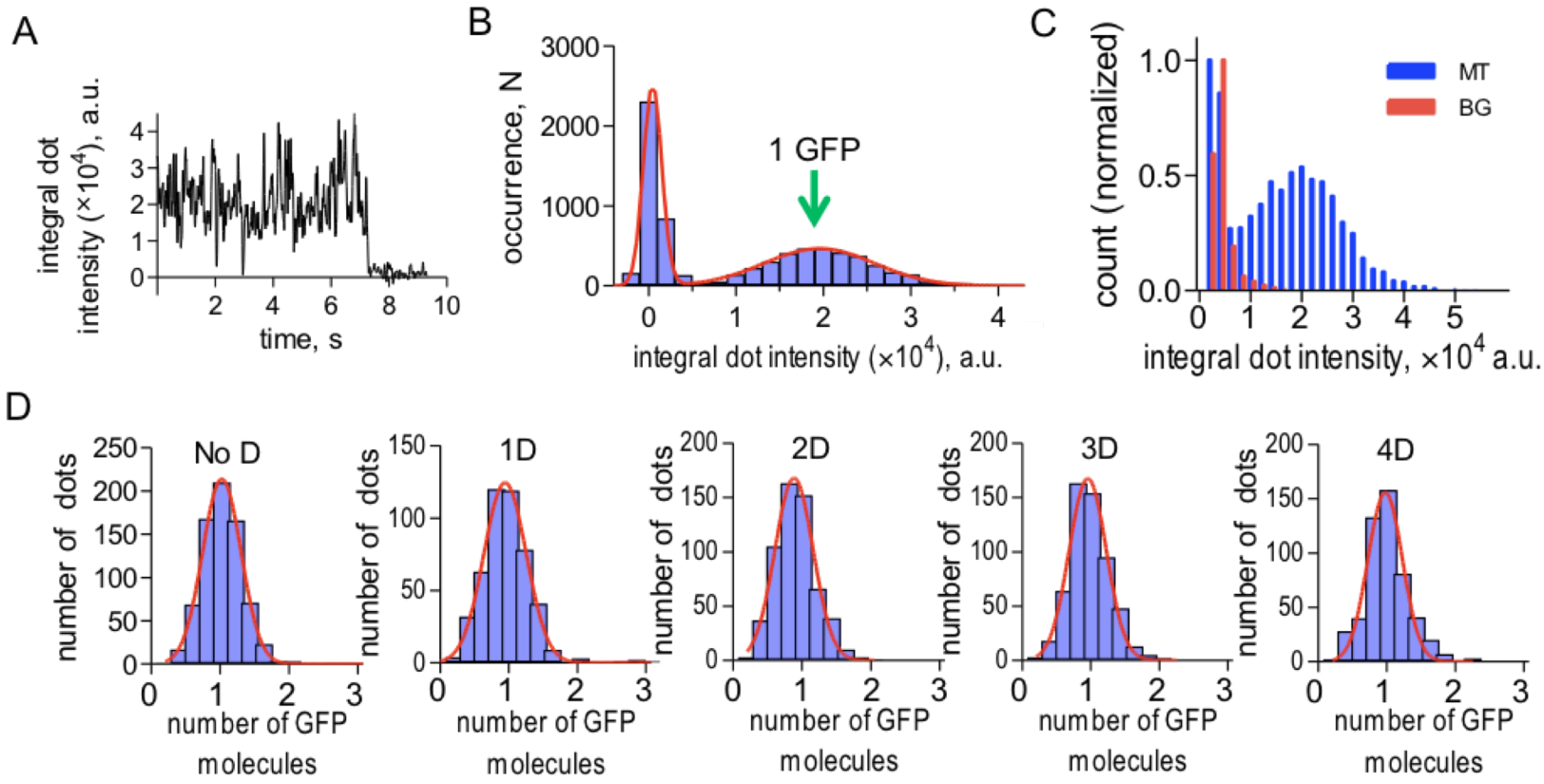
A
integral dot intensity (×10^4), a.u.
time, s
B
occurrence, N
1 GFP
integral dot intensity (×10^4), a.u.
C
count (normalized)
MT
BG
integral dot intensity, ×10^4 a.u.
D
No D
1D
2D
3D
4D
number of dots
number of GFP molecules

**Figure 5.4. Photobleaching kinetics of GFP molecules using TIRF microscopy. A)** Example of a photobleaching curve for GFP -Dam1 complexes immobilized of the surface of a coverslip. **B)** Histogram of integral intensities for the bleaching NDC80$^{Bonsai}$-GFP dots (n = 10). Fluorescence intensity of single GFP molecule was analyzed by fitting this histogram with equidistant Gaussian distributions. **C)** Automatic analysis of the maximal intensity of dots (n = 10000 analyzed frames; MT = microtubule; BG = background). **D)** Histogram distributions of the intensity of NDC80$^{Bonsai}$-GFP fusion proteins. Predominant species are single NDC80$^{Bonsai}$-GFP complexes. For all proteins >95% dots have a fluorescence intensity that corresponds to single GFP (with 95% confidence). At least 300 dots were analyzed for each NDC80$^{Bonsai}$-GFP mutant. Red lines are Gaussian fit.

**Table 5.1. Summary of experimental data collected from single molecule experiments and TIRF-based microtubule affinity measurements.** "N" denotes the number of experimental replicates; "n" denotes the number of individual events analyzed.

| | No D | 1D | 2D | 3D | 4D |
|---|---|---|---|---|---|
| | | | | | |
| Diffusion coefficient (D), $\mu m^2/s$ | 0.096±0.007 (N=2, n=719) | 0.111±0.002 (N=2, n=1324) | 0.197±0.004 (N=2, n=712) | 0.251±0.013 (N=2, n=830) | 0.343±0.001 (N=2, n=833) |
| Residency time (τ), ms | 417±23 | 250±14 | 143±5 | 117±5 | 100±8 |
| Dissociation rate ($k_{off}$), $s^{-1}$ | 2.40±0.13 (N=2, n=2682) | 4.00±0.22 (N=2, n=2643) | 7.00±0.20 (N=2, n=2779) | 8.56±0.35 (N=2, n=2652) | 10.01±0.84 (N=2, n=2819) |
| Association rate ($k_{on}$), $s^{-1}\mu m^{-1}nM^{-1}$ | 12.13±1.59 (N=2) | 12.86±0.93 (N=2) | 11.62±0.41 (N=2) | 12.41±0.52 (N=2) | 12.44±1.05 (N=2) |
| | | | | | |
| Initial slopes, a.u./nM | 177±16 (N=5) | 133±1 (N=3) | 90±3 (N=5) | 59±2 (N=3) | 44±3 (N=5) |
| Binding plateau ($B_{max}$), $x10^4$ a.u. | 7.6 ±0.2 (N=5) | 9.4±0.7 (N=3) | 8.8±0.8 (N=5) | 9.0±0.9 (N=3) | 6.3±0.5 (N=5) |
| Cooperativity factor (w) | 0.30±0.04 (N=5) | 0.50±0.1 (N=3) | 0.40±0.05 (N=5) | 0.45±0.05 (N=3) | 0.25±0.1 (N=5) |
| Dissociation constant ($K_D$), nM | 157±17 (N=5) | 306±36 (N=3) | 504±52 (N=5) | 767±89 (N=3) | 1801±113 (N=5) |

phospho-mimetic NDC80$^{Bonsai}$-GFP complexes on microtubules, as well as the association and dissociation rate constants $k_{on}$ and $k_{off}$. We found that the residency time decreased as the number of phospho-mimetic substitutions increased (Figure 5.3D). We also showed that $k_{on}$ is similar for No D and all of the NDC80$^{Bonsai}$ mutants tested, but $k_{off}$ increases about 4-fold from No D-Ndc80$^{Bonsai}$-GFP to 4D-Ndc80$^{Bonsai}$-GFP (Figure 5.3E). These data suggest that phosphorylation even at a single residue in the Hec1 tail domain affects the direct interactions between the NDC80 complex and microtubules, with the interactions becoming less persistent with increasing phosphorylation (Figure 5.3E and Table 5.1). Additionally, these data support a model of phospho-regulation of kinetochore-microtubule attachment strength that is mediated via direct contacts between the Hec1 tail and the microtubule, instead of through tail-mediated oligomerization of adjacent NDC80 complexes.

### 5.2.4 Phospho-mimetic substitutions do not change the cooperativity of NDC80 complexes binding to microtubules

We also tested how phosphorylation of the Hec1 tail affects NDC80-NDC80 interactions on the microtubule wall. Previous microtubule binding studies have shown that the NDC80 complex binds microtubules in a cooperative manner (Cheeseman et al., 2006). These conclusions, however, were drawn based on microtubule co-pelleting assays in which NDC80-induced bundling of the soluble microtubules may have affected the results. We used a TIRF approach using microtubules that are immobilized on the coverslip and cannot

bundle (Figure 5.3A). A wide range of concentrations of soluble NDC80$^{Bonsai}$-GFP was applied with constant flow to ensure that the measurements were taken at a constant protein concentration (Figure 5.5A). We first examined the fluorescence intensity of microtubules decorated with <10nM soluble NDC80$^{Bonsai}$-GFP. At this low concentration range the intensity of MT decoration increased linearly with increasing NDC80 concentration, indicating that these changes were due to single molecule interactions (Figure 5.5B). When this assay was carried out using higher concentrations, up to 0.8 μM, of NDC80$^{Bonsai}$-GFP, we found that the fluorescence intensity of microtubules increased non-linearly, consistent with NDC80-NDC80 interactions on the microtubule lattice (Figure 5.5C). To determine how phospho-mimetic substitutions affect interactions of adjacent NDC80$^{Bonsai}$-GFP complexes, we fit these binding curves to a model developed by McGhee and Hippel (1974) that explicitly includes intramolecular interactions (Figure 5.5D). We found that the $K_D$ of NDC80$^{Bonsai}$-GFP for microtubules decreased with an increasing number of phospho-mimetic substitutions but that the cooperativity ($w$) was unaffected (Figure 5.5E). The calculated packing density of NDC80$^{Bonsai}$-GFP complexes on the microtubule lattice, $B_{max}$, was also similar for No D NDC80$^{Bonsai}$-GFP and each of the phospho-mimetic mutants, corresponding to ~1.9±0.2 complexes per tubulin dimer at saturation, consistent with previous reports (Figure 5.5E) (Alushin et al., 2010). Together these data suggest that Hec1 phosphorylation directly affects the binding affinity between kinetochores and microtubules and that phosphorylation of the Hec1 tail disrupts direct interactions between NDC80

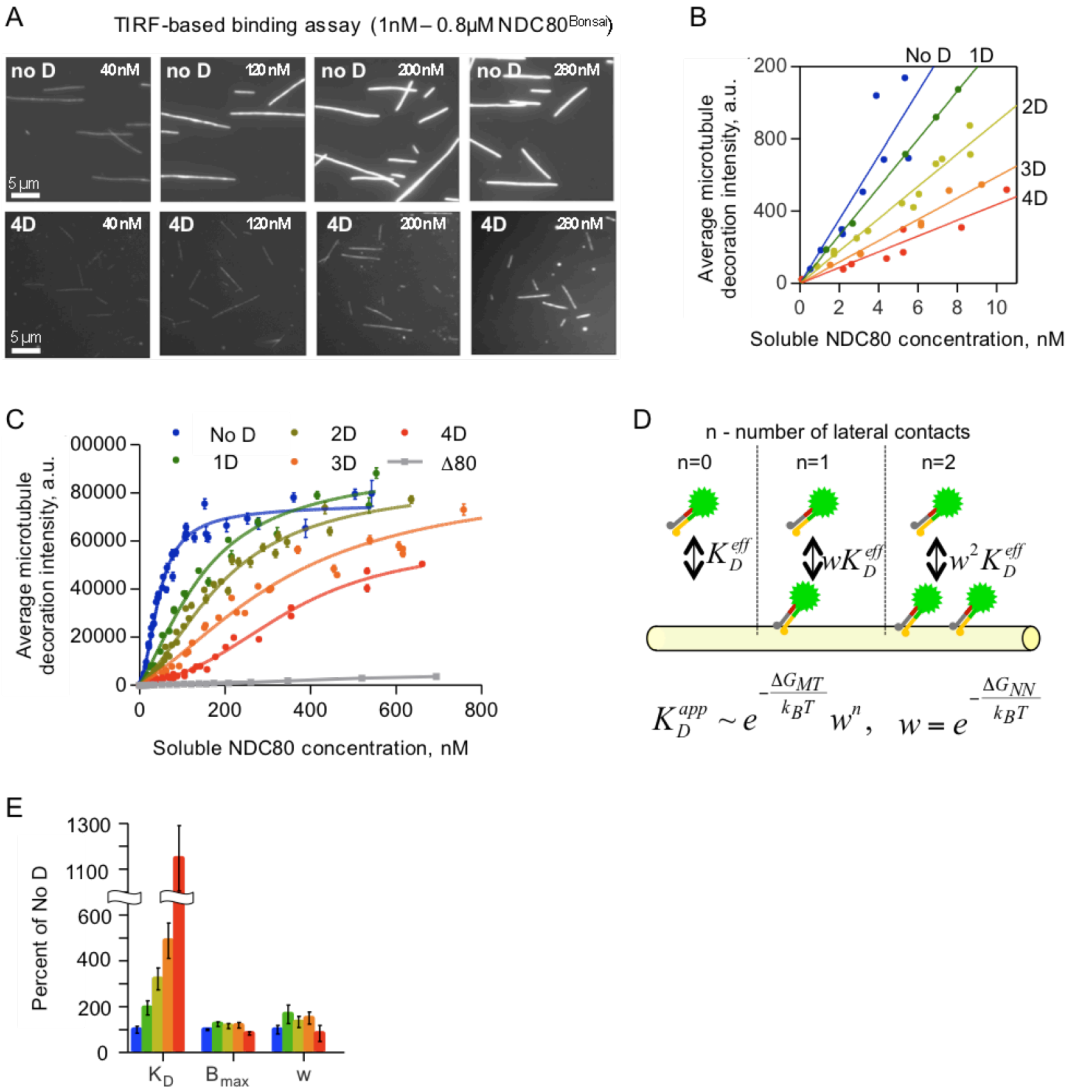


**Figure 5.5. Phospho-mimetic subsitutions to the Hec1 tail reduce the binding affinity of NDC80$^{Bonsai}$-GFP complexes for microtubules. A)** Representative images of fields of different concentrations of NDC80$^{Bonsai}$-GFP bound to unlabeled microtubules. Upper row of images are No D NDC80$^{Bonsai}$-GFP, bottom row are 4D NDC80$^{Bonsai}$-GFP. Each panel is the average of ten frames. **B)** Quantification of microtubule fluorescence intensities at very low concentrations of NDC80$^{Bonsai}$-GFP, showing the linear change in microtubule binding in response to phospho-mimetic substitutions. **C)** $K_D$ plotted for different NDC80$^{Bonsai}$ mutants based on fluorescence intensities of microtubules (Panel A). **D)** Schematic of model for NDC80 binding to microtubules. $K_D$ – dissociation constant for single molecules, $w$ – cooperativity factor. **E)** Comparison of $K_D$, cooperativity factor ($w$), and $B_{max}$ for different NDC80$^{Bonsai}$-GFP mutants.

complexes and microtubules instead of inhibiting oligomerization of adjacent NDC80 complexes.

### 5.2.5 Mathematical modeling predicts that small changes in Hec1 tail phosphorylation translate into changes in kinetochore-microtubule attachment stability

Several models of force generation at the kinetochore-microtubule interface have been proposed, including sleeves, rings, fibrils, and networks (Margolis and Wilson 1981; Hill, 1985; McIntosh et al., 2008; Dong et al., 2007). Structural studies of the kinetochore have not been able to unequivocally resolve how the microtubule binding site is organized. The placement of microtubule binding components will not only affect the physical arrangement of the kinetochore, but also how kinetochore-microtubule attachment stability is regulated. Using our in vivo data and the in vitro TIRF measurements, we have generated two models of the kinetochore, one with individual, pre-defined microtubule binding sites, and another with a continuous, fluid microtubule binding interface (Figure 5.6, A and B, respectively). Using these models we were able to ask how microtubule dynamics changed in response to phosphorylation of Hec1.

We first asked how many kinetochore-microtubules could accumulate at an individual kinetochore in response to an increasing number of phosphorylated residues on the Hec1 tail. In prophase, when the nuclear envelope is intact, interactions between kinetochores and microtubules are unable to occur. After

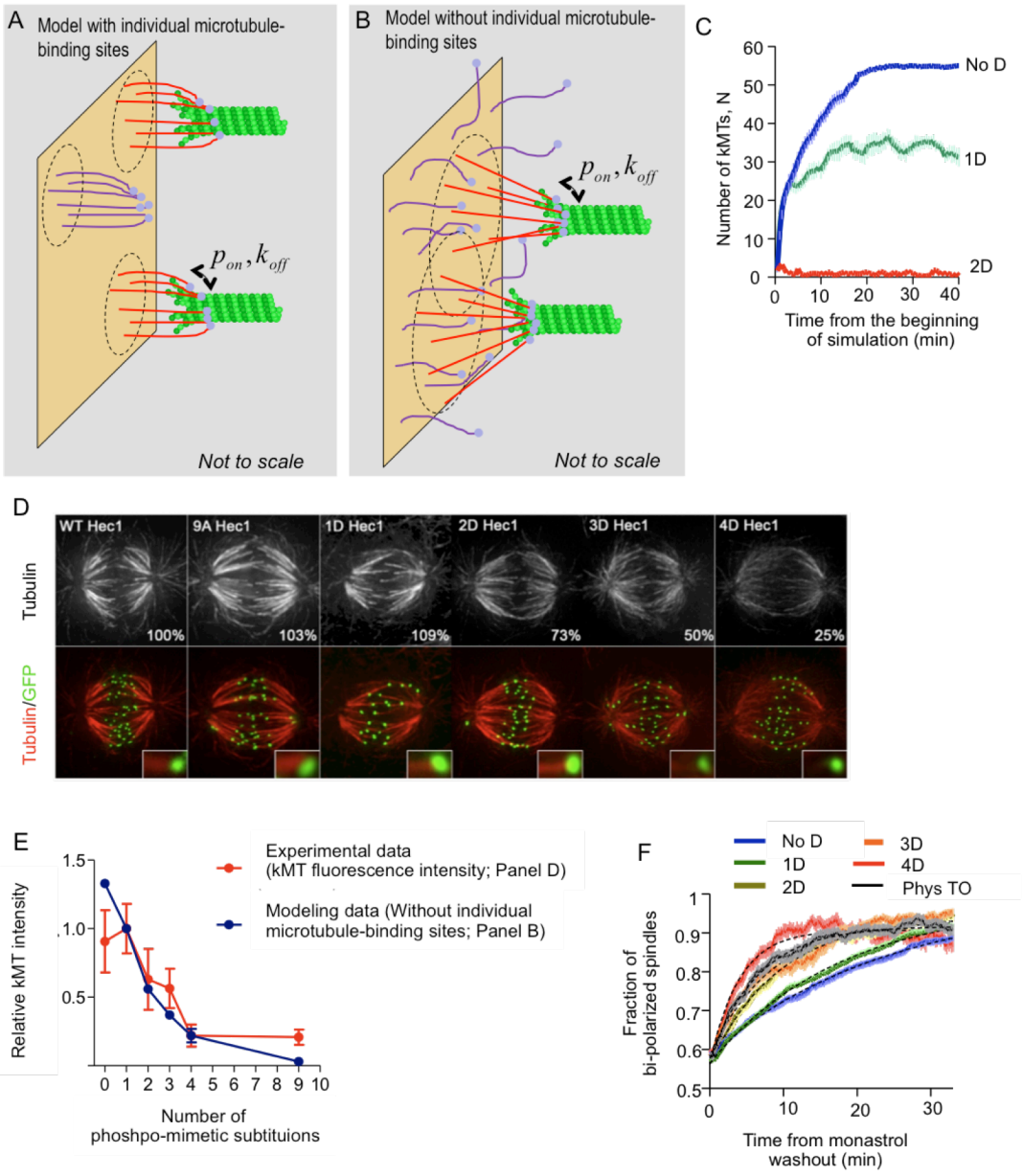
A
Model with individual microtubule-binding sites
$p_{on}, k_{off}$
Not to scale
B
Model without individual microtubule-binding sites
$p_{on}, k_{off}$
Not to scale
C
Number of kMTs, N
60
50
40
30
20
10
0
0
10
20
30
40
Time from the beginning of simulation (min)
No D
1D
2D
D
Tubulin
Tubulin/GFP
WT Hec1
9A Hec1
1D Hec1
2D Hec1
3D Hec1
4D Hec1
100%
103%
109%
73%
50%
25%
E
Relative kMT intensity
1.5
1.0
0.5
0 1 2 3 4 5 6 7 8 9 10
Number of phoshpo-mimetic subtituions
Experimental data (kMT fluorescence intensity; Panel D)
Modeling data (Without individual microtubule-binding sites; Panel B)
F
No D
1D
2D
3D
4D
Phys TO
Fraction of bi-polarized spindles
1
0.9
0.8
0.7
0.6
0.5
0
10
20
30
Time from monastrol washout (min)

**Figure 5.6. Small changes in Hec1 phosphorylation affect kinetochore-microtubule attachment stability. A and B)** Schematic representation of a model of microtubule interactions with a kinetochore. NDC80 complexes are attached to the kinetochore at one end. When a microtubule encounters the kinetochore, NDC80 complexes that can reach it (dotted circle) bind to the microtubule with $p_{on}/k_{off}$ probability. NDC80 complexes attached to microtubules are shown in red. If another microtubule approaches the kinetochore within the binding radius of neighboring NDC80 complexes (dotted circle), there is no redistribution of NDC80 complexes between kinetochore-microtubules (kMTs) in a model with predefined microtubule binding sites (Panel A). In a model where there the microtubule binding interface is continuous, NDC80 complexes redistribute between these two microtubules (Panel B). **C)** Simulation of kMT accumulation through mitosis in response to phosphophorylation of Hec1. **D)** PtK1 cells were depleted of Hec1 by siRNA and rescued with either WT or phospho-mimetic mutant Hec1 proteins fused to GFP. Cells were fixed in cold buffer and stained with anti-tubulin antibodies. The fluorescence intensity of kMT bundles was measured according to Cimini et al., 2003 (see Materials and Methods). **E)** The number of kMTs present in the context of phospho-mimetic $NDC80^{Bonsai}$ complexes was calculated from our model and normalized to 1D $NDC80^{Bonsai}$ (blue) and compared to experimental data from cold-treated PtK1 cells (red). **F)** Calculations, based on the model, of error correction efficiency in response to increasing phosphorylation of the Hec1 tail ("Phys TO" indicates calculations based on the microtubule turnover rate under physiological conditions).

nuclear envelope breakdown, microtubules encounter kinetochores and in human cells, for example, approximately 16 microtubules will bind a single kinetochore at metaphase (Wendell et al., 1993; McEwen et al., 2001). As shown in Figure 5.6C, simulations using microtubule binding parameters for No D NDC80$^{Bonsai}$-GFP indicate that a maximum number of kinetochore-microtubules (kMTs) could accumulate. As the number of phosphorylated sites increased, the accumulation of microtubules was drastically decreased. To test our model, we measured the fluorescence intensity of kinetochore-microtubule bundles in PtK1 cells depleted of Hec1 and rescued with WT and phospho-mimetic Hec1-GFP fusion proteins (Figure 5.6D). We found that in cells rescued with 9A or 1D Hec1-GFP the microtubule bundle fluorescence intensity was increased compared to cells rescued with WT Hec1-GFP. As the number of phospho-mimetic substitutions was increased, the fluorescence intensity of microtubules decreased, consistent with predictions from a model of the microtubule attachment site that lacks pre-defined binding sites (Figure 5.6E). Finally, we used the model to predict the number of bi-polarized spindles after monastrol washout in response to phosphorylation of Hec1. We found that the fraction of mitotic spindles that could bi-polarize was dependent on the number of phosphorylated residues, and as the number of substitutions increased the rate of spindle bi-polarization increased, consistent with our in vivo data (Figures 5.2C and 5.6F). Together these data suggest that small changes in the phosphorylation state of the Hec1 tail can translate into large changes in microtubule stability in the context of a complete kinetochore. Furthermore,

these data support a model of the kinetochore-microtubule interface that is made of a fluid and continuous array of microtubule binding proteins, rather than pre-defined microtubule binding sites, consistent with the previously suggested 'fibrous network' model of the outer kinetochore (Dong et al., 2007).

### 5.3 Discussion

Here we have shown that kinetochore-microtubule attachment strength is sensitive to small changes in phosphorylation of Hec1. Even a single phospho-mimetic substitution is enough to change NDC80-microtubule interactions in vivo and in vitro. One phospho-mimetic mutation promotes wild-type kinetochore oscillations and increasing the number of phospho-mimetic substitutions increases the error correction efficiency in cells. In vitro, the association and dissociation rate constants ($k_{on}$ and $k_{off}$), diffusion coefficient, and residency time for single molecules of $NDC80^{Bonsai}$ changed commensurately with the number of phospho-mimetic substitutions. These data suggest that phospho-regulation of kinetochore-microtubule attachment is mainly through interactions between the NDC80 complex and microtubules rather than NDC80-NDC80 interactions. Interestingly, the affect on the $K_D$ measured from $NDC80^{Bonsai}$ complexes in bulk solution is more pronounced than the change in the off rate for single NDC80 molecules suggesting a modest decrease in NDC80-NDC80 interactions. However, phospho-mimetic substitutions to Hec1 only weakly affect the cooperativity of NDC80 complexes binding to microtubules. Together these data suggest that the tail domain principally functions to bind microtubules directly and

does not make a significant contribution to the cooperative nature of NDC80-microtubule interactions.

Finally, using mathematical modeling we have demonstrated that small changes in Hec1 tail phosphorylation can translate into large changes in kinetochore-microtubule attachment stability in the context of a complete kinetochore (Figure 5.7, Top Panel). As the number of phosphorylated sites increases, the lifetime of microtubule bundles decreases, ultimately resulting in an increased rate of microtubule turnover at the kinetochore promoting functions like error correction. When phosphorylation is low, however, microtubule bundles are more stable and have a longer lifetime, which translates into stable kinetochore-microtubule attachments that can support chromosome alignment and kinetochore oscillations. Together these data indicate that the regulation of kinetochore-microtubule attachment strength is not an all-or-nothing mechanism and that phospho-regulation acts as a sensitive tuner rather than a simple toggle between microtubule binding and release (Figure 5.7, Bottom Panel). This mode of regulation is important in cells to facilitate discrete functions of the kinetochore during mitotic progression that ultimately culminate with chromosome alignment at the spindle equator and accurate chromosome segregation in anaphase.

Our data highlight the molecular mechanism of regulation of kinetochore-microtubule attachment strength through phosphorylation of the Hec1 tail domain. Although phosphorylation has been long shown to regulate protein-protein interactions, to the best of our knowledge, incremental phosphorylation is a novel mechanism of regulating microtubule binding proteins. Interestingly,

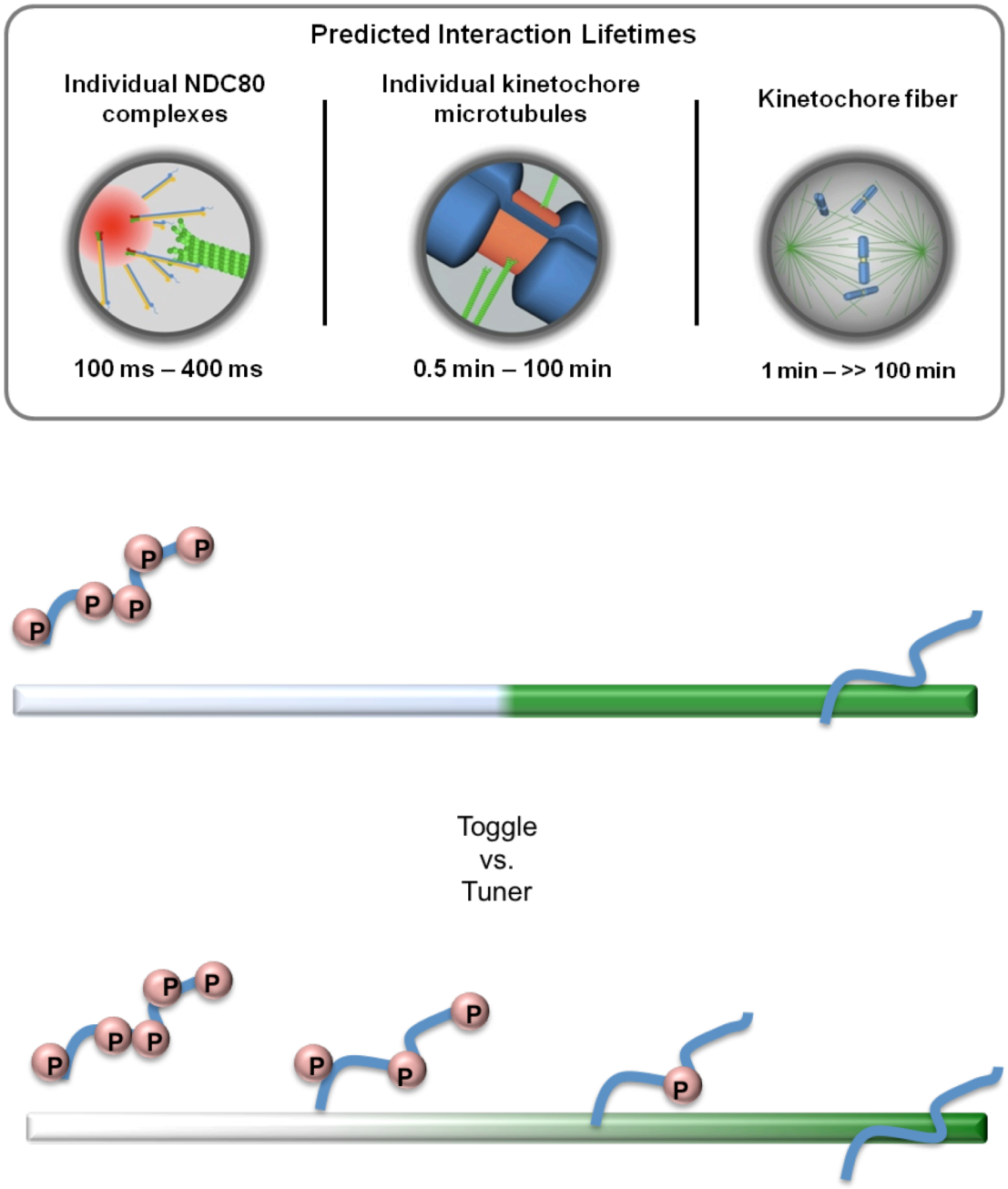


**Figure 5.7. Phosphoregulation of kinetochore-microtubule attachments acts as a sensitive tuner to facilitate varied functions of the kinetochore through mitosis.** In the top panel, the interaction lifetimes at the kinetochore as predicted from the model. In the bottom panel, a schematic illustrates that incremental phosphorylation of the Hec1 tail results in a finely tuned gradient of binding affinities for microtubules instead of a simple toggle for binding or release of microtubules.

incremental phosphorylation is not a new way of regulating protein interactions with other molecules, such as DNA. The transcriptional cofactor PC4 has a 60 amino acid, lysine-rich, unstructured N-terminal domain that contains multiple phosphorylation sites that regulate its DNA binding activity (Jonker et al., 2006). Although functionally distinct, the structural and compositional similarities between the N-terminal domains of Hec1 and PC4 may imply a common mechanism of phospho-regulation by masking electrostatically driven interactions.

Our in vivo and in vitro systems allow for precise control of the number and position of phosphorylated sites within the Hec1 tail. Although we have clearly demonstrated that incremental phosphorylation can facilitate distinct functions of kinetochores, these studies open up the possibility that an exact subset of phosphorylated sites, not only in number but also in position, may be required for regulation of kinetochore-microtubule attachment in cells. Furthermore, these data support the idea that the Hec1 tail is never fully dephosphorylated during mitosis. This suggests that dephosphorylation of the Hec1 tail is selective; some sites are dephosphorylated while others remain. How the process of dephosphorylation is regulated, and how a phosphatase may play a role in phospho-regulation, is not clear in this instance. In yeast, it has been shown that meiotic kinases Cdk1 and Ime2 phosphorylate an overlapping set of substrates, leading to differential dephosphorylation by phosphatases (Holt et al., 2007). The Hec1 tail is phosphorylated on several sites by the mitotic kinase Mps1, some of which overlap with ABK sites (Kemmler et al., 2009). In

yeast it has been shown that PP1 opposes ABK-dependent phosphorylation of kinetochore components, but the activity of PP1 against Mps1-dependent phosphorylation of the Hec1 tail has not been tested (Liu et al., 2010). Directed mutagenesis to the overlapping ABK and Mps1 sites may offer insight into the mechanism of phospho-regulation at the level of both the kinase and the phosphatase. Additionally, this would implicate the phosphatase as an active player in phospho-regulation of kinetochore-microtubule attachments. The site-specificity of Hec1 tail phosphorylation and regulation of its dephosphorylation will certainly be an active area of further research.

### 5.4 Acknowledgements

The data in Chapter V are a collaborative effort between Jennifer DeLuca's laboratory at Colorado State University and Ekaterina Grishchuk's laboratory at the University of Pennsylvania. Special thanks to Keith DeLuca (CSU) for collecting and analyzing the kinetochore oscillation data and to Jeanne Mick (CSU) for purifying all of the proteins used for the in vitro assays. Anatoly Zaytsev (UPenn) carried out the in vitro studies and the mathematical modeling, as well as the analyses of those data.

# CHAPTER VI

## Conclusions and perspectives

The kinetochore is large molecular machine made of at least 100 parts. Here we have focused on characterizing the NDC80 complex, which is part of the KMN network, a supercomplex of proteins that form the core microtubule binding site at the outer kinetochore. In doing so we have been able to elucidate some of the molecular details of how kinetochore-microtubule attachments are generated and regulated. We have shown that the Hec1 N-terminus – the "toe" of the CH domain and the tail domain – are required to make direct contacts with microtubules. It is remarkable that such a small region within one protein at the kinetochore mediates such an important function. We have also shown that, unlike the Hec1 CH domain, the CH domain of Nuf2 does not likely interface the microtubule lattice. Although we were able to generate data to support structural work suggesting that the Nuf2 CH domain does not directly interface with the microtubule lattice, the explicit function of this protein motif is not known. Experiments using Hec1 and Nuf2 mutants in which the respective CH domains are 'swapped' may yield results that help answer this question. Likewise, if there are ~22 NDC80 complexes per microtubule, then the dimensions of the Hec1/Nuf2 dimer can lead one to believe that adjacent NDC80 complexes could

nearly encircle the outer diameter of a microtubule. This is not to imply that proper rings would form around the microtubule, but structural data indicate that the Nuf2 CH domain could interface with a negatively charged portion of the Hec1 CH domain, perhaps leading to a mode of NDC80-NDC80 oligomerization mediated by the Nuf2 CH domain. Although not definitive, experiments such as these may yield interesting results that help elucidate the function of the Nuf2 CH domain at the outer kinetochore.

Although Hec1 is typically considered a direct microtubule binding protein, it is now clear from our characterization that the loop domain does not likely bind microtubules directly and instead recruits accessory proteins to the kinetochore to promote stable kinetochore-microtubule attachments. These data emphasize the diverse functions of a single kinetochore component in the process of kinetochore-microtubule attachment and the importance of protein architecture at the microtubule binding site.

Here we have also shown that the N-terminal tail domain of Hec1 is absolutely required for not only directly binding microtubules, but also regulating kinetochore-microtubule attachment strength in cells. Our data support the idea that the tail domain regulates microtubule interactions with kinetochores through direct binding to the microtubule lattice instead of explicitly promoting oligomerization of adjacent NDC80 complexes. Furthermore, our data expose the possibility that phospho-regulation of kinetochore-microtubule attachment strength may rely on a specific subset of phosphorylated amino acids in the Hec1 tail. It will be important to determine if kinetochore function responds not only to

the number of phosphorylated residues in the Hec1 tail, but also the position of these phosphorylated sites.

Interestingly, our data show that neither the Hec1 CH domain nor the tail domain can support kinetochore-microtubule attachment alone. What remains to be defined, however, is how these two domains form a functional microtubule binding site together. With the answer to this question will undoubtedly come important insight into the molecular mechanism of kinetochore-microtubule attachment.

Importantly, our data implicate the NDC80 complex as the principal site of direct microtubule attachments in cells. Furthermore, we have shown that the NDC80 complex is required for regulating kinetochore-microtubule attachment strength, allowing the kinetochore to carry out discrete functions during mitosis. Taken together our data indicate that the NDC80 complex has distinct protein domains that are required for generating and regulating kinetochore-microtubule attachments in cells, a process that culminates with chromosome alignment, ultimately leading to accurate chromosome segregation.

## REFERENCES


Akhmanova, A., Steinmetz, M. O. (2008). Tracking the ends: a dynamic protein network controls the fate of microtubule tips. *Nature Reviews Molecular Cell Biology* **9**, 309-322.

Alushin, G. M., Ramey, V. H., Pasqualato, S., Ball, D. A., Grigorieff, N., Musacchio, A., Nogales, E. (2010). The Ndc80 kinetochore complex forms oligomeric arrays along microtubules. *Nature* **467**, 805-810.

Arentson, E., Faloon, P., Seo, J., Moon, E., Studts, J. M., Fremont, D. H., Choi, K. (2002). Oncogenic potential of the DNA replication licensing protein CDT1. *Oncogene* **21**, 1150.

Asbury, C. L., Gestaut, D. R., Powers, A. F., Franck, A. D., Davis, T. N. (2006). The Dam1 kinetochore complex harnesses microtubule dynamics to produce force and movement. *Proceedings of the National Academy of Sciences* **103**, 9873.

Baker, D. J., Dawlaty, M. M., Galardy, P., Deursen, J. M. v. (2007). Mitotic regulation of the anaphase-promoting complex. *Cellular and Molecular Life Sciences* **64**, 589-600.

Bakhoum, S. F., Compton, D. A. (2011). Kinetochores and disease: keeping microtubule dynamics *in check!*. *Current Opinion in Cell Biology* **24,** 64-70.

Barisic, M., Sohm, B., Mikolcevic, P., Wandke, C., Rauch, V., Ringer, T., Hess, M., Bonn, G., Geley, S. (2010). Spindly/CCDC99 is required for efficient chromosome congression and mitotic checkpoint regulation. *Molecular Biology of the Cell* **21**, 1968-1981.

Biggins, S., Murray, A. W. (2001). The budding yeast protein kinase Ipl1/Aurora allows the absence of tension to activate the spindle checkpoint. *Genes & Development* **15**, 3118-3129.

Black, B. E., Foltz, D. R., Chakravarthy, S., Luger, K., Woods, V. L., Cleveland, D. W. (2004). Structural determinants for generating centromeric chromatin. *Nature* **430**, 578-582.

Black, B. E., Jansen, L. E. T., Maddox, P. S., Foltz, D. R., Desai, A. B., Shah, J. V., Cleveland, D. W. (2007). Centromere identity maintained by nucleosomes assembled with histone H3 containing the CENP-A targeting domain. *Molecular Cell* **25**, 309-322.

Bloom, K. (2007). Centromere dynamics. *Current Opinion in Genetics & Development* **17**, 151-156.

Bomont, P., Maddox, P., Shah, J. V., Desai, A. B., Cleveland, D. W. (2005). Unstable microtubule capture at kinetochores depleted of the centromere-associated protein CENP-F. *The EMBO Journal* **24**, 3927-3939.

Brinkley, B. R., Stubblefield, E. (1966). The fine structure of the kinetochore of a mammalian cell in vitro. *Chromosoma* **19**, 28-43.

Burrack, L. S., Applen, S. E., Berman, J. (2011). The requirement for the Dam1 complex is dependent upon the number of kinetochore proteins and microtubules. *Current Biology* **21,** 889-896.

Campbell, M. S., Chan, G. K. ,Yen, T. J. (2001). Mitotic checkpoint proteins HsMAD1 and HsMAD2 are associated with nuclear pore complexes in interphase. *Journal of Cell Science* **114**, 953-963.

Carmena, M., Earnshaw, W. C. (2003). The cellular geography of aurora kinases. *Nature Reviews Molecular Cell Biology* **4**, 842-854.

Chan, Y. W., Jeyaprakash, A. A., Nigg, E. A., Santamaria, A. (2012). Aurora B controls kinetochore-microtubule attachments by inhibiting Ska complex-KMN network interaction. *The Journal of Cell Biology* **5,** 563-571.

Cheeseman, I. M., Brew, C., Wolyniak, M., Desai, A., Anderson, S., Muster, N., Yates, J. R., Huffaker, T. C., Drubin, D. G., Barnes, G. (2001a). Implication of a novel multiprotein Dam1p complex in outer kinetochore function. *The Journal of Cell Biology* **155**, 1137-1146.

Cheeseman, I. M., Enquist-Newman, M., Müller-Reichert, T., Drubin, D. G., Barnes, G. (2001b). Mitotic spindle integrity and kinetochore function linked by the Duo1p/Dam1p complex. *The Journal of Cell Biology* **152**, 197-212.

Cheeseman, I. M., Anderson, S., Jwa, M., Green, E. M., Kang, J., Yates, J. R., Chan, C. S. M., Drubin, D. G., Barnes, G. (2002). Phospho-regulation of kinetochore-microtubule attachments by the Aurora kinase Ipl1p. *Cell* **111**, 163-172.

Cheeseman, I. M., Chappie, J. S., Wilson-Kubalek, E. M., Desai, A. (2006). The conserved KMN network constitutes the core microtubule-binding site of the kinetochore. *Cell* **127**, 983-997.

Cheeseman, I. M. Desai, A. (2008). Molecular architecture of the kinetochore-microtubule interface. *Nat Rev Mol Cell Biol* **9**, 33-46.

Cheeseman, I. M., Hori, T., Fukagawa, T., Desai, A. (2008). KNL1 and the CENP-H/I/K complex coordinately direct kinetochore assembly in vertebrates. *Molecular Biology of the Cell* **19**, 587-594.

Churchman, L. S., Ökten, Z., Rock, R. S., Dawson, J. F., Spudich, J. A. (2005). Single molecule high-resolution colocalization of Cy3 and Cy5 attached to macromolecules measures intramolecular distances through time. *Proceedings of the National Academy of Sciences of the United States of America* **102**, 1419-1423.

Ciferri, C., De Luca, J., Monzani, S., Ferrari, K. J., Ristic, D., Wyman, C., Stark, H., Kilmartin, J., Salmon, E. D. ,Musacchio, A. (2005). Architecture of the human Ndc80-Hec1 complex, a critical constituent of the outer kinetochore. *Journal of Biological Chemistry* **280**, 29088-29095.

Ciferri, C., Pasqualato, S., Screpanti, E., Varetti, G., Santaguida, S., Dos Reis, G., Maiolica, A., Polka, J., De Luca, J. G., De Wulf, P. (2008). Implications for kinetochore-microtubule attachment from the structure of an engineered Ndc80 complex. *Cell* **133**, 427-439.

Cimini, D., Howell, B., Maddox, P., Khodjakov, A., Degrassi, F., Salmon, E. D. (2001). Merotelic kinetochore orientation is a major mechanism of aneuploidy in mitotic mammalian tissue cells. *The Journal of Cell Biology* **153**, 517-528.

Cimini, D., Moree, B., Canman, J. C. ,Salmon, E. D. (2003). Merotelic kinetochore orientation occurs frequently during early mitosis in mammalian tissue cells and error correction is achieved by two different mechanisms. *Journal of Cell Science* **116**, 4213-4225.

Cimini, D., Wan, X., Hirel, C. B., Salmon, E. D. (2006). Aurora kinase promotes turnover of kinetochore microtubules to reduce chromosome segregation errors. *Current Biology* **16**, 1711-1718.

Cleveland, D. W., Mao, Y., Sullivan, K. F. (2003). Centromeres and kinetochores from epigenetics to mitotic checkpoint signaling. *Cell* **112**, 407-421.

Cooke, C. A., Schaar, B., Yen, T. J., Earnshaw, W. C. (1997). Localization of CENP-E in the fibrous corona and outer plate of mammalian kinetochores from prometaphase through anaphase. *Chromosoma* **106**, 446-455.

Coquelle, F. M., Caspi, M., Cordelieres, F. P., Dompierre, J. P., Dujardin, D. L., Koifman, C., Martin, P., Hoogenraad, C. C., Akhmanova, A. ,Galjart, N. (2002). LIS1, CLIP-170's key to the dynein/dynactin pathway. *Molecular and Cellular Biology* **22**, 3089-3102.

Coue, M., Lombillo, V. A., McIntosh, J. R. (1991). Microtubule depolymerization promotes particle and chromosome movement in vitro. *The Journal of Cell Biology* **112**, 1165-1175.

Daum, J. R., Wren, J. D., Daniel, J. J., Sivakumar, S., McAvoy, J. N., Potapova, T. A. ,Gorbsky, G. J. (2009). Ska3 is required for spindle checkpoint silencing and the maintenance of chromosome cohesion in mitosis. *Current Biology* **19**, 1467-1472.

De Wulf, P., McAinsh, A. D., Sorger, P. K. (2003). Hierarchical assembly of the budding yeast kinetochore from multiple subcomplexes. *Genes & Development* **17**, 2902-2921.

DeLuca, J. G., Moree, B., Hickey, J. M., Kilmartin, J. V. ,Salmon, E. D., (2002). hNuf2 inhibition blocks stable kinetochore-microtubule attachment and induces mitotic cell death in HeLa cells. *The Journal of Cell Biology* **159,** 549-555.

DeLuca, J. G., Howell, B. J., Canman, J. C., Hickey, J. M., Fang, G., Salmon, E. D. (2003). Nuf2 and Hec1 are required for retention of the checkpoint proteins Mad1 and Mad2 to kinetochores. *Current Biology* **13**, 2103-2109.

DeLuca, J. G., Dong, Y., Hergert, P., Strauss, J., Hickey, J. M., Salmon, E. D., McEwen, B. F. (2005). Hec1 and Nuf2 are core components of the kinetochore outer plate essential for organizing microtubule attachment sites. *Molecular Biology of the Cell* **16**, 519-531.

DeLuca, J. G., Gall, W. E., Ciferri, C., Cimini, D., Musacchio, A., Salmon, E. D. (2006). Kinetochore microtubule dynamics and attachment stability are regulated by Hec1. *Cell* **127**, 969-982.

DeLuca, J. G., Musacchio, A. (2011). Structural organization of the kinetochore-microtubule interface. *Current Opinion in Cell Biology* **24,** 48-56.

DeLuca, K. F., Lens, S. M. A., DeLuca, J. G. (2011). Temporal changes in Hec1 phosphorylation control kinetochore-microtubule attachment stability during mitosis. *Journal of Cell Science* **124**, 622-634.

Desai, A., Rybina, S., Müller-Reichert, T., Shevchenko, A., Shevchenko, A., Hyman, A., Oegema, K. (2003). KNL-1 directs assembly of the microtubule-binding interface of the kinetochore in C. elegans. *Genes & Development* **17**, 2421-2435.

Diaz-Rodríguez, E., Sotillo, R., Schvartzman, J. M., Benezra, R. (2008). Hec1 overexpression hyperactivates the mitotic checkpoint and induces tumor formation in vivo. *Proceedings of the National Academy of Sciences* **105**, 16719-16724.

Ditchfield, C., Johnson, V. L., Tighe, A., Ellston, R., Haworth, C., Johnson, T., Mortlock, A., Keen, N., Taylor, S. S. (2003). Aurora B couples chromosome alignment with anaphase by targeting BubR1, Mad2, and Cenp-E to kinetochores. *The Journal of Cell Biology* **161**, 267-280.

Dong, Y., Beldt, K. J. V., Meng, X., Khodjakov, A., McEwen, B. F. (2007). The outer plate in vertebrate kinetochores is a flexible network with multiple microtubule interactions. *Nature Cell Biology* **9**, 516-522.

Dougherty, G. W., Adler, H. J., Rzadzinska, A., Gimona, M., Tomita, Y., Lattig, M. C., Merritt Jr, R. C., Kachar, B. (2005). CLAMP, a novel microtubule-associated protein with EB-type calponin homology. *Cell Motility and the Cytoskeleton* **62**, 141-156.

Dujardin, D., Wacker, U. I., Moreau, A., Schroer, T. A., Rickard, J. E., De Mey, J. R. (1998). Evidence for a role of CLIP-170 in the establishment of metaphase chromosome alignment. *The Journal of Cell Biology* **141**, 849-862.

Enquist-Newman, M., Cheeseman, I. M., Van Goor, D., Drubin, D. G., Meluh, P. B., Barnes, G. (2001). Dad1p, third component of the Duo1p/Dam1p complex involved in kinetochore function and mitotic spindle integrity. *Molecular Biology of the Cell* **12**, 2601-2613.

Franck, A. D., Powers, A. F., Gestaut, D. R., Gonen, T., Davis, T. N., Asbury, C. L. (2007). Tension applied through the Dam1 complex promotes microtubule elongation providing a direct mechanism for length control in mitosis. *Nature Cell Biology* **9**, 832-837.

Gaitanos, T. N., Santamaria, A., Jeyaprakash, A. A., Wang, B., Conti, E., Nigg, E. A. (2009). Stable kinetochore-microtubule interactions depend on the Ska complex and its new component Ska3/C13Orf3. *The EMBO Journal* **28**, 1442-1452.

Gascoigne, K. E., Takeuchi, K., Suzuki, A., Hori, T., Fukagawa, T., Cheeseman, I. M. (2011). Induced Ectopic Kinetochore Assembly Bypasses the Requirement for CENP-A Nucleosomes. *Cell* **145**, 410-422.

Gassmann, R., Holland, A. J., Varma, D., Wan, X., Çivril, F., Cleveland, D. W., Oegema, K., Salmon, E. D., Desai, A. (2010). Removal of Spindly from microtubule-attached kinetochores controls spindle checkpoint silencing in human cells. *Genes & Development* **24**, 957-971.

Gestaut, D. R., Graczyk, B., Cooper, J., Widlund, P. O., Zelter, A., Wordeman, L., Asbury, C. L., Davis, T. N. (2008). Phosphoregulation and depolymerization-driven movement of the Dam1 complex do not require ring formation. *Nature Cell Biology* **10**, 407-414.

Gimona, M., Djinovic-Carugo, K., Kranewitter, W. J., Winder, S. J. (2002). Functional plasticity of CH domains. *FEBS Letters* **513**, 98-106.

Goshima, G., Kiyomitsu, T., Yoda, K., Yanagida, M. (2003). Human centromere chromatin protein hMis12, essential for equal segregation, is independent of CENP-A loading pathway. *The Journal of Cell Biology* **160**, 25-39.

Griffis, E. R., Stuurman, N., Vale, R. D. (2007). Spindly, a novel protein essential for silencing the spindle assembly checkpoint, recruits dynein to the kinetochore. *The Journal of Cell Biology* **177**, 1005-1015.

Grishchuk, E. L., Efremov, A. K., Volkov, V. A., Spiridonov, I. S., Gudimchuk, N., Westermann, S., Drubin, D., Barnes, G., McIntosh, J. R., Ataullakhanov, F. I. (2008). The Dam1 ring binds microtubules strongly enough to be a processive as well as energy-efficient coupler for chromosome motion. *Proceedings of the National Academy of Sciences* **105**, 15423-15428.

Guimaraes, G. J., Dong, Y., McEwen, B. F., DeLuca, J. G. (2008). Kinetochore-microtubule attachment relies on the disordered N-terminal tail domain of Hec1. *Current Biology* **18**, 1778-1784.

Guse, A., Carroll, C. W., Moree, B., Fuller, C. J., Straight, A. F. (2011). In vitro centromere and kinetochore assembly on defined chromatin templates. *Nature* **477,** 354-358.

Hanisch, A., Silljé, H. H. W., Nigg, E. A. (2006). Timely anaphase onset requires a novel spindle and kinetochore complex comprising Ska1 and Ska2. *The EMBO Journal* **25**, 5504-5515.

Hauf, S., Cole, R. W., LaTerra, S., Zimmer, C., Schnapp, G., Walter, R., Heckel, A., Van Meel, J., Rieder, C. L., Peters, J. M. (2003). The small molecule Hesperadin reveals a role for Aurora B in correcting kinetochore-microtubule attachment and in maintaining the spindle assembly checkpoint. *The Journal of Cell Biology* **161**, 281-294.

Hayashi, I., Ikura, M. (2003). Crystal structure of the amino-terminal microtubule-binding domain of end-binding protein 1 (EB1). *Journal of Biological Chemistry* **278**, 36430-36434.

Heun, P., Erhardt, S., Blower, M. D., Weiss, S., Skora, A. D., Karpen, G. H. (2006). Mislocalization of the Drosophila centromere-specific histone CID promotes formation of functional ectopic kinetochores. *Developmental Cell* **10**, 303-315.

Helenius, J., Brouhard, G., Kalaidzidis, Y., Diez, S. ,Howard, J. (2006). The depolymerizing kinesin MCAK uses lattice diffusion to rapidly target microtubule ends. *Nature* **441**, 115-119.

Hill, T. L. (1985). Theoretical problems related to the attachment of microtubules to kinetochores. *Proceedings of the National Academy of Sciences* **82**, 4404-4408.

Hofmann, C., Cheeseman, I. M., Goode, B. L., McDonald, K. L., Barnes, G., Drubin, D. G. (1998). Saccharomyces cerevisiae Duo1p and Dam1p, novel proteins involved in mitotic spindle function. *The Journal of Cell Biology* **143**, 1029-1040.

Hoffman, D. B., Pearson, C. G., Yen, T. J., Howell, B. J., Salmon, E. D. (2001). Microtubule-dependent changes in assembly of microtubule motor proteins and mitotic spindle checkpoint proteins at PtK1 kinetochores. *Molecular Biology of the Cell* **12**, 1995-2009.

Holt, L. J., Hutti, J. E., Cantley, L. C., Morgan, D. O. (2007). Evolution of Ime2 phosphorylation sites on Cdk1 substrates provides a mechanism to limit the effects of the phosphatase Cdc14 in meiosis. *Molecular Cell* **25**, 689-702.

Hori, T., Haraguchi, T., Hiraoka, Y., Kimura, H. ,Fukagawa, T. (2003). Dynamic behavior of Nuf2-Hec1 complex that localizes to the centrosome and centromere and is essential for mitotic progression in vertebrate cells. *Journal of Cell Science* **116**, 3347-3362.

Hori, T., Amano, M., Suzuki, A., Backer, C. B., Welburn, J. P., Dong, Y., McEwen, B. F., Shang, W. H., Suzuki, E., Okawa, K. (2008). CCAN makes multiple contacts with centromeric DNA to provide distinct pathways to the outer kinetochore. *Cell* **135**, 1039-1052.

Howard, W. D., Timasheff, S. N. (1986). GDP state of tubulin: stabilization of double rings. *Biochemistry* **25**, 8292-8300.

Howell, B. J., McEwen, B. F., Canman, J. C., Hoffman, D. B., Farrar, E. M., Rieder, C. L., Salmon, E. D. (2001). Cytoplasmic dynein/dynactin drives kinetochore protein transport to the spindle poles and has a role in mitotic spindle checkpoint inactivation. *The Journal of Cell Biology* **155**, 1159-1172.

Hsu, K. S., Toda, T. (2011). Ndc80 internal loop interacts with Dis1/TOG to ensure proper kinetochore-spindle attachment in fission yeast. *Current Biology* **21,** 214-220.

Inoue, S., Salmon, E. D. (1995). Force generation by microtubule assembly/disassembly in mitosis and related movements. *Molecular Biology of the Cell* **6**, 1619-1640.

Janke, C., Ortíz, J., Tanaka, T. U., Lechner, J., Schiebel, E. (2002). Four new subunits of the Dam1-Duo1 complex reveal novel functions in sister kinetochore biorientation. *The EMBO Journal* **21**, 181-193.

Joglekar, A. P., Bouck, D. C., Molk, J. N., Bloom, K. S., Salmon, E. D. (2006). Molecular architecture of a kinetochore-microtubule attachment site. *Nature Cell Biology* **8**, 581-585.

Joglekar, A. P., Bouck, D., Finley, K., Liu, X., Wan, Y., Berman, J., He, X., Salmon, E. D., Bloom, K. S. (2008). Molecular architecture of the kinetochore-microtubule attachment site is conserved between point and regional centromeres. *The Journal of Cell Biology* **181**, 587-594.

Joglekar, A. P., Bloom, K., Salmon, E. D. (2009). In vivo protein architecture of the eukaryotic kinetochore with nanometer scale accuracy. *Current Biology* **19**, 694-699.

Joglekar, A. P., Bloom, K. S. ,Salmon, E. D. (2010). Mechanisms of force generation by end-on kinetochore-microtubule attachments. *Current Opinion in Cell Biology* **22**, 57-67.

Johnston, K., Joglekar, A., Hori, T., Suzuki, A., Fukagawa, T., Salmon, E. D. (2010). Vertebrate kinetochore protein architecture: protein copy number. *The Journal of Cell Biology* **189**, 937-943.

Jokelainen, P. T. (1967). The ultrastructure and spatial organization of the metaphase kinetochore in mitotic rat cells. *Journal of Ultrastructure Research* **19**, 19-44.

Jones, M. H., Bachant, J. B., Castillo, A. R., Giddings Jr, T. H., Winey, M. (1999). Yeast Dam1p is required to maintain spindle integrity during mitosis and interacts with the Mps1p kinase. *Molecular Biology of the Cell* **10**, 2377-2391.

Jonker, H. R. A., Wechselberger, R. W., Pinkse, M., Kaptein, R., Folkers, G. E. (2006). Gradual phosphorylation regulates PC4 coactivator function. *FEBS Journal* **273**, 1430-1444.

Jordan, M. A., Thrower, D. ,Wilson, L. (1992). Effects of vinblastine, podophyllotoxin and nocodazole on mitotic spindles. Implications for the role of microtubule dynamics in mitosis. *Journal of Cell Science* **102**, 401-416.

Kemmler, S., Stach, M., Knapp, M., Ortiz, J., Pfannstiel, J., Ruppert, T., Lechner, J. (2009). Mimicking Ndc80 phosphorylation triggers spindle assembly checkpoint signalling. *The EMBO Journal* **28**, 1099-1110.

King, R. W., Peters, J. M., Tugendreich, S., Rolfe, M., Hieter, P., Kirschner, M. W. (1995). A 20S complex containing CDC27 and CDC16 catalyzes the mitosis-specific conjugation of ubiquitin to cyclin B. *Cell* **81**, 279-288.

Kiyomitsu, T., Murakami, H., Yanagida, M. (2011). Protein interaction domain mapping of human kinetochore protein Blinkin reveals a consensus motif for binding of spindle assembly checkpoint proteins Bub1 and BubR1. *Molecular and Cellular Biology* **31**, 998-1011.

Kline, S. L., Cheeseman, I. M., Hori, T., Fukagawa, T., Desai, A. (2006). The human Mis12 complex is required for kinetochore assembly and proper chromosome segregation. *The Journal of Cell Biology* **173**, 9-17.

Kline-Smith, S. L., Sandall, S., Desai, A. (2005). Kinetochore–spindle microtubule interactions during mitosis. *Current Opinion in Cell Biology* **17**, 35-46.

Koshland, D. E., Mitchison, T. J., Kirschner, M. W. (1988). Polewards chromosome movement driven by microtubule depolymerization in vitro. *Nature* **331**, 499-504.

Kulukian, A., Han, J. S., Cleveland, D. W. (2009). Unattached kinetochores catalyze production of an anaphase inhibitor that requires a Mad2 template to prime Cdc20 for BubR1 binding. *Developmental Cell* **16**, 105-117.

Lampson, M. A., Kapoor, T. M. (2005). Unraveling cell division mechanisms with small-molecule inhibitors. *Nature Chemical Biology* **2**, 19-27.

Lawrimore, J., Bloom, K. S., Salmon, E. D. (2011). Point centromeres contain more than a single centromere-specific Cse4 (CENP-A) nucleosome. *The Journal of Cell Biology* **195**, 573-582.

Li, Y., Bachant, J., Alcasabas, A. A., Wang, Y., Qin, J., Elledge, S. J. (2002). The mitotic spindle is required for loading of the DASH complex onto the kinetochore. *Genes & Development* **16**, 183-197.

Liontos, M., Koutsami, M., Sideridou, M., Evangelou, K., Kletsas, D., Levy, B., Kotsinas, A., Nahum, O., Zoumpourlis, V., Kouloukoussa, M. (2007). Deregulated overexpression of hCdt1 and hCdc6 promotes malignant behavior. *Cancer Research* **67**, 10899-10909.

Liu, D., Vleugel, M., Backer, C. B., Hori, T., Fukagawa, T., Cheeseman, I. M., Lampson, M. A. (2010). Regulated targeting of protein phosphatase 1 to the

outer kinetochore by KNL1 opposes Aurora B kinase. *The Journal of Cell Biology* **188**, 809-820.

Lombillo, V. A., Nislow, C., Yen, T. J., Gelfand, V. I., McIntosh, J. R. (1995). Antibodies to the kinesin motor domain and CENP-E inhibit microtubule depolymerization-dependent motion of chromosomes in vitro. *The Journal of Cell Biology* **128**, 107-115.

Machida, Y. J., Hamlin, J. L., Dutta, A. (2005). Right place, right time, and only once: replication initiation in metazoans. *Cell* **123**, 13-24.

Maiato, H., Fairley, E. A. L., Rieder, C. L., Swedlow, J. R., Sunkel, C. E., Earnshaw, W. C. (2003). Human CLASP1 is an outer kinetochore component that regulates spindle microtubule dynamics. *Cell* **113**, 891-904.

Maiato, H., DeLuca, J., Salmon, E. D., Earnshaw, W. C. (2004). The dynamic kinetochore-microtubule interface. *Journal of Cell Science* **117,** 5461-5477.

Maiolica, A., Cittaro, D., Borsotti, D., Sennels, L., Ciferri, C., Tarricone, C., Musacchio, A., Rappsilber, J. (2007). Structural analysis of multiprotein complexes by cross-linking, mass spectrometry, and database searching. *Molecular & Cellular Proteomics* **6**, 2200-2211.

Malureanu, L. A., Jeganathan, K. B., Hamada, M., Wasilewski, L., Davenport, J., van Deursen, J. M. (2009). BubR1 N terminus acts as a soluble inhibitor of Cyclin B degradation by APC/C Cdc20 in interphase. *Developmental Cell* **16**, 118-131.

Mandelkow, E. M., Mandelkow, E., Milligan, R. A. (1991). Microtubule dynamics and microtubule caps: a time-resolved cryo-electron microscopy study. *The Journal of Cell Biology* **114**, 977-991.

Mandelkow, E. M. , Mandelkow, E. (1992). Microtubule oscillations. *Cell Motility and the Cytoskeleton* **22**, 235-244.

Manning, A. L., Bakhoum, S. F., Maffini, S., Correia-Melo, C., Maiato, H., Compton, D. A. (2010). CLASP1, astrin and Kif2b form a molecular switch that regulates kinetochore-microtubule dynamics to promote mitotic progression and fidelity. *The EMBO Journal* **29**, 3531-3543.

Mao, Y., Desai, A., Cleveland, D. W. (2005). Microtubule capture by CENP-E silences BubR1-dependent mitotic checkpoint signaling. *Science's STKE* **170**, 873-880.

Maresca, T. J., Salmon, E. D. (2010). Welcome to a new kind of tension: translating kinetochore mechanics into a wait-anaphase signal. *Journal of Cell Science* **123**, 825-835.

Margolis, R. L., Wilson, L. (1981). Microtubule treadmills— possible molecular machinery. *Nature* **293,** 705-711.

Martin-Lluesma, S., Stucke, V. M., Nigg, E. A. (2002). Role of Hec1 in spindle checkpoint signaling and kinetochore recruitment of Mad1/Mad2. *Science* **297**, 2267-2270.

Maure, J. F., Komoto, S., Oku, Y., Mino, A., Pasqualato, S., Natsume, K., Clayton, L., Musacchio, A., Tanaka, T. U. (2011). The Ndc80 loop region facilitates formation of kinetochore attachment to the dynamic microtubule plus end. *Current Biology* **21,** 207-213.

McCleland, M. L., Kallio, M. J., Barrett-Wilt, G. A., Kestner, C. A., Shabanowitz, J., Hunt, D. F., Gorbsky, G. J., Stukenberg, P. T. (2004). The vertebrate Ndc80 complex contains Spc24 and Spc25 homologs, which are required to establish and maintain kinetochore-microtubule attachment. *Current biology* **14**, 131-137.

McEwen, B. F., Arena, J. T., Frank, J., Rieder, C. L. (1993). Structure of the colcemid-treated PtK 1 kinetochore outer plate as determined by high voltage electron microscopic tomography. *The Journal of Cell Biology* **120,** 301-312.

McEwen, B. F., Hsieh, C. E., Mattheyses, A. L., Rieder, C. L. (1998). A new look at kinetochore structure in vertebrate somatic cells using high-pressure freezing and freeze substitution. *Chromosoma* **107**, 366-375.

McEwen, B. F., Chan, G. K. T., Zubrowski, B., Savoian, M. S., Sauer, M. T., Yen, T. J. (2001). CENP-E is essential for reliable bioriented spindle attachment, but chromosome alignment can be achieved via redundant mechanisms in mammalian cells. *Molecular Biology of the Cell* **12**, 2776-2789.

McEwen, B. F., Dong, Y. (2010). Contrasting models for kinetochore microtubule attachment in mammalian cells. *Cellular and Molecular Life Sciences* **67**, 2163-2172.

McGhee, J. D., von Hippel, P. H. (1974). Theoretical aspects of DNA-protein interactions: co-operative and non-co-operative binding of large ligands to a one-dimensional homogeneous lattice. *Journal of Molecular Biology* **86**, 469-489.

McIntosh, J. R. (2005). Rings around kinetochore microtubules in yeast. *Nature Structural & Molecular Biology* **12**, 210-212.

McIntosh, J. R., Grishchuk, E. L., Morphew, M. K., Efremov, A. K., Zhudenkov, K., Volkov, V. A., Cheeseman, I. M., Desai, A., Mastronarde, D. N., Ataullakhanov, F. I. (2008). Fibrils connect microtubule tips with kinetochores: a mechanism to couple tubulin dynamics to chromosome motion. *Cell* **135**, 322-333.

Miller, S. A., Johnson, M. L., Stukenberg, P. T. (2008). Kinetochore attachments require an interaction between unstructured tails on microtubules and Ndc80$^{Hec1}$. *Current Biology* **18,** 1785-1791.

Miranda, J. J. L., De Wulf, P., Sorger, P. K., Harrison, S. C. (2005). The yeast DASH complex forms closed rings on microtubules. *Nature Structural & Molecular Biology* **12**, 138-143.

Musacchio, A., Hardwick, K. G. (2002). The spindle checkpoint: structural insights into dynamic signalling. *Nature Reviews Molecular Cell Biology* **3**, 731-741.

Nishino, T., Takeuchi, K., Gascoigne, K. E., Suzuki, A., Hori, T., Oyama, T., Morikawa, K., Cheeseman, I. M., Fukagawa, T. (2012). CENP-TWSX forms a unique centromeric chromatin structure with a histone-like fold. *Cell* **148**, 487-501.

Obuse, C., Iwasaki, O., Kiyomitsu, T., Goshima, G., Toyoda, Y., Yanagida, M. (2004). A conserved Mis12 centromere complex is linked to heterochromatic HP1 and outer kinetochore protein Zwint-1. *Nature Cell Biology* **6**, 1135-1141.

Ohta, S., Bukowski-Wills, J. C., Sanchez-Pulido, L., Alves, F. L., Wood, L., Chen, Z. A., Platani, M., Fischer, L., Hudson, D. F. ,Ponting, C. P. (2010). The protein composition of mitotic chromosomes determined using multiclassifier combinatorial proteomics. *Cell* **142**, 810-821.

Okada, M., Cheeseman, I. M., Hori, T., Okawa, K., McLeod, I. X., Yates, J. R., Desai, A., Fukagawa, T. (2006). The CENP-H,—I complex is required for the efficient incorporation of newly synthesized CENP-A into centromeres. *Nature Cell Biology* **8**, 446-457.

Peters, J. M. (2006). The anaphase promoting complex/cyclosome: a machine designed to destroy. *Nature Reviews Molecular Cell Biology* **7**, 644-656.

Petrovic, A., Pasqualato, S., Dube, P., Krenn, V., Santaguida, S., Cittaro, D., Monzani, S., Massimiliano, L., Keller, J., Tarricone, A. (2010). The MIS12 complex is a protein interaction hub for outer kinetochore assembly. *The Journal of Cell Biology* **190**, 835-852.

Pinsky, B. A., Kung, C., Shokat, K. M. ,Biggins, S. (2005). The Ipl1-Aurora protein kinase activates the spindle checkpoint by creating unattached kinetochores. *Nature cell biology* **8**, 78-83.

Powers, A. F., Franck, A. D., Gestaut, D. R., Cooper, J., Gracyzk, B., Wei, R. R., Wordeman, L., Davis, T. N., Asbury, C. L. (2009). The Ndc80 kinetochore complex forms load-bearing attachments to dynamic microtubule tips via biased diffusion. *Cell* **136**, 865-875.

Przewloka, M. R., Venkei, Z., Bolanos-Garcia, V. M., Debski, J., Dadlez, M., Glover, D. M. (2011). CENP-C is a structural platform for kinetochore assembly. *Current Biology* **21,** 399-405.

Raaijmakers, J. A., Tanenbaum, M. E., Maia, A. F. ,Medema, R. H. (2009). RAMA1 is a novel kinetochore protein involved in kinetochore-microtubule attachment. *Journal of Cell Science* **122**, 2436-2445.

Rieder, C. L. (1981). The structure of the cold-stable kinetochore fiber in metaphase PtK1 cells. *Chromosoma* **84**, 145-158.

Rieder, C. L., Salmon, E. D. (1998). The vertebrate cell kinetochore and its roles during mitosis. *Trends in Cell Biology* **8**, 310-318.

Roos, U. P. (1973). Light and electron microscopy of rat kangaroo cells in mitosis. II. Kinetochore structure and function. *Chromosoma* **41**, 195-220.

Salmon, E. D., Begg, D. A. (1980). Functional implications of cold-stable microtubules in kinetochore fibers of insect spermatocytes during anaphase. *The Journal of Cell Biology* **85**, 853-865.

Santaguida, S., Musacchio, A. (2009). The life and miracles of kinetochores. *The EMBO Journal* **28**, 2511-2531.

Sclafani, R. A., Holzen, T. M. (2007). Cell cycle regulation of DNA replication. *Annual Review of Genetics* **41**, 237-280.

Screpanti, E., De Antoni, A., Alushin, G. M., Petrovic, A., Melis, T., Nogales, E., Musacchio, A. (2011). Direct binding of Cenp-C to the Mis12 complex joins the inner and outer kinetochore. *Current Biology* **21,** 391-398.

Shah, J. V., Cleveland, D. W. (2000). Waiting for anaphase Mad2 and the spindle assembly checkpoint. *Cell* **103**, 997-1000.

Slep, K. C., Vale, R. D. (2007). Structural basis of microtubule plus end tracking by XMAP215, CLIP-170, and EB1. *Molecular Cell* **27**, 976-991.

Stumpff, J., Von Dassow, G., Wagenbach, M., Asbury, C. ,Wordeman, L. (2008). The kinesin-8 motor Kif18A suppresses kinetochore movements to control mitotic chromosome alignment. *Developmental Cell* **14**, 252-262.

Sudakin, V., Ganoth, D., Dahan, A., Heller, H., Hershko, J., Luca, F. C., Ruderman, J. V., Hershko, A. (1995). The cyclosome, a large complex containing cyclin-selective ubiquitin ligase activity, targets cyclins for destruction at the end of mitosis. *Molecular Biology of the Cell* **6**, 185-197.

Sudakin, V., Chan, G. K. T., Yen, T. J. (2001). Checkpoint inhibition of the APC/C in HeLa cells is mediated by a complex of BUBR1, BUB3, CDC20, and MAD2. *The Journal of Cell Biology* **154**, 925-936.

Sundin, L. J. R., DeLuca, J. G. (2010). Kinetochores: NDC80 toes the line. *Current Biology* **20**, R1083-R1085.

Sundin, L. J. R., Guimaraes, G. J., DeLuca, J. G. (2011). The NDC80 complex proteins Nuf2 and Hec1 make distinct contributions to kinetochore-microtubule attachment in mitosis. *Molecular Biology of the Cell* **22**, 759-768.

Tanaka, K., Li Chang, H., Kagami, A., Watanabe, Y. (2009). CENP-C functions as a scaffold for effectors with essential kinetochore functions in mitosis and meiosis. *Developmental Cell* **17**, 334-343.

Tanaka, T. U., Rachidi, N., Janke, C., Pereira, G., Galova, M., Schiebel, E., Stark, M. J. R., Nasmyth, K. (2002). Evidence that the Ipl1-Sli15 (Aurora kinase-INCENP) complex promotes chromosome bi-orientation by altering kinetochore-spindle pole connections. *Cell* **108**, 317-329.

Tanaka, T. U., Stark, M. J. R., Tanaka, K. (2005). Kinetochore capture and bi-orientation on the mitotic spindle. *Nature Reviews Molecular Cell Biology* **6**, 929-942.

Tatsumi, Y., Sugimoto, N., Yugawa, T., Narisawa-Saito, M., Kiyono, T., Fujita, M. (2006). Deregulation of Cdt1 induces chromosomal damage without rereplication and leads to chromosomal instability. *Journal of Cell Science* **119**, 3128-3140.

Thakur, J., Sanyal, K. (2011). The essentiality of the fungus-specific Dam1 complex is correlated with a one-kinetochore-one-microtubule interaction present throughout the cell cycle, independent of the nature of a centromere. *Eukaryotic Cell* **10**, 1295-1305.

Theis, M., Slabicki, M., Junqueira, M., Paszkowski-Rogacz, M., Sontheimer, J., Kittler, R., Heninger, A. K., Glatter, T., Kruusmaa, K., Poser, I. (2009). Comparative profiling identifies C13orf3 as a component of the Ska complex required for mammalian cell division. *The EMBO Journal* **28**, 1453-1465.

Tooley, J. G., Miller, S. A., Stukenberg, P. T. (2011). The Ndc80 complex uses a tripartite attachment point to couple microtubule depolymerization to chromosome movement. *Molecular Biology of the Cell* **22**, 1217-1226.

Van Hooser, A. A., Ouspenski, I. I., Gregson, H. C., Starr, D. A., Yen, T. J., Goldberg, M. L., Yokomori, K., Earnshaw, W. C., Sullivan, K. F., Brinkley, B. R. (2001). Specification of kinetochore-forming chromatin by the histone H3 variant CENP-A. *Journal of Cell Science* **114**, 3529-3542.

Varga, V., Helenius, J., Tanaka, K., Hyman, A. A., Tanaka, T. U., Howard, J. (2006). Yeast kinesin-8 depolymerizes microtubules in a length-dependent manner. *Nature Cell Biology* **8**, 957-962.

Varma, D., Chandrasekaran, S., Sundin, L. J. R., Reidy, K. T., Wan, X., Chasse D. A. D., Nevis, K. R., DeLuca, J. G., Salmon, E. D., Cook, J. G. In press. *Nature Cell Biol*ogy.

Wan, X., O'Quinn, R. P., Pierce, H. L., Joglekar, A. P., Gall, W. E., DeLuca, J. G., Carroll, C. W., Liu, S. T., Yen, T. J., McEwen, B. F. (2009). Protein architecture of the human kinetochore microtubule attachment site. *Cell* **137**, 672-684.

Wang, F., Dai, J., Daum, J. R., Niedzialkowska, E., Banerjee, B., Stukenberg, P. T., Gorbsky, G. J., Higgins, J. M. G. (2010). Histone H3 Thr-3 phosphorylation by Haspin positions Aurora B at centromeres in mitosis. *Science* **330**, 231-235.

Wei, R. R., Sorger, P. K., Harrison, S. C. (2005). Molecular organization of the Ndc80 complex, an essential kinetochore component. *Proceedings of the National Academy of Sciences* **102**, 5363-5367.
Wei, R. R., Al-Bassam, J., Harrison, S. C. (2007). The Ndc80/HEC1 complex is a contact point for kinetochore-microtubule attachment. *Nature Structural & Molecular Biology* **14**, 54-59.

Welburn, J. P. I., Grishchuk, E. L., Backer, C. B., Wilson-Kubalek, E. M., Yates, J. R., Cheeseman, I. M. (2009). The human kinetochore Ska1 complex facilitates microtubule depolymerization-coupled motility. *Developmental Cell* **16**, 374-385.

Welburn, J. P. I., Vleugel, M., Liu, D., Yates Iii, J. R., Lampson, M. A., Fukagawa, T. ,Cheeseman, I. M. (2010). Aurora B phosphorylates spatially distinct targets to differentially regulate the kinetochore-microtubule interface. *Molecular Cell* **38**, 383-392.

Wendell, K. L., Wilson, L., Jordan, M. A. (1993). Mitotic block in HeLa cells by vinblastine: ultrastructural changes in kinetochore-microtubule attachment and in centrosomes. *Journal of cell science* **104**, 261-274.

Westermann, S., Avila-Sakar, A., Wang, H. W., Niederstrasser, H., Wong, J., Drubin, D. G., Nogales, E., Barnes, G. (2005). Formation of a dynamic kinetochore-microtubule interface through assembly of the Dam1 ring complex. *Molecular Cell* **17**, 277-290.

Westermann, S., Wang, H. W., Avila-Sakar, A., Drubin, D. G., Nogales, E., Barnes, G. (2006). The Dam1 kinetochore ring complex moves processively on depolymerizing microtubule ends. *Nature* **440**, 565-569.

Wigge, P. A., Kilmartin, J. V. (2001). The Ndc80p complex from Saccharomyces cerevisiae contains conserved centromere components and has a function in chromosome segregation. *The Journal of Cell Biology* **152**, 349-360.

Wilson-Kubalek, E. M., Cheeseman, I. M., Yoshioka, C., Desai, A., Milligan, R. A. (2008). Orientation and structure of the Ndc80 complex on the microtubule lattice. The *Journal of Cell Biology* **182**, 1055-1061.

Wojcik, E., Basto, R., Serr, M., Scaërou, F., Karess, R., Hays, T. (2001). Kinetochore dynein: its dynamics and role in the transport of the Rough deal checkpoint protein. *Nature Cell Biology* **3**, 1001-1008.

Zinkowski, R. P., Meyne, J., Brinkley, B. R. (1991). The centromere-kinetochore complex: a repeat subunit model. *The Journal of Cell Biology* 1091-1110.